

Regulation of phenotypic plasticity in high ambient temperature:
ELF3 and BZR1 as major thermostats gating PIF4 signaling

Dissertation
zur Erlangung des
Doktorgrades der Naturwissenschaften (Dr. rer. nat.)

der

Naturwissenschaftlichen Fakultät III
Agrar-und Ernährungswissenschaften,
Geowissenschaften und Informatik

der Martin-Luther-Universität Halle-Wittenberg

vorgelegt von

Carla Ibáñez Robles

Geb. am 24.11.1988 in Valencia (Spanien)

Halle, 2017

A mis padres

Abstract – English Version

Together with light, temperature is one of the major environmental cues regulating plant growth. In *Arabidopsis thaliana*, growth responses to high ambient temperature occur already in early stages of seedling development, hypocotyl elongation being one of the best characterized model phenotypes. At the molecular level, temperature-mediated plant morphology (also named thermomorphogenesis) is largely dependent on the transcription factor PHYTOCHROME INTERACTOR FACTOR 4 (PIF4). However, regulation of PIF4 on both transcriptional and post-transcriptional level is very complex and remains rather poorly understood. To exploit both the phenotypic and genotypic variation observed and to identify novel components of the temperature signaling pathway, temperature-induced hypocotyl elongation (TIHE) was used as a model response to perform a QTL analysis in the Bay x Sha RIL population and an EMS-mutagenesis screen in the Rrs-7 ecotype. As a result, the circadian clock component EARLY FLOWERING 3 (ELF3) and the brassinosteroid transcription factor BRASSINAZOLE RESISTANT 1 (BZR1) are highlighted here as novel components by gating PIF4 in the control of thermomorphogenesis.

Key words: *Arabidopsis*, ecotype, hypocotyl, thermomorphogenesis, PIF4, brassinosteroids, BZR1, auxin, ELF3, temperature, signaling.

Abstract – Deutsche Version

Neben Licht ist Temperatur einer der wichtigsten Umwelteinflüsse, die pflanzliches Wachstum regulieren. Das Wachstum von *Arabidopsis thaliana* reagiert bereits in den frühen Stadien der Keimlingsentwicklung sehr sensitiv auf erhöhte Umgebungstemperaturen. Hypokotylelongation ist hierbei einer der am besten charakterisierten Phänotypen. Auf molekularer Ebene hängt die temperaturregulierte Morphologie (Thermomorphogenese) zu großen Teilen vom Transkriptionsfaktor PHYTOCHROME-INTERACTING FACTOR 4 (PIF4) ab. Die Regulation von PIF4 ist jedoch sowohl auf transkriptioneller als auch auf translationeller Ebene sehr komplex und bislang wenig verstanden. Zur Identifizierung neuer Komponenten eines Temperatursignalweges wurde die genotypische und phänotypische Variation temperaturinduzierter Hypokotylelongation als Modelphänotyp in einer QTL-Analyse (Bay x Sha RIL Population) und einem EMS-Mutagenesecscreen (Rrs-7 Ökotyp) genutzt. Als Ergebnis dieser Ansätze konnten sowohl eine Komponente der circadianen Uhr, EARLY FLOWERING 3 (ELF3), als auch ein in der Brassinosteroidsignalkette relevanter Transkriptionsfaktor, BRASSINAZOLE RESISTANT 1 (BZR1), identifiziert und ihre Rollen in der temperaturinduzierten Signaltransduktion charakterisiert werden.

Stichworte: *Arabidopsis*, Ökotyp, Hypokotyl, Thermomorphogenese, PIF4, Brassinosteroide, BZR1, Auxin, ELF3, Temperatursignalweges.

Namen der Gutachter: Prof. Dr. Marcel Quint and Prof. Dr. Ute Höcker

Verteidigungsdatum: 10.07.2017

Index

1. Introduction	1
1.1 Effect of globally increasing ambient temperature on plant performance.....	1
1.2 Thermomorphogenesis	1
1.3 Temperature sensing in plants	2
1.4 The temperature signal transduction	4
1.5 The relevance of brassinosteroids in growth-associated responses	6
1.5.1 The brassinosteroid signaling network.....	6
2. Objectives.....	8
3. Materials and Methods	9
3.1 <i>Escherichia coli</i>	9
3.1.1 <i>E.coli</i> strains	9
3.1.2 Luria-Bertani (LB) medium	9
3.1.3 Growth conditions.....	9
3.1.4 Heat shock transformation and selection of positive clones	9
3.2 <i>Agrobacterium tumefaciens</i>	10
3.2.1 <i>A.tumefaciens</i> strain	10
3.2.2 Growth media	10
3.2.3 Growth conditions.....	10
3.2.4 Heat shock transformation and selection	10
3.3 <i>Arabidopsis thaliana</i>	10
3.3.1 Seeds sterilization and stratification.....	10
3.3.2 Growth conditions.....	10
3.3.3 Hormone/Inhibitor treatments	11
3.3.4 Temperature-Induced Hypocotyl Elongation (TIHE) assay.....	11
3.3.5 Chlorophyll quantification.....	11
3.3.6 Flowering time estimation	12
3.3.7 Rosette and petiole measurements	12
3.3.8 <i>Arabidopsis thaliana</i> transformation by floral dip.....	12
3.3.9 Selection of transformed <i>Arabidopsis thaliana</i> seedlings	12
3.4 Molecular biology methods	13
3.4.1 Semi-quantitative PCR	13
3.4.2 Genomic DNA extraction for mapping.....	13
3.4.2.1 Extraction buffer	13

3.4.2.2 Protocol.....	14
3.4.3 Mapping by CAPS markers	14
3.4.4 RNA Extraction, cDNA Synthesis, and qRT- PCR	14
3.4.5 Protoplast assay by the Tape- <i>Arabidopsis</i> Sandwich method	15
3.4.5.1 Solutions	15
3.4.5.2 Protoplast preparation.....	15
3.4.5.3 Protoplast transformation	16
3.4.5.4 Luciferase assay	16
3.4.5.5 GUS assay.....	16
3.4.5.6 LUC normalization	17
3.4.6 Western blot	17
3.4.6.1 Protein extraction	17
3.4.6.2 SDS-PAGE electrophoresis.....	18
3.4.6.3 Electrotransfer (semi-dry transference)	18
3.4.7 Chromatin-immunoprecipitation-PCR (ChIP-PCR).....	18
3.4.7.1 Buffers/Material.....	18
3.4.7.2 Protocol.....	19
3.4.8 Golden Gate cloning.....	22
3.5 Statistics	22
3.5.1 Q10 temperature coefficient.....	23
3.5.2 Index of phenotypic divergence (Pst).....	23
4. Results.....	24
4.1 CHAPTER I. Variation of thermomorphogenesis among <i>Arabidopsis</i> accessions	24
4.2 CHAPTER II. Natural variants of <i>ELF3</i> in thermomorphogenesis signaling.....	30
4.2.1 Previous work - QTL analysis	30
4.2.2 Verification of <i>GIR2.1</i> and <i>GIR2.2</i> confidence intervals	31
4.2.3 Fine-mapping and identification of the causal SNP for <i>GIR2.1</i>	32
4.2.4 Confirmation of <i>ELF3</i> as candidate gene for <i>GIR2.1</i>	32
4.3 CHAPTER III. The <i>okapi (opi)</i> -EMS screen.....	35
4.3.1 Previous work.....	35
4.3.2 <i>opi2</i>	36
4.3.2.1 Identification of the <i>opi2</i> causal mutation.....	36
4.3.2.2 <i>BIG/TIR3</i> cloning by the Golden Gate technique.....	37
4.3.3 <i>opi3</i> and <i>opi7</i>	40
4.3.3.1 Identification of the causal mutation	40
4.3.3.2 Pharmacological and transgenic complementation	43
4.3.3.3 Brassinosteroids are essential in temperature signaling.....	45

4.3.4 The auxin-brassinosteroid hierarchy in temperature signal transduction	46
4.3.5 The role of BRs in thermomorphogenesis: Gating PIF4	47
4.3.6 PIF4 and BZR1 in thermomorphogenesis responses.....	53
5. Discussion	55
5.1 Thermomorphogenic responses in plant adaptation	55
5.2 Temperature vs. light crosstalk.....	57
5.3 ELF3 as a negative regulator of temperature signaling	59
5.4 Brassinosteroids are essential for thermomorphogenesis	62
5.5 Auxin-brassinosteroid crosstalk in temperature response	65
5.6 BZR1 regulates temperature signaling by gating PIF4	67
5.7 BZR1 and ELF3 as antagonistic regulators of PIF4 expression and activity	69
5.8 The current model of temperature signal transduction.....	71
6. Conclusions	72
7. Bibliography.....	73
Appendix I.....	84
Appendix II.....	85
Appendix III.....	86
Appendix IV	87
Appendix V	88
Appendix IV	89
Acknowledgments	90
Curriculum Vitae	92

Abbreviations

A.thaliana	Arabidopsis thaliana
AFB2	AUXIN SIGNALING F-BOX 2
ANOVA	Analysis of variance
ARF	AUXIN RESPONSE FACTOR
ATHB2	ARABIDOPSIS THALIANA HOMEODOMAIN PROTEIN 2
ATS	Arabidopsis thaliana solution
BAK1	BRI1-ASSOCIATED RECEPTOR KINASE
Bay-0	Bayreuth
BC1	Back-cross 1
BFA	Brefeldin A
bHLH	basic helix-loop-helix
BIN2	BRASSINOSTEROID-INSENSITIVE 2
BKI1	BRASSINOSTEROID KINASE INHIBITOR 1
BRI1	BRASSINOSTEROID INSENSITIVE1
BRRE	Brassinosteroid responsive element
BRs	Brassinosteroids
BSK1	BRI1-SUPPRESSOR KINASE1
BSU1	BRI1 SUPPRESSOR 1
BZR1	BRASSINAZOLE-RESISTANT 1
BZR2	BRASSINAZOLE-RESISTANT 2
CAB	CHLOROPHYLL A/B BINDING PROTEIN
CAPS	Cleaved amplified polymorphic sequences
CCB	Coloidal comassie Blue
CDG1	CONSTITUTIVE DIFFERENTIAL GROWTH 1
CDS	Coding sequence
ChIP	Chromatin Immunoprecipitation
Col-0	Columbia-0
COP1	CONSTITUTIVE PHOTOMORPHOGENIC 1
CRY1	CRYPTOCHROME 1
CRY2	CRYPTOCHROME 2
DET1	DE-ETIOLATED 1
DET2	DE-ETIOLATED 2
DNA	Deoxyribonucleic acid
DWF7	DWARF7
E.coli	Escherichia coli
EC	Evening complex
ELF3	EARLY FLOWERING 3
ELF4	EARLY FLOWERING 4
EMS	Ethyl-methanesulfonate
Epi-BL	Epi-brassinolide
FLM	FLOWERING LOCUS M
GA	Gibberellic acid
GFP	GREEN FLUORESCENT PROTEIN
GG	Golden gate
GIR	GIRAFFE
GUS	Beta-glucuronidase
HFR1	LONG HYPOCOTYL IN FAR-RED
HIFs	Heterogeneous inbred families

Abbreviations

HY5	ELONGATED HYPOCOTYL 5
IAA	Indole-3-acetic-acid
IAA19	INDOLE-3-ACETIC ACID INDUCIBLE 19
Kyn	Kynurenin
LBS	LUX binding sites
Ler-1	Landsberg erecta
LHY	LATE ELONGATED HYPOCOTYL
LRR-RK	Leucine rich repeat receptor kinase
LUC	LUCIFERASE
NGS	Next-generation sequencing
OPI	Okapi
ORF	Open reading frame
PCR	Polymerase chain reaction
PHYB	PHYTOCHROME B
PIC	Picloram
PIF4	PHYTOCHROME INTERACTOR FACTOR 4
PIF5	PHYTOCHROME INTERACTOR FACTOR 5
PIN1	ARABIDOPSIS THALIANA PIN-FORMED 1
polyQ	Polyglutamine
PI	Protease inhibitor
PS	Ponceau staining
PP	protoplasts
PP2A	PROTEIN PHOSPHATASE 2A
PPZ	Propiconazole
PRE5	PACLOBUTRAZOL RESISTANCE 5
QTL	Quantitative trait locus
QTN	Quantitative trait nucleotide
RIL	Recombinant inbreed line
ROT3	ROTUNDIFOLIA3
SAR2	SHADE AVOIDANCE2
SAUR19	SMALL AUXIN UP RNA 19
SAUR23	SMALL AUXIN UP RNA 23
SDS	sodium dodecyl sulfate
SNP	Single nucleotide polymorphism
SPA1	SUPRESSOR OF PHYA
STE1	STEROL1
TAR1	TRYPTOPHAN AMINOTRANSFERASE RELATED 1
TIHE	Temperature-induced hypocotyl elongation
TIR1	TRANSPORT INHIBITOR RESPONSE 1
TIR3	TRANSPORT INHIBITOR RESPONSE 3
TOC1	TIMMING OF CAB EXPRESSION 1
UTR	Untranslated region
WEI8	WEAK ETHYLENE INSENSITIVE 8
Wt	Wild type
Yuc	Yucasin
ZT	Zeituple

1. Introduction

1.1 Effect of globally increasing ambient temperature on plant performance

The global average surface temperature has increased over the 20th century by about 0.6°C. In fact, the 10 warmest years in the past 134-year have occurred since 2000, 2016 being the warmest year on record (NASA). Future projections show that ambient temperature will rise, presuming a 1°C increase by 2050 and up to 6.4°C by 2100 (IPCC 2014; Woodward et al., 2014).

An increase in ambient temperature has a detrimental effect on light use efficiency when the temperature is above the “photosynthetic thermal optimum”. As yield production is largely dependent on photosynthesis efficiency, increases in ambient temperature become a potential problem for food security and a challenge for global agriculture. For major crops like cereals, wheat and barley (C_3), there is a negative correlation between yield and high temperature (Taiz, 2015); while C_4 (maize, sugarcane, sorghum...) plants have a wider optimal temperature range, thus yield is less affected by increasing temperature (Figure 1). For instance, global wheat (C_3) production is estimated to fall by 6% for each °C of temperature increase. It will furthermore become more variable over space and time, meaning yield stability will likewise decrease (Asseng et al., 2015). Other studies have revealed a 10% rice yield reduction for each 1°C in night time temperature increase (Peng et al., 2004). Economically, recent temperature increase is estimated to cause global loss of \$5 billion for these crops per year, as occurred in 2002 (Lobell and Field, 2007). Based on that, and although higher temperatures are projected to boost growth in cold climates; they may also impede growth in the tropics, or restrict growth exclusively to C_4 plants (Christin and Osborne, 2014), compromising the survival of species that will not be able to adapt. Indeed, some studies suggest that plant species unable to adjust flowering time in response to temperature are disappearing from certain environments (Hoffmann and Sgrò, 2011).

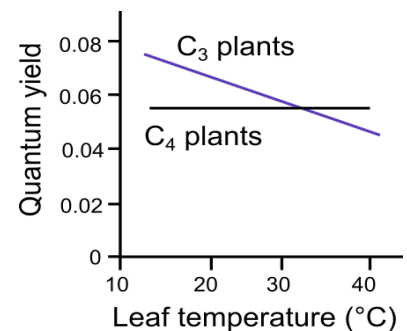


Figure 1. Effect of temperature into quantum yield efficiency. Increasing ambient temperature above the quantum optimum has detrimental effects on C_3 plants (black) while C_4 (purple) have a wider optimal temperature in photosynthesis efficiency.

1.2 Thermomorphogenesis

Plants exposed to high ambient temperature are characterized to change morphology as part of a buffering capacity. Developmental acclimatation (Athanasidou et al., 2010) or

thermomorphogenesis (Erwin et al., 1989) was defined as the adjustment of development during plant growth to high ambient temperatures. Most of the traits that are affected by temperature are directly or indirectly relevant for agriculture. Among these are seed dormancy, germination, flowering time and grain filling capacity; all of them essential to ensure food sustainability (Parent and Tardieu, 2012; Schmuths et al., 2006).

Although stem elongation or adult plant height has not been directly related to plant production, it may contribute to the capability of the plant to adapt to warm environments. In addition, leaves and inflorescences appear to be the organs most sensitive to high temperature. Because of that, tissue temperature moderation is frequently accomplished by changes in morphology and positioning of sensitive organs. Leaves tend to be small and vertically oriented to reduce solar irradiation, also called hyponastic growth. Beside changes in leaf morphology, plants growing under high ambient temperature exhibit high transpiration rates and steep leaf angles. All these mechanisms contribute to moderate leaf temperature and enhance cooling capacity of the plant (Crawford et al., 2012).

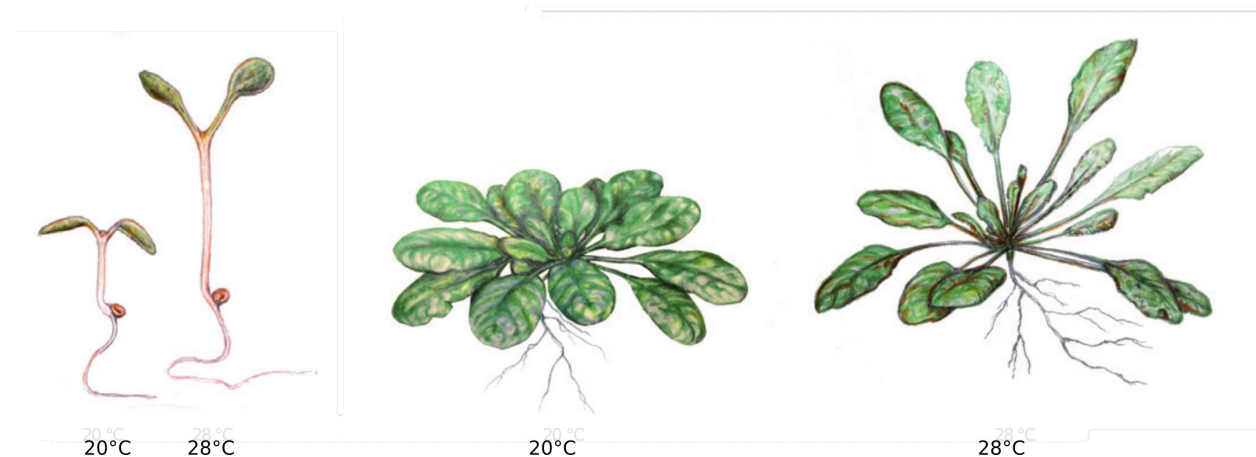


Figure 2. Temperature-induced growth in *Arabidopsis thaliana*. Hypocotyl elongation (left) and rosette opening (right) in response to high ambient temperature. Figure adapted from Quint et al. (2016).

In the model organism *Arabidopsis thaliana*, one of the earliest and best characterized thermomorphogenic responses is temperature-induced hypocotyl elongation (TIHE). Together with the phenotypes described above, petiole elongation and flowering time are also affected in further developmental stages (Figure 2).

1.3 Temperature sensing in plants

For morphological changes to occur in the plant, ambient temperature must be perceived. Temperature sensing mechanisms can be distinguished between the ones controlling configuration or assembly of molecules (passive sensing) or those integrated into a downstream signal transduction creating an active signal regulating a process of adaptive significance (Penfield et al., 2012). Potential temperature sensing mechanisms will be explained next. The

signal transduction cascade activated in response to temperature will be addressed in the next chapter.

Since ambient temperature varies between day and night, plants have to sense small fluctuations in temperature, and at the same time, distinguish daily fluctuations from warmth or cold stress. Hence, plants are extremely sensitive to temperature variations and even 1°-3°C change is enough to activate a signal transduction with potential dramatic developmental responses (Germination, flowering time; McClung and Davis, 2010). Nevertheless, the sensing mechanisms plants use to obtain this information from the environment remain poorly understood. Changes in membrane fluidity was hypothesized to be one of the primary sites of temperature perception. In fact, alterations in the lipid bilayer membranes together with changes in protein conformation are likely mechanisms “sense” ambient temperature also in plants (McClung and Davis, 2010; Penfield et al., 2012). However, this mechanism has only been shown in prokariotic systems. The major role of membrane fluidity may be to regulate downstream activity of fatty acid desaturases that ultimately will be controlling the lipid composition. Changes in membrane fluidity have been connected with the activation of other mechanisms such as the activation of ion channels (Ca²⁺) and protein folding by chaperones action (Saidi et al., 2009).

Chromatin complexity and thermodynamic changes are considered additional ways for plants to sense and activate transcriptional responses to ambient temperature. In fact, transcription and enzyme activity increase by 3.5-fold for a 10°C temperature rise (Q₁₀; Franklin and Wigge, 2014). Furthermore, Kumar and Wigge (2010) identified a histone H2A variant, H2A.Z, which may contribute to passive temperature sensing. Under high ambient temperatures, the occupancy of H2A.Z at promoters of temperature-induced genes decreases allowing accessibility of the transcription machinery. In addition to temperature-induced transcriptomic responses, epigenetic changes such as DNA methylation and histone de-acetylation appear to have a strong impact on plant responses to high ambient temperature (Lee et al., 2014). In recent years, these epigenetic changes have been described to be transgenerationally inherited and determined by the maternal plant (Whittle et al., 2009). In addition, protein conformation has also been proposed as an extra mechanism of temperature sensing and the light photoreceptor PhyB has recently been highlighted as novel temperature sensor (Delker et al., 2017; Legris et al., 2016).

Besides changes in protein confirmation and activity, the circadian clock is considered the most relevant component involved in temperature buffering. In fact, rhythmicity and periodicity of clock genes are affected by temperature fluctuations, which ultimately will regulate growth. Specifically, genetic studies have predicted LATE ELONGATED HYPOCOTYL (LHY) as one of the major temperature-sensitive clock proteins (Gould et al., 2013). Under high temperatures, LHY protein levels increase, slowing the clock and allowing to maintain a 24-hour period at warmer temperatures. In that way, the circadian clock appears as the major temperature

integrator that shapes plant growth to different temperature conditions. Other factors such as FLOWERING LOCUS M (FLM) have been found to modulate the sensitivity to temperature by having different splicing variants less capable to repress flowering under warm temperatures (Balasubramanian and Weigel, 2006; Lutz et al., 2015; Sureshkumar et al., 2016). Altogether, these players will trigger the activation of temperature signal transduction which will ultimately induce temperature responsive growth.

1.4 The temperature signal transduction

Being one of the earliest thermomorphogenic responses, hypocotyl elongation is often used to identify novel components in the temperature signaling pathway. Independently of the temperature cue, elongation of the hypocotyl is considered anisotropic (directional) and it is produced by a combination of cell expansion and division that ultimately will increase cell size. Recently, microtubule alignment and hormonal balance have been implicated in hypocotyl elongation in response to different light conditions by controlling cell division and elongation (Sambade et al., 2012). Similarly to light, in the temperature-induced hypocotyl elongation response, auxin, brassinosteroids and gibberellins have been tightly involved, and biosynthesis or signaling mutants of each of these pathways exhibit an impairment of hypocotyl elongation at 28°C (Gray et al., 1998; Stavang et al., 2009). However, whether similar mechanisms were conserved between light and temperature was rather poorly understood at the beginning of my work.

In 2009, the basic helix-loop-helix (bHLH) transcription factor PHYTOCHROME INTERACTOR FACTOR 4 (PIF4) was proposed as one of the major regulators of high temperature-mediated hypocotyl and petiole elongation, as well as hyponastic responses by the regulation of the hormonal balance (Koini et al., 2009; Figure 3). PIFs belong to a subfamily of 15 members (Toledo-Ortiz et al., 2003) and are considered master regulators of growth. In contrast to shade avoidance, where redundancy between multiple PIFs is observed, PIF4 dominates in the regulation of high temperature acclimation (Koini et al., 2009; Li et al., 2012; Stavang et al., 2009). As a consequence, *pif4* mutants exhibit an impairment in hypocotyl elongation at high temperature, demonstrating its importance in controlling the response to warmth. Furthermore, *PIF4* expression and protein stability increases in response to warmth. However, as *pif4* displays residual elongation in response to temperature, other players are likely involved. While PIF4-controlled downstream factors are not fully identified, it has been generally proposed that auxin-mediated signal transduction is crucially implicated (Franklin et al., 2011; de Wit et al., 2014). Actually, PIF4 is involved in temperature response in an auxin dependent manner (Gray et al., 1998) by activating auxin biosynthesis (Sun et al., 2012). Based on that, mutants deficient in PIF4 show lower auxin levels at high temperature and display significantly reduced architectural responses in these conditions (Franklin et al., 2011; Sun et al., 2012). Whether auxin-induced

growth is sufficient or other components are needed remains unknown. As a core component of the temperature signaling pathway, PIF4 is also tightly regulated at the protein level. For instance, the DELLAs (negative regulators of gibberellin signaling) interfere with PIF4 binding activity during the day, restricting growth to the night (Figure 3). Interestingly, these proteins do not only regulate PIF4 under different light conditions, but also at high temperature. Indeed, dark and warm environments trigger DELLA destabilization, allowing PIF4 transcriptional activity (Stavang et al., 2009) and organ elongation.

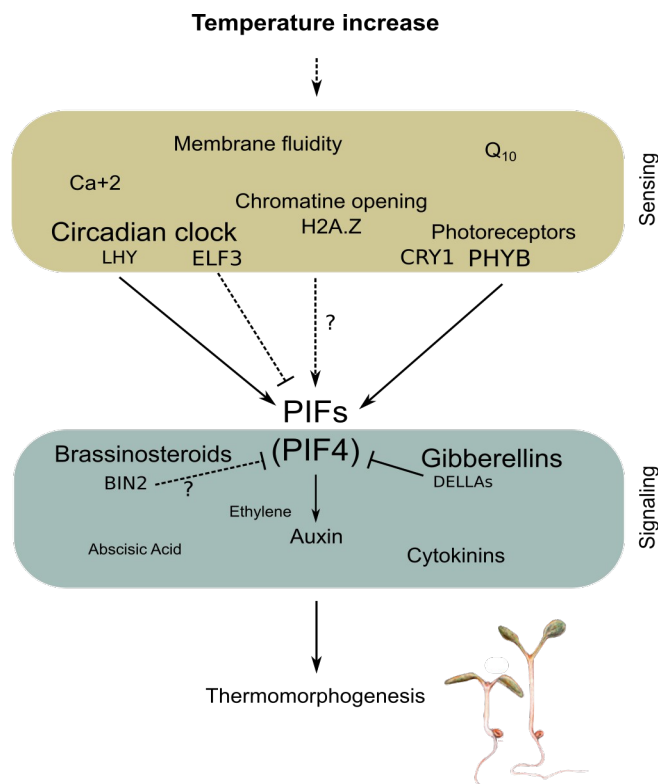


Figure 3. Sensing and signal transduction in response to high ambient temperature. Plant sensing mechanisms perceive increases in ambient temperature. These changes will be integrated into PIF4; considered the major regulator of plant thermomorphogenesis. PIF4, together with a tightly regulated hormonal balance, will activate temperature-induced transcriptomic responses that ultimately will trigger morphological changes in the plant. Solid lines represent known connections in the temperature signaling pathway, Dashed lines stand for regulatory mechanisms predicted from the light signaling pathway but not described for temperature response.

Not surprisingly, most of the known PIF4 regulators in response to temperature are also known to belong to the light signaling pathway. For instance, the light photoreceptors PHYB (PHYTOCHROME B) and CRY1 (CRYPTOCHROME1) are among the light signaling components involved in the regulation of PIF4 protein function also under high ambient temperature (Huq and Quail, 2002; Ma et al., 2016). Specifically, PhyB was described to interfere with PIF4 transcriptional activity by occupying temperature-induced gene promoters (Jung et al., 2016; Legris et al., 2016). Another light component, HFR1, was described to form heterodimers with PIF4 blocking its transcriptional activity (Foreman et al., 2011). Based on that, a strong crosstalk between light and temperature can be expected.

Beside these light components, PIF4 is also tightly regulated by the circadian clock (Nusinow et al., 2011) and exhibits different expression profiles depending on the photoperiod. For instance, in short photoperiods PIF4 mRNA and protein accumulates during the night, when maximum growth occurs, while under long photoperiods maximal growth rate occurs at noon coinciding with PIF4 peak (Nomoto et al., 2012). In shade avoidance responses, the evening-complex component *EARLY FLOWERING3 (ELF3)* emerged as one of the major regulators in repressing *PIF4* expression and controlling PIF4 activity by interfering with its binding to target promoters (Nusinow et al., 2011). Nevertheless, no association with temperature response had been described when my thesis was initiated. In addition to ELF3, one of the negative regulators of the brassinosteroid (BR) signaling pathway, BIN2 was characterized to time PIF4 activity by controlling its phosphorylation status under low BR conditions (Bernardo-García et al., 2014). However, whether this regulatory mechanism is conserved under high ambient temperature remains unknown. Another central component of the brassinosteroid pathway, BRASSINAZOLE-RESISTANT1 (BZR1) acts together with PIF4 in a cooperative manner to activate growth-associated genes (Oh et al., 2012, 2014).

1.5 The relevance of brassinosteroids in growth-associated responses

Together with auxin and gibberellins, BRs are among the most relevant hormones controlling growth. Independently of temperature, BRs have been involved in the control of cell elongation (Azpiroz et al., 1998) and cell division in roots (Lee et al., 2015; Vilarrasa-Blasi et al., 2014). The severe dwarf phenotypes of BR biosynthesis mutants (Choe et al., 1999a) stand out its role during growth and development. However, while the importance of this hormone in temperature-induced growth was highlighted almost 20 years ago with the characterization of the brassinosteroid biosynthesis mutant *de-etiolated 2 (det2)*; Gray et al., 1998); the role that BRs may have in temperature responses is not understood (Stavang et al., 2009).

The BR biosynthesis pathway is based on triterpenoid pathways. At the end of the route, the most abundant and widely occurring BRs are C28 steroids, and among them brassinolide (BL-24-epibrassinolide and 28-homobrassinolide) is the most biologically active.

1.5.1 The brassinosteroid signaling network

The BR signaling network is composed of a kinase signaling cascade in which phosphorylation and dephosphorylation reactions tightly control the activity of the different components of the pathway. The LRR receptor kinase BRASSINOSTEROID INSENSITIVE 1 (BRI1) perceives the active forms of BRs in extracellular domains and activates the intracellular signaling cascade. Under low brassinolide conditions, the BRI1 kinase domain is maintained in the plasma membrane in an inactive state by association with BRI1-KINASE INHIBITOR (BKI1, Wang & Chory, 2006). At the same time, BKI1 is preventing the interaction of BRI1 with BAK1, a LRR kinase with a positive role in BR signaling (Figure 4).

In high BL conditions, active forms of BR will bind to the hydrophobic pocket (also called *island domain*) of the plasma membrane-localized receptor kinase BRI1 (Figure 4). This will trigger the dissociation of BKI1, that will re-localize to the cytosol (Wang & Chory, 2006). BL, then acts as a “molecular bridge” promoting the association between BRI1 and its co-receptor BAK1, resulting in the assembly of a ternary complex BRI1-BL-BAK1 (Wang & Chory, 2006). Auto- and transphosphorylation between BRI1 and BAK1 in a ping-pong mechanism will lead to the transduction of BR signals to downstream targets (Belkhadir and Jaillais, 2015). Activated BRI1 phosphorylates the BRI1-SUPPRESSOR KINASE 1 (BSK1) and CONSTITUTIONAL DIRECTIONAL GROWTH (CDG1) receptor-like cytoplasmic kinases, which activate the BRI1-SUPPRESSOR 1 (BSU1) phosphatase. BSU1 will be responsible for dephosphorylating and thereby inactivating the GSK3-like kinase BRASSINOSTEROID INSENSITIVE 2 (BIN2) (Kim et al., 2009; Figure 4).

While in low BRs conditions, BIN2 autophosphorylates itself and phosphorylates BRASSINAZOLE RESISTANT 1 and its homologue BRASSINAZOLE RESISTANT 2 (BZR1/BZR2), leading to their retention in the cytoplasm and degradation (Gampala et al., 2007; He et al., 2002); in high BRs conditions active forms of BR trigger BIN2 inactivation (Figure 4). In parallel, PROTEIN PHOSPHATASE 2A (PP2A) will dephosphorylate BZR1/BZR2, allowing the accumulation of these transcription factors in the nucleus. After BR perception, BZR1/BZR2 multimerize as either homodimers or heterodimers on the promoter of target genes, to either activate or repress gene expression. BZR1/BZR2 have an atypical basic helix–loop–helix (bHLH) DNA-binding domain that can bind to E-boxes (CANNTG) and/or to BR response elements (BRREs, CGTGT/CG; He, 2005; Yin et al., 2005).

Genome-wide chromatin immunoprecipitation (ChIP) analysis indicate that BRRE sites mediate BR repression of gene expression, while E-boxes are predominantly associated with BR-induced genes (Sun et al., 2010). BZR1 can act as a negative regulator of BR biosynthesis in a feedback mechanism by repressing the expression of genes coding for BR biosynthetic enzymes (He, 2005; Figure 4). However, in contrast to PIF4, it is not known whether BZR1 exerts its normal growth-regulating function also in response to high ambient temperature.

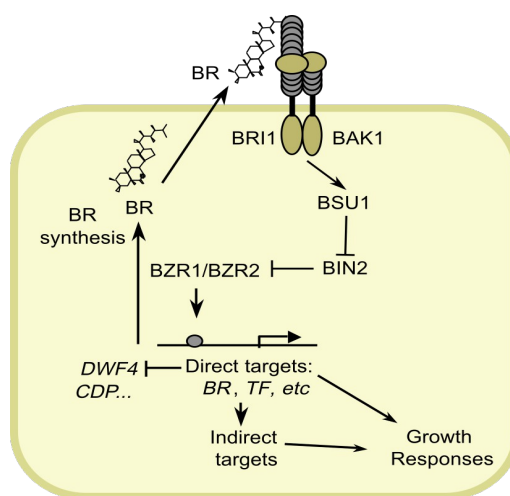


Figure 4. Brassinosteroid signaling pathway. BR signaling is initiated by the activation of the receptor kinases BRI1 and BAK1 on the cell surface. BRI1 activation will trigger a kinase cascade that ultimately leads to dephosphorylation by PP2A and accumulation of BZR1/BZR2 in the nucleus. Activated BZR1/BZR2 will induce expression of growth-associated responses and repress brassinosteroid biosynthesis gene expression as part of a feed-back mechanism. Figure adapted from Wang et al. (2006). Light green represents intracellular space.

2. Objectives

At the beginning of my thesis work, PIF4 was considered the main regulator of thermomorphogenesis by fine-tuning the hormonal balance and temperature-induced gene expression, although the molecular mechanisms that integrate hormone signaling into the pathway was poorly understood. In addition, temperature sensing and regulatory mechanisms upstream of PIF4 were not known (Figure 3). At phenotypic level, previous published studies had highlighted hypocotyl elongation as a classical response to warm environments, while temperature effects on a comprehensive life cycle scale were not described. Surprisingly, natural variation for thermomorphogenic responses was still an untapped resource.

Thus, the objectives of my work were:

1. To perform a comprehensive profiling of morphological responses to a range of ambient temperatures over the complete life cycle of 10 *Arabidopsis thaliana* accessions.
2. To identify novel components of the temperature signal transduction pathway via forward-genetic approaches.

To better understand the molecular mechanism underlying plant thermomorphogenesis and to identify novel components of the signaling pathway, I got involved in two previously initiated projects: an EMS mutagenesis screen and a QTL analysis. The aims of my work were to identify the causal mutations underlying the variation of hypocotyl elongation observed in response to warmth and further study the relevance of those players in the canonical PIF4 signaling pathway. Additionally, I performed an extensive temperature profiling in 10 *Arabidopsis thaliana* accessions grown at four constant ambient temperatures. From the data collected, I expected to identify and cluster phenotypes differently affected by ambient temperature increases. Additionally, I wanted to assess the susceptibility of each individual trait to be affected by temperature and natural variation and to study the conservation of these responses between accessions. These data would potentially reveal key phenotypes in the adaptation process across natural variation and highlight other sensitive traits to analyze in the mutants isolated in the EMS-screen and the QTL analysis.

3. Materials and Methods

3.1 *Escherichia coli*

3.1.1 *E.coli* strains

- *DH5α*: *fhuA2 lac(del)U169 phoA glnV44 Φ80' lacZ(del)M15 gyrA96 recA1 relA1 endA1 thi-1 hsdR17*
- *DH10β*: *F- mcrA Δ(mrr-hsdRMS-mcrBC) φ80lacZΔM15 ΔlacX74 nupG recA1 araD139 Δ(ara-leu)7697 galE15 galK16 rpsL(Str^R) endA1 λ⁻*
- *DB3.1:F-* *gyrA462 endA1 glnV44 Δ(sr1-recA) mcrB mrr hsdS20(rB-, mB-) ara14 galK2 lacY1 proA2 rpsL20(Smr) xyl5 Δleu mtl1*

3.1.2 Luria-Bertani (LB) medium

According to Bertani, (1951): Ten grams of Bacto-tryptone, 5gr yeast extract, 10gr NaCl to 800 ml of H₂O was added to 1L dH₂O. Media was sterilized by autoclaving. For LB plates, 15 gr/L agar was added to the LB medium. In case of the use of antibiotics, these were added after medium was cooled down. Kanamycin, spectinomycin in a stock concentration of 50 mM were used (working concentration was 50 μM). Together with kanamycin, gentamycin (25 μM) and rifamycin (15 μM) were used for agrobacterium selection. LacZ diluted in DMF was used for the white-blue selection during Golden Gate cloning.

3.1.3 Growth conditions

E.coli was grown on plates (LB + agar) or in liquid LB media at 37°C for 16 hours. In case of growth in liquid media, tubes were placed in a shaker at 500 rpm.

3.1.4 Heat shock transformation and selection of positive clones

E.coli transformation was done using chemically competent cells (*TOP10/DH5α*) by heat shock:

1. Competent cells were taken out of -80°C and thawed on ice (2-3 min)
2. 1-5 μl DNA (usually 10 pg-100 ng) were mixed with 50 μl of competent cells
3. Competent cells were incubated for 20 min on ice
4. Transformation tubes were heat shocked as follows:
 - 42°C for 1 min
 - 2 min on ice
 - 1h at 37°C
5. Transformation was plated on a 10 cm LB agar plate containing the appropriate antibiotic
6. Positive colonies were confirmed by colony-PCR and restriction digestion

3.2 *Agrobacterium tumefaciens*

3.2.1 *A.tumefaciens* strain

GV3101

Chromosomal information: C58

3.2.2 Growth media

Agrobacterium was grown in LB media (detailed in 3.1.2)

3.2.3 Growth conditions

The growth conditions for *Agrobacterium* were LB + agar or liquid LB medium at 28°C for 16-24 hours. In case of growth in liquid media, tubes were placed in a shaker at 500 rpm

3.2.4 Heat shock transformation and selection

Transformation was done using chemically competent cells by heat shock:

1. Competent cells were taken out of -80°C and thawed on ice (2-3 min)
2. 1-5 µl DNA (usually 10 pg-100 ng) were mixed into 100 µl of competent cells
3. Competent cells were incubated for 20 min on ice
4. Transformation tubes were heat shocked as follows:
 - 42°C for 1 min
 - 2 min on ice
 - 2h at 28°C
5. Transformation was plated on a 10 cm LB agar plate containing the appropriate antibiotic
6. Positive colonies were confirmed by colony-PCR the next day

3.3 *Arabidopsis thaliana*

Plant material used in chapters I, II and III is detailed in *Appendix I*

3.3.1 Seeds sterilization and stratification

Seeds were surface-sterilized by washing with 50X volume of 70% ethanol for 10 min. Subsequently, ethanol was removed and a volume of 50% bleach/50% water was added. Next, bleach solution was removed and seeds were washed with sterile water 3 times. Seeds in water were stratified at 4°C for 3 days in darkness.

3.3.2 Growth conditions

Arabidopsis thaliana solution (ATS) was prepared according to Lincoln et al. (1990).

Chapter I (Temperature profiling): Seeds were germinated and cultivated in climate-controlled growth cabinets (Percival, AR66-L2) at constant temperatures of 16, 20, 24 or 28 °C under long day photoperiods (16h light/8h dark) and a fluence rate of 95 $\mu\text{mol}\cdot\text{m}^{-2}\cdot\text{sec}^{-1}$ white light. Germination rates and rosette development were assessed daily and hypocotyl, root length, and petiole angles were measured in 7 days-old seedlings grown on plates.

Chapter II (Natural variants of ELF3): The growth assays for the original QTL analysis were done at 250 $\mu\text{mol m}^{-2} \text{s}^{-1}$ white light and a long day photoperiod (16h light /8h dark). Described in detail in Raschke et al. (2015).

Chapter III (The *okapi* screen): Wild type (Wt) and mutant lines in the Rrs-7 background were grown with 250 $\text{mmol m}^{-2}\text{s}^{-1}$ light intensity at both temperatures. Wt and mutant lines in Col-0, Ws-2 and Ler backgrounds were grown at 95 $\mu\text{mol}\cdot\text{m}^{-2}\cdot\text{sec}^{-1}$. In both cases, plants were grown in a constant long day photoperiod (16h light/8h dark). Temperature treatment (shift) was done 4 days after germination. Described in detail Delker et al. (2014).

3.3.3 Hormone/Inhibitor treatments

ATS plates were supplemented with the hormones/inhibitors at the concentrations specified for each assay. For short-time responses, hormone/inhibitor treatments were done in liquid ATS medium. Hormone or inhibitors were added to the medium after autoclaving and cooling in the following concentrations:

Compound	Supplier-Cat.no	Solvent	Working concentration
Picloram	Sigma-P5575	DMSO	5 μM
Epibrassinolide	Sigma-E1641	Ethanol 70%	100 nM
Propiconazole	Sigma-45899	Methanol	1 μM
Yucasin	Dr.Hayashi	DMSO	50 μM
L-kynurenin	Dr.Hayashi	DMSO	100 μM

3.3.4 Temperature-Induced Hypocotyl Elongation (TIHE) assay

Seeds were surface-sterilized and kept in deionized H₂O for 3 days at 4°C before sowing. Seedlings were germinated and grown under sterile conditions and the indicated temperatures on vertical ATS plates. Plates were placed at 20°C for 3 days to allow equal germination. After three-days, seedlings were transferred to 28°C while a second batch was kept at 20°C as control treatment. After 4 days, plates were photographed and hypocotyl length was measured by the Root Detection software (<http://www.labutils.de/rd.html>).

3.3.5 Chlorophyll quantification

Chlorophyll quantification was done according to Porra et al. (1989)

3.3.6 Flowering time estimation

Flowering time was recorded by two independent protocols:

- Number of days needed for the inflorescence (bolt) to be higher than > 1cm
- Total number of rosette leaves at first opened flower. Number of plants used to estimate this parameter was always n>15.

3.3.7 Rosette and petiole measurements

Seeds were surface-sterilized, and incubated in sterile water at 4°C for 3 days. After stratification, seeds were placed on soil and equally germinated at 20°C during 3 days. After 3 days at 20°C, one tray containing 20 replicates of each line was shifted to 28°C. Rosette pictures of the equally developed plants (n>15) were taken. Rosette area and petiole length were measured with ImageJ (<https://imagej.nih.gov/ij/>).

3.3.8 *Arabidopsis thaliana* transformation by floral dip

Arabidopsis transformation was done according to Logemann et al. (2006):

1. The plasmid *pGWB406:ROT3 (35S:GFP:ROT3)* DNA construct was transformed into *Agrobacterium*. Transformed *Agrobacterium* was grown on LB plates containing kanamycin [50 µg/ml] + Rifamycin [15 µg/ml] + Gentamycin [25 µg/ml] antibiotics in a 28°C incubator for 2-3 days. Positive colonies were selected by restriction digestion and colony-PCR
2. Positive colonies were plated on 2x LB plates with kanamycin [50 µg/ml] + Rifamycin [15 µg/ml] + Gentamycin [25 µg/ml] antibiotics and incubated at 28°C for 2–3 days.
3. Densely grown *Agrobacterium* was collected from the plate by scraping, and resuspended in 30 ml LB in a sterile falcon tube. The O.D 600 should be about 2.0.
4. Per transformation 120 ml of 5% sucrose solution containing 0.03% of Silwet L-77 were prepared.
5. Inflorescences of the plants were dipped into the *Agrobacterium* solution for 10 seconds, under gentle agitation.
6. Dipped plants were placed under a lid or cover for 16 to 24 hours to maintain high humidity.
7. Plants were grown until senescence and ripe seeds were collected.

3.3.9 Selection of transformed *Arabidopsis thaliana* seedlings

Selection of transgenic seeds was done according to Harrison et al. (2006)

3.4 Molecular biology methods

3.4.1 Semi-quantitative PCR

Oligonucleotides and vector maps used in chapter I, II and III are collected in *Appendix II and III*.

Dream Taq polymerase PCR reaction was set up with the following components:

1 μ l	10x PCR Buffer
0.75 μ l	dNTPs 10 mM
1 μ l	Oligonucleotides (F + R) 20 μ M
0.05 μ l	DreamTaq TM Green DNA-Polymerase 5U/ μ l
0.75 μ l	DNA
10 μ l	Milliq H ₂ O

PCR cycle was the followed:

Step	Temperature °C	Time	Cycles
Initial denaturation	95	2 min	1
Denaturation	95	30s	
Annealing	Tm-5	30s	35
Extension	72	1 min/Kb	
Final extension	72	5-10 min	1
Hold	4	-	-

For high accuracy in the cloning of *ROT3*, *BZR1* and *PIF4p Phusion High-Fidelity DNA* polymerase was used. Amounts per reaction are specified below.

Component	50 μ L reaction	Final Concentration
H2O	add to 50 μ L	
5x Phusion HF Buffer	10 μ L	1X
10 mM dNTPs	1 μ L	200 μ M each
Forward primer	x μ L	0.5 μ M
Reverse primer	x μ L	0.5 μ M
Template DNA	x μ L	
Phusion DNA polymerase	0.5 μ L	0.02 U/ μ L

PCR cyler was programmed with the following variations to the *Dream Taq* polymerase: Denaturation step was done at 98°C and extension time was calculated for 15-30 sec/Kb instead.

3.4.2 Genomic DNA extraction for mapping

3.4.2.1 Extraction buffer

Tris-HCl (pH 7.5)	200 mM
NaCl	250 mM
EDTA (pH 7.5)	25 mM
SDS	0.5%

3.4.2.2 Protocol

1. Approx. 100 mg frozen tissue was homogenized in a 2 ml tube.
2. To each tube, 400 μ l extraction buffer (see 2.1.5) was added and mixed for 5 sec. During this time, samples were kept at RT.
3. Tubes were centrifuged for 2-4 min at max. speed (13.000 rpm).
4. A total of 300 μ l of the supernatant was transferred into a new 1.5 ml tube.
5. To this, 300 μ l isopropanol was added and mixed. Samples were kept at RT for 2 minutes.
6. Next, samples were centrifuged for 5 minutes at max. speed (13.000 rpm)
7. Supernatant was removed by inverting tubes.
8. Pellet was cleaned by adding 500 μ l ethanol 70%.
Samples were centrifuged for extra 5 minutes at max. speed (13.000 rpm).
9. Ethanol was removed and pellet was dried until ethanol was gone.
10. Pelleted DNA was diluted in 50 μ l H₂O.

3.4.3 Mapping by CAPS markers

Fine mapping was performed by the use of CAPS markers (cleaved amplified polymorphic sequences). A CAPS assay uses amplified DNA fragments that are digested with a restriction endonuclease restricting a different digestion pattern between Wt plants and mutant of segregating populations.

CAPS marker design was done in: <http://helix.wustl.edu/dcaps/dcaps.html>

The CAPS assay was performed in 3 main steps:

1. Amplification of the region of interest in Wt and mutant/segregating line
2. Digestion with the specified enzyme
3. Electrophoresis gel

When the difference between fragments was > 100 bp, 1% standard agarose was used. When differences between fragments was <100, eletrophoresis gel was done using Pure agarose 3:1.

3.4.4 RNA Extraction, cDNA Synthesis, and qRT- PCR

Surface-sterilized and stratified seeds were placed on ATS medium and grown for 7 days under long day photoperiods (16h light/ 8 dark) and 95 μ mol m⁻²s⁻¹ white light at 20°C. Temperature-induced samples were shifted to 28°C when lights were switched off (ZT:16), while control plants remained at 20°C. Samples for qRT-PCR analyses were harvested 4 hours after shift (ZT: 20).

Expression analyses were performed essentially as described previously (Franklin et al., 2011). RNA was extracted from three independent pools of 7-day-old seedlings grown at 20°C or 28°C in long day conditions. In case of hormone pre-treated samples, the incubation of mock controls and treated samples were done in 6-well plates with ATS liquid media in shaking. RNA extraction

was performed with RNA purification kit (Macherey-Nagel) including the on-column DNase digestion step according to the manufacturer's protocols. Two microgram of total RNA was reverse-transcribed using the Revert Aid First Strand cDNA Synthesis Kit (Thermo Scientific). qRT-PCR analyses were performed using the ABsolute Blue QPCR SYBR Green low ROX Mix and gene-specific oligonucleotides listed in *Appendix III*. qRT-PCRs were performed of three biological replicates per time point using *At1g13320* as a reference gene (Czechowski et al., 2005). Relative expression levels for each analyzed gene were calculated as $2^{-(Ct_{\text{reference gene}} - Ct_{\text{gene of interest}})}$.

3.4.5 Protoplast assay by the Tape-Arabidopsis Sandwich method

Vector maps of the plasmids used in this work are shown in *Appendix II*.

Protoplast transient expression assays were done according to Wu et al. (2009) and Yoo et al. (2007). *BZR1* coding sequence was amplified from cDNA and cloned by the pENTR/D-TOPO Cloning kit into the pENTR vector. Next, *BZR1* was introduced into the expression vector pGWB406 (Gateway). *PIF4* promoter (2 Kb upstream from the start codon) was amplified from genomic DNA and cloned into a pNHL10 vector (*PIF4p:LUC*) using *PstI* and *NcoI* restriction enzymes.

Arabidopsis mesophyll protoplasts were isolated by the Tape-Arabidopsis Sandwich method (Wu et al., 2009). After protoplast isolation, 10 µg total DNA was transfected as described in Yoo et al. (2007). *PIF4* promoter fused to a firefly luciferase reporter gene was co-transfected with *35S:BZR1*. A CFP (*35S:CFP*) construct was co-transfected with *PIF4p:LUC* as a negative control. Transfected protoplasts were incubated overnight and luciferase expression was quantified next day. The firefly luciferase activities were normalized by β-glucuronidase (GUS) as an internal control of expression.

3.4.5.1 Solutions

Solutions used in the protoplast isolation are detailed in *Appendix VI*

3.4.5.2 Protoplast preparation

1. Paper tape was fixed on the desk, with the adhesive part facing up. Then, a cutted clean and dry leaf was attached to the upper side of the paper tape.
2. Using normal scotch tape, the lower side of the leaf was peeled off. The tape around the leaf was cut and the leaves were placed quickly into the enzyme solution to prevent protoplasts from drying out.
3. Leaves in solution were placed into a shaker at approx. 45 rpm for 3 hours until the protoplasts are released into the solution.
4. 20ml protoplasts were split into two 10 ml aliquots using 5 ml or 10ml pipet into 12 ml cell culture tubes. Protoplasts were centrifuged at 100 x g for 3 min.

- Supernatant was discarded by inversion and resuspended in 5 ml per tube using W5 solution and incubated on ice for 30 min.
- During the incubation period, protoplasts were counted using a hemocytometer.
- By now protoplasts pelleted by gravity and supernatant was removed with the 5 ml pipet and carefully resuspended in MMG solution to a final concentration of 2 to 5×10^5 cells/ml

3.4.5.3 Protoplast transformation

New 12ml tubes were used for transformation with $V < 1$ ml

- A total of 10 μ l DNA/100 μ l protoplasts (pp) was prepared in the tube. One V pp. was added. To this, 1.1V of a freshly-prepared solution of PEG was added and gently mixed very well by inversion for 3-4min.
- The mixture was incubated at room temperature for 10 min in total (vertically). After incubation, 4.4V of W5 solution was added and mixed. Protoplasts were pelleted by centrifugation at $200 \times g$ for 1 min.
- Supernatant was removed with a pipet and resuspended gently in the initial volume of W1 and incubated o/n in the dark. Tubes were placed horizontally.
After o/n incubation, an aliquot for western blot was taken.

3.4.5.4 Luciferase assay

- After overnight incubation, 0,2 μ l of 100 mM luciferin was added per 100 μ l pp (final concentration 200 μ M).
- Protoplasts were transferred into a 96-well microtiter plate suitable for luminescence measurements. A total of 90 μ l pp were pipetted per well. Protoplasts were incubated for 30 to 40 min in the dark at RT (20-22°C).
- Luciferase activity kinetics was measured with a 96-well plate luminescence reader (Thermo Fluoroscan).

3.4.5.5 GUS assay

Extraction buffer (10X):

500 mM NaPO_4 (pH 7.0), 10 mM EDTA, 1 % Triton, 100 mM β -mercaptoethanol, proteinase inhibitors
10 mM 4-MUG (4-Methylumbelliferyl- β -D-glucuronide), dissolved in 1X extraction buffer
0,2 M Na_2CO_3

- Two 96-well plates with 200 μ l 0,2 M Na_2CO_3 in each well were prepared.
- A 96-well PCR plate with 50 μ l 10 mM 4-MUG in each well was prepared. Plate was placed in a PCR machine and cooled to 4°C.

3. Preparation of extract: 10 μ l 10x concentrated extraction buffer was added directly to the protoplasts in the LUC-plate, plate was sealed with adherent foil and vortexed for 20 seconds.
4. Preparation of reaction mixture: 50 μ l extract was pipetted into a prepared PCR-plate (containing 4-MUG at 4 °C) and mixed by pipetting.
5. Time point 0 min: 20 μ l of reaction mixture was pipetted into the prepared "time point 0 min" microtiter plate containing Na₂CO₃.
6. Reaction was started by running PCR machine at 37 °C for 20 min, then cooled down to 4°C.
7. Time point 20 min: 20 μ l of reaction mixture was pipetted into the prepared "time point 20 min" microliter plate containing Na₂CO₃.
8. Plates were measured in the Cytofluor II: 5 sec shaking, 10 reads per well, excitation 360/ 40 nm, emission 460/40 nm.

3.4.5.6 LUC normalization

1. GUS values were calculated by subtraction: 20 min – 0 min = GUS value
2. For normalization, protoplast values were divided by the corresponding gus value
3. Average of "biological" replicates of each time point were calculated

3.4.6 Western blot

3.4.6.1 Protein extraction

Protein extraction was done using RIPA lysis and extraction buffer:

TRIS-Cl (pH 7.6)	50 mM
NaCl	150 mM
NaF	20 mM
Nonidet P-40	1 % (v/v)
Deoxycholate	0.5 % (v/v)
Na ₄ P ₂ O ₇	10 mM
EDTA	1 mM
EGTA	0.5 mM
add fresh:	1 mM PMSF/DTT + Protease inhibitor

A total of 50 mg of plant material was harvested in 2 ml tubes and frozen in liquid nitrogen. Homogenization of the material was done using metal beads. RIPA buffer was added to each sample (200 μ l buffer/50 mg plant material). Tubes were incubated in a shaker (200 rpm/ 4°C) for 15 min. After incubation samples were centrifuged at max. speed (14.000 rpm/ 4°C) for 20 min.

The supernatant was collected and added to the protein loading buffer (4X). Tubes were incubated at 96°C for 10 min. A total of 30 μ l sample was loaded on the SDS gel.

3.4.6.2 SDS-PAGE electrophoresis

Denatured samples were loaded with the protein loading gel on a 8% SDS-acrylamide gel. Voltage was settled to 80V until samples got into the resolving gel. Voltage was then increased to 100-120 V until samples ran through the complete gel.

Protein loading buffer (4X):

Tris-HCl pH 6.8	2.0 ml 1M
SDS	0.8 g
100% glycerol	4.0 ml
β-mercaptoethanol	0.4 ml 14.7 M
EDTA	1.0 ml 0.5 M
bromophenol Blue	8 mg

3.4.6.3 Electrotransfer (semi-dry transference)

The membrane used in the electrotransfer was PVDF previously activated by methanol

1. Electrotransfer was calculated in miliAmperes depending on the size of the membrane: $L \times W \times 1.5$.
2. After the transfer was completed, the membrane was blocked by immersing the membrane in 10 ml TBS 1X Tween 20 containing 2% non-fat milk during 30 min on a rocker.
3. The membrane was incubated with the primary antibody (1:1000, anti-GFP, Life Tech) for one hour at room temperature.
4. Next, the membrane was incubated with the HRP labeled secondary antibody (anti-rabbit) for one hour at room temperature in a rocker. A 1:5000 dilution was used.
5. The membrane was washed 3 x 10 minutes with 10 ml TBS 1X Tween 20.
6. Detection was done using the "SuperSignal West substrate" (Thermo).

3.4.7 Chromatin-immunoprecipitation-PCR (ChIP-PCR)

3.4.7.1 Buffers/Material

- MinElute Reaction Cleanup Kit, 28204
- DNA beads (Dynabeads Protein G- Invitrogen 100.03D)
- Low affinity eppendorf tubes (Sigma-T4816-250A)
- GFP antibody - MBL (code 598)
- ChIP Dilution Buffer (500 ml):

0.01% SDS,	0.5 ml 10%
1.1% Triton X- 100,	27.5 ml 20%
1.2 mM EDTA,	1.2 ml 0.5 M
16.7 mM Tris-HCl, pH 8.1,	8.35 ml 1 M
167 mM NaCl,	16.7 ml 5 M
- Low Salt Immune Complex Wash Buffer (500 ml):

0.1% SDS,	5 ml 10%
-----------	----------

4. The seedlings were submerged at the bottom of the 50 ml falcon, and then crosslinked in a vacuum for 15 minute (on ice). Vacuum was released slowly. Crosslinking was stopped by adding glycine to a final concentration of 0.125 M.
5. The seedlings were removed from the vacuum and the formaldehyde was rinsed off with 40 ml of pre-cooled milli-Q water. This step was repeated 1x. Following the two rinses, as much water as possible was removed from the seedlings.
6. The seedlings in liquid nitrogen were homogenized to a fine powder.
7. The powder was added to 30 ml of Extraction Buffer 1 (with the proteinase inhibitors added) in a 50 ml falcon tube (pre-cooled).
8. The solution was filtered through Miracloth (2 layers) into a fresh 50 ml ultracentrifuge tube.
9. The supernatant was removed by inversion and the pellet was resuspended in 10 ml of Extraction Buffer 2.
10. Resuspended was centrifuged at 12,000 g for 20 minutes at 4°C. After this centrifugation, a white pellet was visible.
11. The supernatant was removed and the pellet was resuspended with a brush in 300 µl of Extraction Buffer 3.
12. In a clean eppendorf tube, 300 µl of Extraction Buffer 3 was added. The 300 µl solution (resuspended pellet) from step 16 was carefully added on top of the clean 300 µl of Extraction Buffer 3.
13. Samples were centrifuged for 1 hour at 16.000g at 4°C.
14. The supernatant was removed and the chromatin pellet was resuspended in 200 µl of Nuclei Lysis Buffer.
15. The pellet was resuspended by pipetting up and down and vortexed.
16. Once resuspended, the chromatin solution was sonicated into 0.2-1.0 Kb. Fragments. 3 x (30" sonication-5min in ice) cycles were done.
17. The chromatin solution was centrifuged for 5 minutes at 4°C to pellet the debris. Supernatant was transferred to a new tube. To confirm shearing efficiency and determine DNA content, an electrophoresis gel was done.
18. Electrophoresis: From each sample, a 10 µl aliquot was incubated at 95°C for 10 min to denature protein-DNA complexes. In addition, DNA/proteins were quantified with a Nanodrop.
19. The remaining volume of sonicated chromatin was measured (step 20). The volume was brought up to 0.3 ml with Nuclei Lysis buffer. Samples were diluted 10 fold with ChIP Dilution Buffer to 3 ml.
20. From the 3 ml, aliquots were taken for the PCR and Western blot (input fraction)
100 µl → input PCR
30 µl → input western → -80°C

Rest of volume → step 21

21. To the 3 ml (step 20) 1µl of antibody (anti-GFP) was added. Samples were incubated overnight at 4°C in the rotator. Note: “Input” sample was incubated together with this to ensure all samples are exposed to the same conditions.
22. On the next day, 10 µl DNA beads/sample (4 samples → 40 µl) were placed in an 1.5 ml tube and equilibrated with ChIP elution buffer.
23. After washing the beads, 10 µl DNA beads were added to the 3 ml sample pre-incubated with the antibody. Incubation time: 2h/4°C in the rotor.
24. After incubation, the beads (with the chromatin) were separated from the liquid by placing the eppendorf tube in the magnet holder. The liquid and the beads were collected separately. A 50 µl aliquot was collected for the western blot (“UNBOUND” fraction).
25. Once the beads were collected from each sample, the washing steps started:
 - a) Low Salt Wash Buffer: 150mM NaCl, 0.1% SDS, 1% TritonX-100, 2mM EDTA, 20mM Tris-HCl (pH8.1). Two washes: One quick (rotating), second for 5 minutes (on ice).
 - b) High Salt Wash Buffer: 500mM NaCl, 0.1% SDS, 1% TritonX-100, 2mM EDTA, 20mM Tris-HCl (pH8.1). Two washes: One quick (rotating), second for 5 minutes (on ice).
 - c) LiCl Wash Buffer: 0.25M LiCl, 1% NP40, 1% sodium deoxycholate, 1mM EDTA, 10mM Tris-HCl (pH 8.1). Two washes: One quick (rotating), second for 5 minutes (on ice).
 - d) TE Buffer: 10mM Tris-HCl pH 8, 1mM EDTA. Two washes: One quick, second for 5 minutes.
26. Immune complexes were eluted by adding 250 µl (125 + 125) of Elution Buffer to the pelleted beads. Samples were mixed briefly and incubated at 65°C for 15 minutes with gentle agitation (500 rpm). Beads were collected by centrifugation. The supernatant fraction (eluted) was transferred carefully to another tube and the elution was repeated (+125 µl). The two eluates were combined.
27. The “input” volume (100 µl) was rise to the “elution” samples (250 µl) by adding elution buffer to the first one (150 µl).

Aliquots from “eluted” fractions and the “beads” were collected for the western blot. To each tube loading extraction protein buffer was added, and tubes were stored at -80°C until western was done.
28. To each tube (Eluted and Input) the amounts below were added:

Samples were incubated at 65°C in a shaker (500 rpm) overnight.

 - 10 µl NaCl 5M
 - 5 µl EDTA 0.5M1
 - 0.5 µl Tris 1M pH 6.5
 - 0.5 µl RNAase Qiagen

Incubation was done for 30 min at 65°C.
29. Next, 2.5 µl Proteinase K (from the LR kit) was added to a final concentration of 20 mg/ml

30. Genomic DNA was purified by Mini elute CleanUp kit (see Materials). Pellets were resuspended in 50 μ l of distilled water.
31. qRT-PCRs with the input and the eluted DNA were performed.
32. Data was normalized to Wt, input and PP2A.

3.4.8 Golden Gate cloning

Vector maps of the plasmids used in this work are shown in *Appendix II*.

Golden Gate cloning was performed according to Engler and Marillonnet. (2014). For the *BIG* cloning, *BsaI* and *BpiI* restriction endonucleases were used in consecutive levels together with *T4* DNA ligase.

A total of 20 femtomols DNA per construct was used. Restriction – ligation cycles were done as described:

Cycles	Time	Temperature
x45	2 min	37 °C
	5 min	16 °C
	5 min	50 °C
	10 min	80 °C
	hold	4°C

The total volume of reaction (20 μ l) was transformed into 100 μ l DH10 β *E.coli* competent cells. Transformation was plated on LB agar plates with the specific antibiotic and the substrate of β -galactosidase (X-gal):

Level -2 \rightarrow Constructed with *BpiI/T4*. spectinomycin resistant. *BsaI* compatible.

Confirmed by colony-PCR and sequenced. Vector pAGM9121

Level -1 \rightarrow Constructed with *BsaI/T4*. Kanamycin resistant. *BpiI* compatible. Vector pAGM1311

Level 0 \rightarrow Constructed with *BpiI/T4*. Spectinomycin resistant. *BsaI* compatible. Vector pICH41308

Level 1 \rightarrow Constructed with *BsaI/T4*. Kanamycin resistant. *BpiI* compatible. Vector pICH75044

Since the plasmids used in each of the levels were carrying the LacZ within the insertion site (see *Appendix II*) recombinant clones from every level were selected by the antibiotic resistance and its inability to produce functional β -galactosidase enzyme due to the alfa recombination. Based on that, white colonies were selected. Colony-PCR and restriction digestion were performed in order to confirm positive clones.

3.5 Statistics

Data visualization and statistical analyses of the data were performed using the software R (Team R Core, 2012). The *boxplot* and *heatmap2* functions were used for visualization of the data set and statistical measures. In the temperature profiling (Chapter I), for a single factor (either accession or temperature) analysis, the *anova* function contained in the R stats package

was used. In case of temperature, the factor had four levels. In case of accession, the factor had ten levels. Tukey's Honest Significant Difference' test was used as post hoc test using the function *TukeyHSD* contained in the stats package.

The variation in phenotype expression was analyzed by 2-way ANOVA according to (Nicotra et al., 2010a) and (Whitman and Agrawal, 2009) to test the effect on each phenotype for a significant effect of genotype (*G*, accession) or environment (*E*, temperature), and a significant genotype by environment interaction (*GxE*).

3.5.1 Q_{10} temperature coefficient

The Q_{10} temperature coefficient was calculated according to (Loveys et al., 2003).

$$Q_{10} = \left(\frac{P_w}{P_c} \right)^{\frac{10}{T_w - T_c}}$$

where P_w and P_c are the trait values at the warmer and colder temperatures,

respectively. T_w and T_c represent the corresponding temperatures in °C.

3.5.2 Index of phenotypic divergence (P_{st})

Calculation of the index of phenotypic divergence (P_{st} , Storz, 2002; Leinonen et al., 2006) was calculated as previously described by Storz (2002):

$$P_{st} = \frac{\sigma_b^2}{\sigma_b^2 + 2\sigma_w^2}$$

where σ_b^2 is the variance between populations, and σ_w^2 is the variance

within populations. The ANOVA framework was used to partition the variances to get unbiased estimates for σ_b^2 and σ_w^2 .

Using the two factorial design, two types of indices of phenotypic variation of a trait/phenotype were considered separately. The index of phenotypic divergence for genotypes (P_{st}^{gen}) at a defined temperature level can be computed to measure the effect/impact of the genotype on the variation whereas the index of phenotypic divergence for temperatures (P_{st}^{temp}) provides a measure for the effect of temperature on the observed variation for individual genotypes.

4. Results

4.1 CHAPTER I. Variation of thermomorphogenesis among *Arabidopsis* accessions

With the aim of generating a comprehensive and extensive understanding of physiological and developmental processes that are responsive to warmth, a phenotypic profiling of 10 different *Arabidopsis thaliana* accessions (Bay-0, C24, Col-0, Cvi-0, Ler-1, No-0, Rrs-7, Sha and Ws-2) was performed at 4 constant ambient temperatures (16°C, 20°C, 24°C and 28°C). More than 30 different phenotypes across the life cycle of the plant were recorded as a systematic characterization of plant growth, including: germination, juvenile vegetative, adult vegetative and reproductive stages as well as morphometric and yield-associated phenotypes (Figure 5). Juvenile vegetative stage is differentiated from the adult vegetative stage based on the ability of the plant to initiate flowering. Here, however, juvenile vegetative stage was defined arbitrary from germination to 6 rosette leaves. The adult vegetative stage ranged accordingly from leaf 7 to flowering.

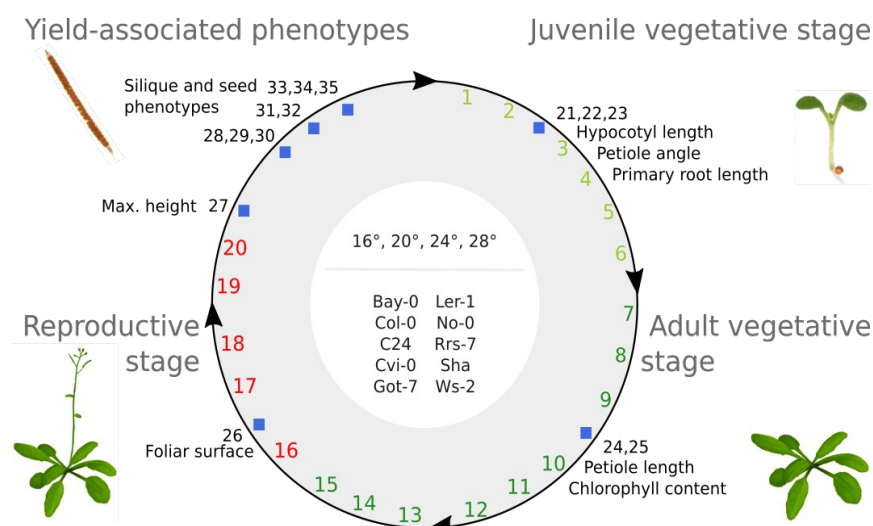
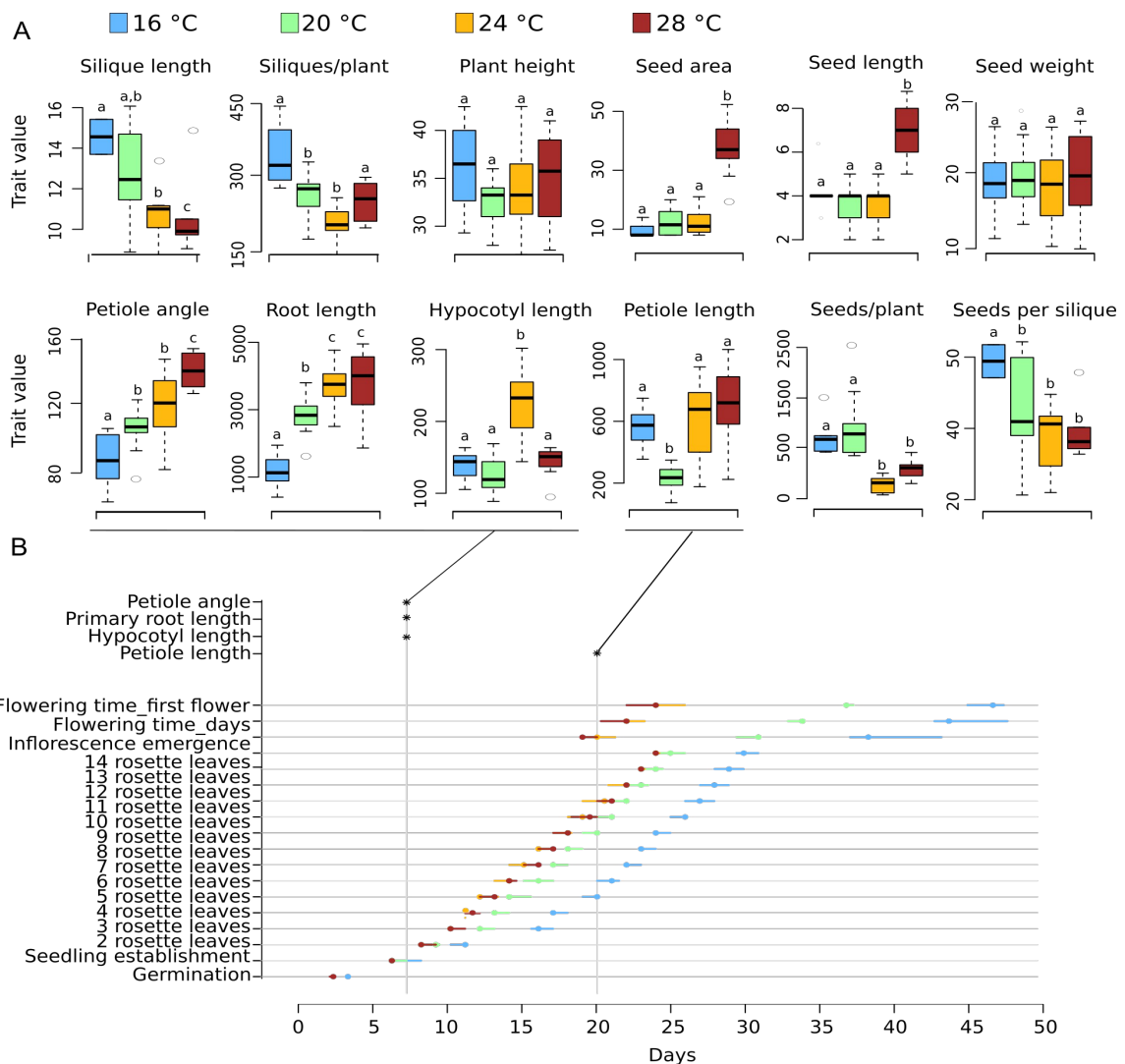


Figure 5. Phenotypes recorded across the *A.thaliana* life cycle. More than 30 different traits were recorded from the vegetative and the reproductive stage. Morphometric traits as well as yield-associated traits are marked with blue squares exemplifying the time when they were collected. Numbers represent individual phenotypes. Phenotype numbers are summarized in *Appendix IV*.

Seeds from every accession were germinated on soil and plants were kept in long day with constant temperature conditions until the senescence of the plant. Daily pictures were taken and individual phenotypes were measured. Juvenile traits such as hypocotyl, root length and petiole angle were measured from 7 days-old seedlings grown on vertical ATS plates. As a commonly used accession, temperature profiling of the reference strain Col-0 is shown here (Figure 6).

The data are presented in two blocks: box plots of quantitative growth traits (Figure 6A) and life cycle-associated traits as developmental plots (Figure 6B). As expected, increases in ambient temperature triggered a general acceleration of plant growth and a shortening of the life cycle (Figure 6B). While the effect of temperature increase appeared to be gradual from 16°C to 28°C in plant development, this effect was more prominent from 16° to 20°C than between 20° and higher temperatures (24° and 28°C, Figure 6A). This observation could be explained for a possible saturation of the response. In contrast, the differences between temperatures in reproductive stage traits (inflorescence emergence and flowering time) appeared to be more susceptible to these changes, especially between 20°C and 24°- 28°C (Figure 6B). Regarding morphometric traits, petiole and root length gradually increased with high ambient temperature.

Figure 6. Col-0 growth and development across an ambient temperature range. Data collected



from the temperature profiling was represented as box plots for morphometric and seed-associated traits (A) or as a line graphs for developmental timing at the four temperatures scored (B). Times of phenotypic assessment for selected traits in (A) are indicated by asterisks. Different letters denote significant differences as assessed by 1-way ANOVA and Tukey-test ($p < 0.05$, $n > 15$).

Similar to what I observed in the graph displaying developmental times (Figure 6B), the 24°C to 28°C effect was less visible than 16°C to 20°C or 24°C to 28°C (Figure 6A). In contrast, silique length, seeds per plant and seeds per silique were reduced by increased ambient temperature, while other yield-associated traits such as seed weight were not significantly affected (Figure 6A).

Once temperature responsive and non-responsive phenotypes were identified in Col-0, I next wanted to study how conserved this response was among the other 9 additional accessions used in this experiment (Bay, C24, Cvi-0, Got-7, No-0, Rrs-7, Sha and Ws-2). From the data obtained, I could observe that not all the traits recorded showed a linear response between temperatures. For example, total production of siliques per plant exhibited a significant decrease from 16° to 24°C that then increased again from 24° to 28°C as observed for Col-0 (Figure 6A). This difference in the response curves was taken into consideration for the next analysis. To compare temperature sensitivity of traits among different accessions, we calculated Q_{10} (temperature coefficient) values for each trait and phenotype class for each analyzed genotype

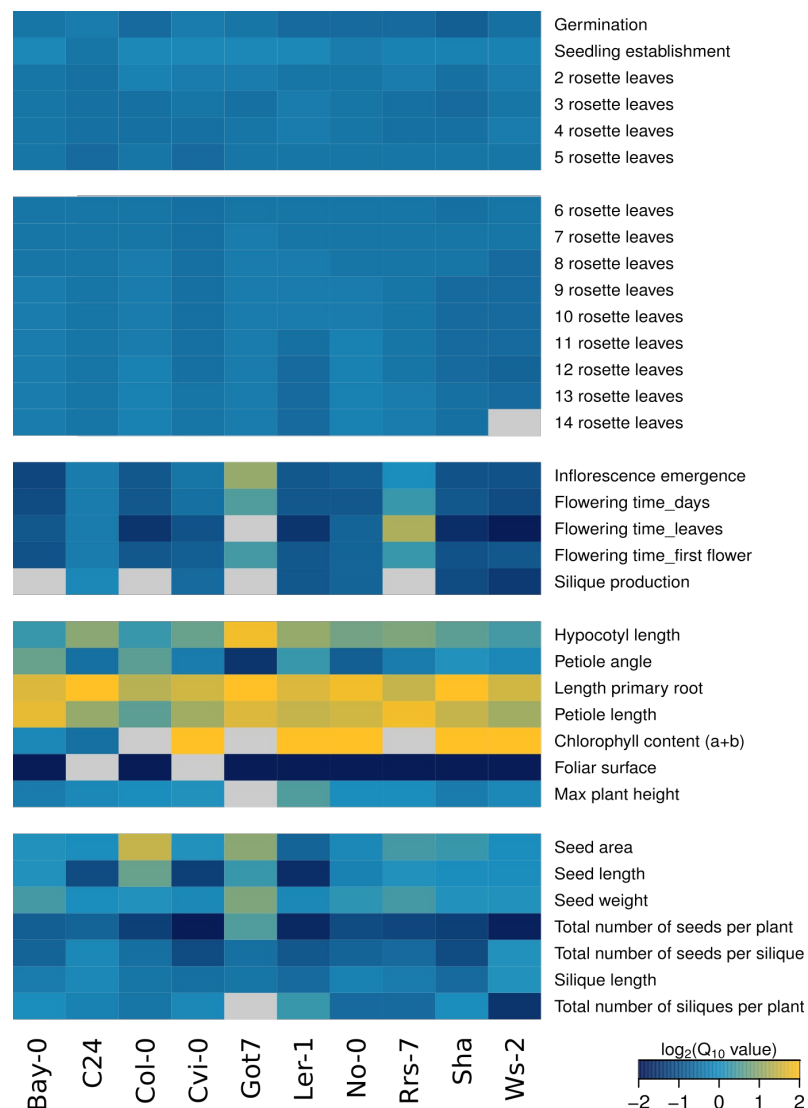


Figure 7. Temperature sensitivity on plant morphology. Representation of the Q_{10} for the effect of temperature on each trait and accession. Positive (increasing) and negative (decreasing) $\log_2 Q_{10}$ values are shown in yellow and blue, respectively with a $\log_2 Q_{10}$ cut-off value of 2 for better resolution. Missing data are denoted in light gray-

(Loveys et al., 2003). The Q_{10} value represents the factor by which a trait value changes if the ambient temperature increases by 10°C (Hegarty 1973). We calculated geometric means of all possible pairwise combinations of temperatures to minimize effects potentially caused by the different response curves mentioned above; and used the $\log_2 Q_{10}$ for visualization as to retain high resolution in the presentation of the data (Ibanez et al., 2015).

As shown in Figure 7, the time of vegetative development (scored as the time of rosette leave initiation) and biomass production (quantified as foliar surface) were accelerated by increasing ambient temperature, exposing negative $\log_2 Q_{10}$ values. Furthermore, I could observe that this response was highly conserved among the 10 accessions (Figure 7).

In contrast, quantitative traits such as hypocotyl elongation, petiole angle, primary root and petiole length (with $\log_2 Q_{10}$ values close to 2) increased with temperature as mentioned before for Col-0 (Figure 6, Figure 7). Specifically, accessions like C24, Got-7 and Rrs-7 appeared to be more susceptible to warmth by exhibiting longer hypocotyl at 28°C than others. While vegetative development was highly conserved, I observed high variability for other traits such as flowering time and yield, meaning that they are less conserved among accessions.

Although Q_{10} is a good measure to estimate the general effect temperature has on specific traits, it is not possible to analyze the degree to which temperature and genotype contribute to the change observed in those phenotypes. To further analyze/quantify the effect that accession (genotype) and temperature have on the phenotypes recorded, we made use of a previously described variance partitioning approach (Storz, 2002; Leinonen et al., 2006; Gay et al., 2008; Whitlock, 2008). Specifically, we calculated the index of phenotypic divergence (P_{st} , Storz, 2002) at each analyzed temperature as a measure of genotype effects (P_{st}^{gen}) on the trait of interest. To complement this analysis, we also estimated the variation occurring across temperatures (P_{st}^{temp}) for each of the analyzed accessions (Ibanez et al., 2015). In Figure 8 we can observe that the juvenile and adult developmental traits exhibited low variability between genotypes (low P_{st}^{gen}) indicative of a high conservation of those traits between accessions. In contrast, the high variability within accessions (with high P_{st}^{temp}), indicated a strong impact of temperature on germination and rosette development (Figure 8). Individual P_{st} values in the reproductive stage and morphometric traits showed a strong impact and variability for both parameters on these traits (Figure 8). In contrast, seed-associated phenotypes were affected to a lesser extent by both parameters.

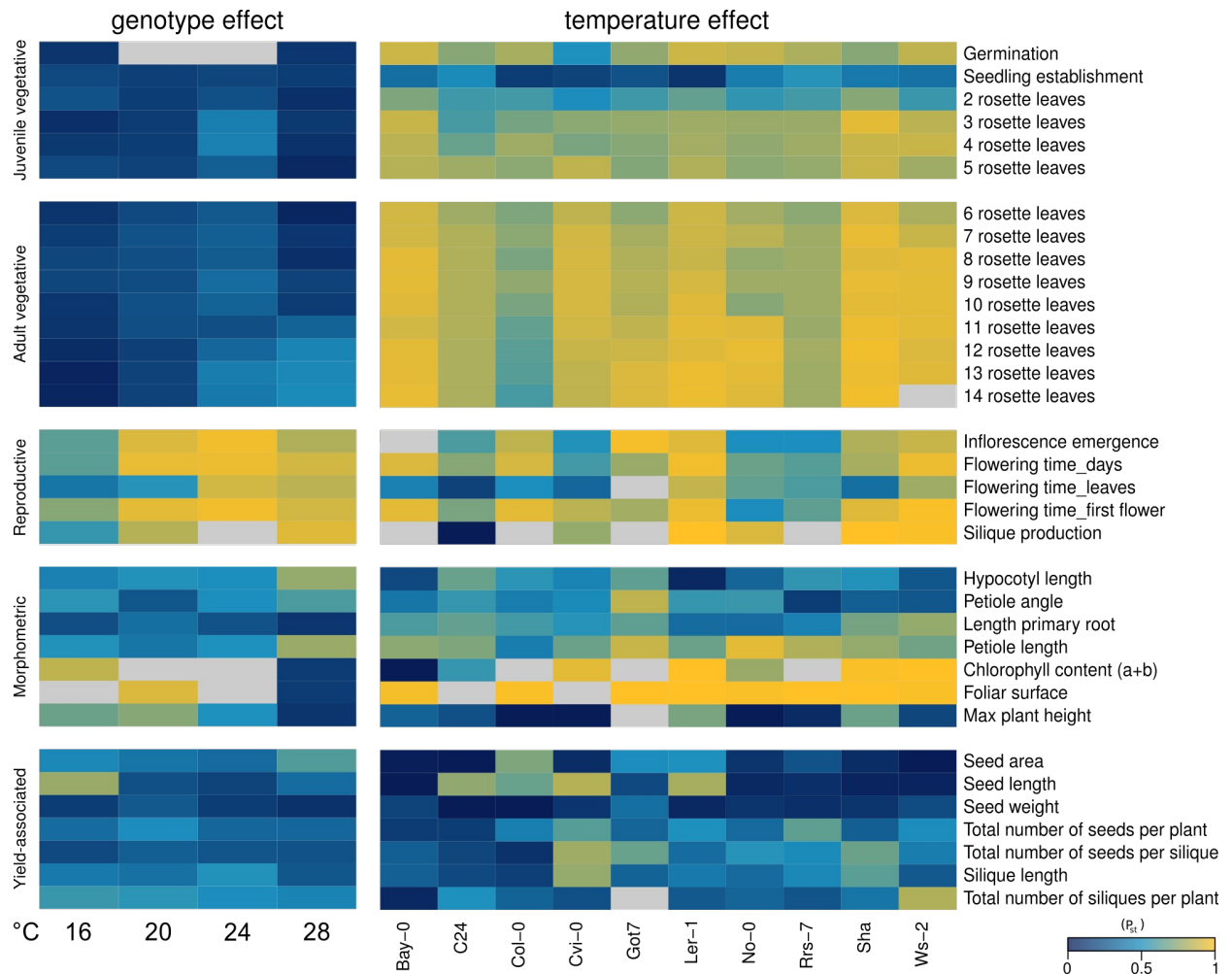


Figure 8. Temperature and genetic background effect on phenotypic variation. The heatmap represents the impact that both variables (temperature and natural variation) have in each trait recorded. Low (blue-ranged) and high impact (yellow-ranged) of each variable are color-coded. Gray boxes represent missing data.

As each phenotypic trait has been assigned a value (P_{st}) for genotype and temperature effects, they can be used to assess which of the two has a stronger influence on the phenotypic plasticity. To allow a direct comparison of effects, P_{st}^{gen} mean values were compared across all temperatures and P_{st}^{temp} across all accessions (Figure 9). With this method we were able to quantify the impact that temperature and genotype have independently on each trait recorded. As Figure 9 shows, the genotype effect was very low during vegetative development (with low P_{st}^{gen}), while the impact that temperature had on this developmental stage was much stronger (with higher P_{st}^{temp}). Furthermore, we could observe that the two variables studied here, temperature and genotype, both had a strong impact in the reproductive stage, with values close to 1. In contrast, yield-associated phenotypes such as seed size and seed production were equally affected by both parameters (Figure 9). Morphometric traits such as hypocotyl and petiole length, and flowering time were among those the phenotypes strongly affected by temperature and natural variation. In contrast, primary root length seemed to be less susceptible to natural variation, while a temperature impact was still observed (Figure 9).

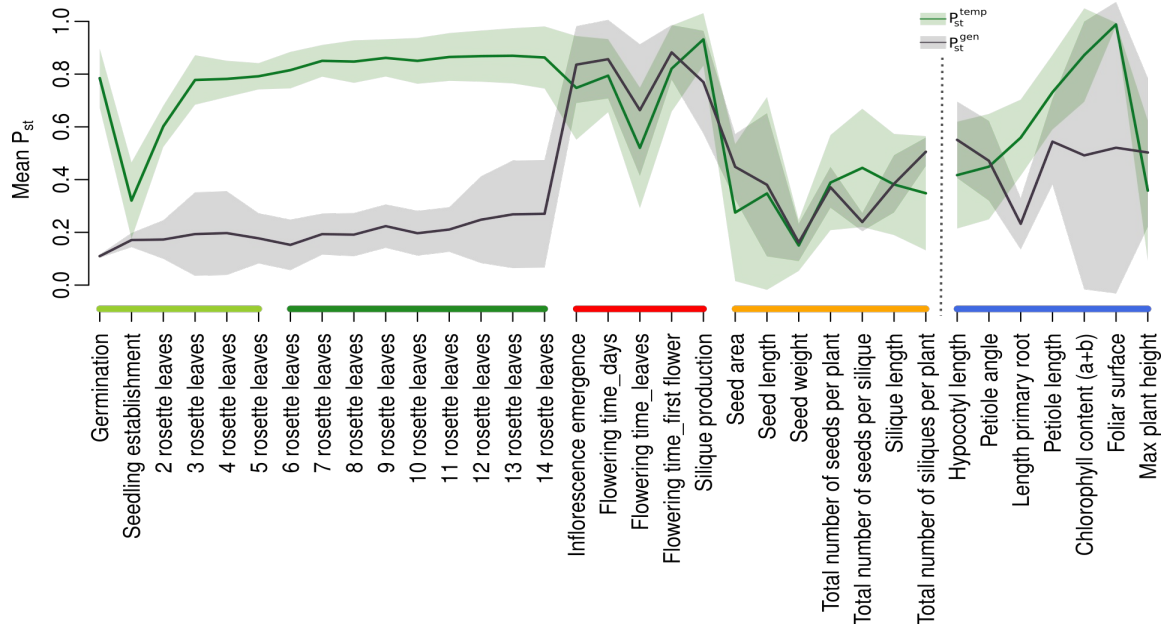


Figure 9. Genotype and temperature effects on phenotypic variation. Genotype (P_{st}^{gen} , black) and temperature (P_{st}^{temp} , green) contribution to variation. Solid lines show mean P_{st} values and shadings indicate standard deviations.

Due to the detrimental effect that high temperature has on yield production, I next wanted to examine the adaptability of the different accessions to warm environments by scoring seed production. Seeds were collected at the end of the plant life cycle and yield production was quantified for each accession and temperature assayed. As figure 10 shows, yield was highly variable among accessions, highlighting Got-7 as a tolerant accession to high ambient temperature. In contrast, other accessions that exhibited early flowering such as Sha and Ws-2 showed a significant decrease in yield production at 28°C compared to 16°C. Taken together, the data I collected from the temperature profiling of

10 *Arabidopsis thaliana* accessions highlighted the tolerance of Got-7 towards high ambient temperature and together with Rrs-7 and C24 were considered very sensitive accessions towards warmth. In addition, hypocotyl elongation appeared here as a highly sensitive morphological response. Therefore, this trait was used as a model response to identify novel players involved in the temperature signal transduction. This will be further explained in Chapter II and III.

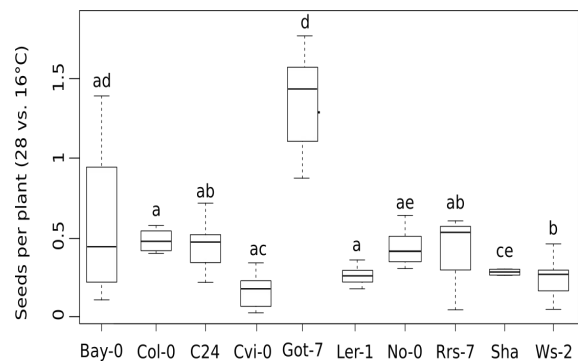


Figure 10. Seed production. Yield was quantified by seeds per plant production at 16°C and 28°C. Different letters denote significant differences as assessed by 1-way ANOVA and Tukey-test ($p < 0.05$, $n > 15$)

4.2 CHAPTER II. Natural variants of ELF3 in thermomorphogenesis signaling

4.2.1 Previous work - QTL analysis

Based on the natural variation present in the temperature-dependent hypocotyl elongation (Delker et al., 2010; Ibanez et al., 2015), a quantitative trait locus (QTL) analysis was performed between two geographically distinct natural accessions Bay-0 and Sha (PhD student A. Raschke). Both accessions differed significantly in the response to warm growth temperature (20°C vs. 28°C) (Figure 11A).

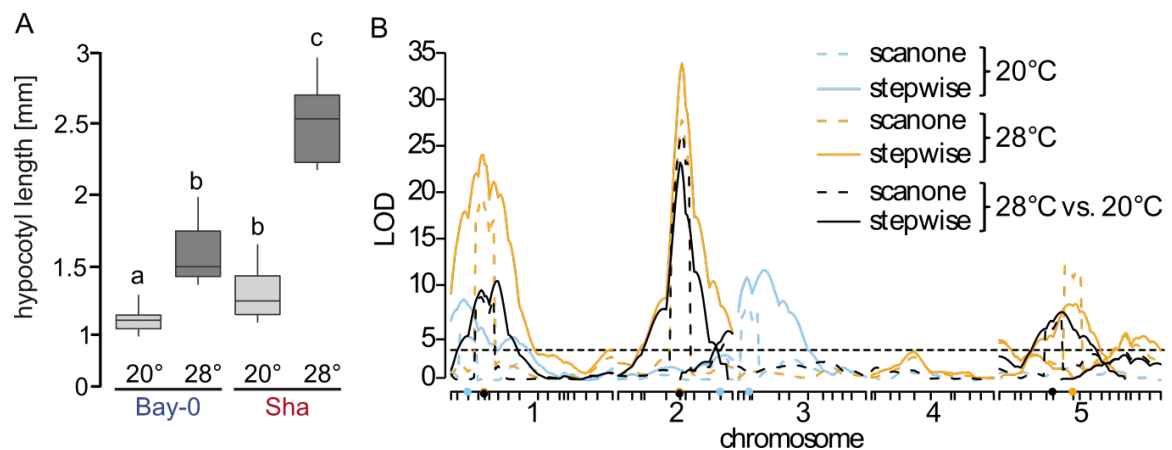


Figure 11. Quantitative trait locus analysis of hypocotyl elongation in response to temperature (A) Hypocotyl elongation (mm) of Bay and Sha at 20°C and 28°C; Different letters denote significant differences as assessed by 1-way ANOVA and Tukey-test ($p < 0.05$, $n > 15$). (B) LOD scores (y-axis) from composite interval mapping and multiple QTL mapping (stepwiseqtl) are plotted against all chromosomes (x-axis). Tick marks on the x-axis correspond to molecular markers in the genetic map. Colored dots on the x-axis show co-variates set for composite interval mapping.

Using a large population of recombinant inbred lines (RILs) derived from a cross between Bay and Sha (Loudet et al., 2002), a QTL analysis was performed for the hypocotyl length of seedlings exposed to a temperature treatment of 10 d 20°C vs. 10 d 28°C. The response ratio between these conditions identified 3 QTLs (Figure 11B), which were named according to chromosome location and the long hypocotyl phenotype, *GIRAFFE1*, *GIRAFFE2* and *GIRAFFE5* (*GIR1*, *GIR2*, *GIR5*).

GIR1, *GIR2* and *GIR5* explained 10%, 23% and 12% of the phenotypic variation in hypocotyl elongation, respectively (Figure 11B). *GIR2* was selected for having a considerable impact on the natural variation between Bay-0 and Sha (major QTL), and the identification of the gene underlying this QTL was established as prime interest.

To confirm/validate the *GIR2* QTL, heterogeneous inbred families (HIFs; Tuinstra et al., 1997) were used. These lines were selected in the progeny of RILs and showed a single residual heterozygous region (in *GIR2*), while they were identical in the rest of the genome (Figure 12). Selfing of such HIFs generated two informative lines: 84-B carried the Bay parental allele at the *GIR2* region, whereas 84-S carried Sha (Figure 12A). Phenotyping of these lines confirmed that

the Sha allele in *GIR2* was responsible for the long hypocotyl of this accession (Figure 12B; Raschke et al., 2015). This clearly demonstrates that the phenotypic differences between two HIF lines, carrying either parental allele in the target region can be attributed to genetic variation in the *GIR2* interval (Figure 12B).

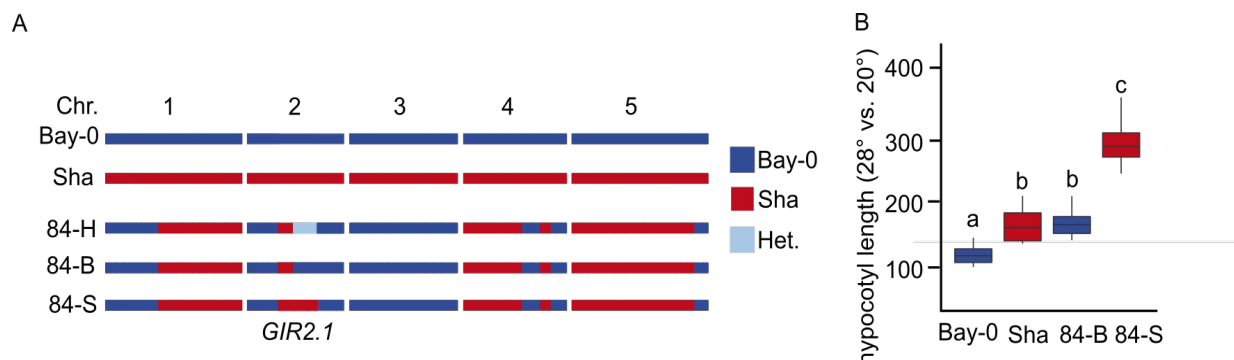


Figure 12. *GIR2.1* validation. (A) Scheme of the genetic background of the HIF lines (84) used for the *GIR2.1* validation shown in B. Bay and Sha allelic regions are represented with blue and red color, respectively. Heterozygous regions are represented with light blue. (B) Box plots show relative hypocotyl elongation (28° vs. 20°C) for the parental lines (Bay and Sha) and the HIFs segregating for Bay or Sha in the *GIR2.1* interval. Different letters denote significant differences as assessed by 1-way ANOVA and Tukey-test ($p < 0.05$, $n > 15$).

Following validation of the QTL, subsequent mapping primarily focused on trying to identify the gene/genes responsible for the variation in TIHE in that interval. Recombinants derived from the isogenic lines (HIFs) suggested that the *GIR2* locus was indeed composed of two genes masked by only one peak, a phenomenon known as “Ghost QTL” (Martínez and Curnow, 1992). The regions were genetically separated and, as a consequence, two new intervals (named *GIR2.1* and *GIR2.2*) were further mapped. In addition to this, the separation of *GIR2* into *GIR2.1* and *GIR2.2* could be additionally confirmed by using the multi QTL method (Uleberg et al., 2005). After the separation of *GIR2.1* and *GIR2.2* by A. Raschke, the aim of my work was the identification of the genes underlying both intervals followed by genetic complementation.

4.2.2 Verification of *GIR2.1* and *GIR2.2* confidence intervals

To verify the confidence interval of *GIR2.1* and *GIR2.2* as previously established by the F2s, I used the next generation of mapping population lines (F3s). Applying cleaved amplified polymorphic sequence (CAPS) markers, *GIR2.1* confidence borders (with a original size of 2 Mbp) were reduced to a total interval length of 0.3 Mbp. Regarding *GIR2.2*, the initial size of this interval was 3.2 Mbp. However, fine-mapping did not allow to reproduce the genetic information obtained previously. Hence, I could not confirm the *GIR2.2* confidence interval. I generated a new mapping population by phenotyping new F3s of HIF lines that were segregating in the F2 generation for the *GIR2.2* interval. However, the differences in TIHE were too weak to have a robust mapping population. As a consequence, the following work was focused on the identification of the gene underlying *GIR2.1*.

4.2.3 Fine-mapping and identification of the causal SNP for *GIR2.1*

The reduced *GIR2.1* interval to 0.3 Mbp, contained a total of 76 genes. Among these genes, I identified *EARLY FLOWERING 3 (ELF3)* as a potential candidate for *GIR2.1*. ELF3 is a component of the evening complex of circadian clock that had previously been isolated in shade avoidance screens (Coluccio et al., 2011; Jiménez-Gómez et al., 2010). In addition, ELF3 has been characterized to repress growth by controlling *PIF4* expression under diurnal conditions (Nusinow et al., 2011). As shade avoidance and temperature signaling pathways are strongly interconnected (Franklin et al., 2014), I considered *ELF3* as a likely candidate for our QTL analysis. *ELF3* coding sequence between Bay-0 and Sha differs in a natural non-synonymous SNP (single nucleotide polymorphism) causing an amino acid exchange at position 362 from alanine to valine. This SNP was related to alterations in the circadian clock (Anwer et al., 2014) caused in the Sha allele. In addition, both accessions differ in the length of a poly-glutamine (poly-Q) tract at the C-terminal of the sequence, although the biological relevance of the polyQ length remains poorly understood. *elf3* loss-of-function mutants exhibited a hyper-elongation of the hypocotyl at high temperatures in comparison to Wt (Figure 13), which may represent a similar response to the hypersensitivity observed in the Sha accession. Altogether, these data highlighted a potential role of ELF3 not only in response to light but also in thermomorphogenesis.

4.2.4 Confirmation of *ELF3* as candidate gene for *GIR2.1*

To confirm *ELF3* as the candidate gene for *GIR2.1*, transgenic complementation lines were used. Transgenic lines were generated in the *elf3-4* mutant (Ws-2) and were previously published by Anwer et al. (2014). Since the *ELF3* coding region differs between Bay and Sha in a non-synonymous SNP (A362V); the relevance of this amino acid change was tested. To do that, the coding regions of Bay or Sha were transformed into the same genetic background (*elf3-4*). Since differences in *ELF3* expression levels could also be expected between different promoters, a third construct was generated, introducing the Sha-SNP into the Bay construct. A summary of the lines used in the complementation assay are detailed below (Figure 13A):

-*ELF3* allele from Bay under native promoter (Bay); designated here as Pro_{Bay-0}:ELF3^{Bay-0}.

-*ELF3* allele from Sha under native promoter (Sha); designated here as Pro_{Sha}:ELF3^{Sha}.

-*ELF3* allele from Bay with a single nucleotide exchange at A362V position under native promoter (Bay); designated here as Pro_{Bay}:ELF3(A362V)_{Bay-0}.

Seedlings were grown in long day conditions with a constant ambient temperature of 20°C or 28°C. After eight days, seedlings were photographed and hypocotyl elongation was measured. As Figure 13 shows, hypocotyl elongation of seedlings carrying Pro_{Bay-0}:ELF3^{Bay-0} were significantly shorter at 28°C than seedlings carrying Pro_{Sha}:ELF3^{Sha} or Pro_{Bay}:ELF3(A362V)_{Bay-0}.

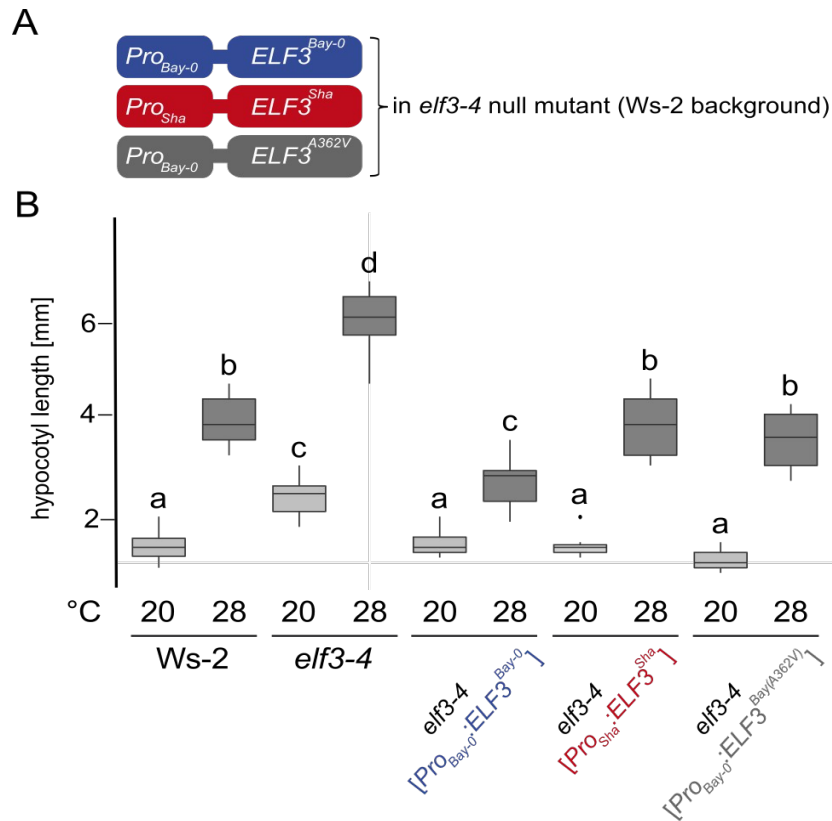


Figure 13. Transgenic complementation with *ELF3* natural variants. (A) Overview of transgenic constructs used for complementation of the *elf3-4* null mutation. (B) Box plots represent hypocotyl elongation (mm) of 8-days old seedlings at 20°C or 28°C. Different letters denote statistical differences as assessed by one-way ANOVA and Tukey HSD ($P < 0.05$).

Since $Pro_{Bay-0} : ELF3^{Bay-0}$ differs from $Pro_{Bay} : ELF3(A362V)_{Bay-0}$ exclusively at the amino acid position 362 (alanine to valine change), I could confirm that a single nucleotide polymorphism in *ELF3* is responsible for the difference observed between Bay-0 and Sha in hypocotyl elongation. Altogether, these data suggest that *ELF3* is the causal gene underlying *GIR2.1*.

ELF3 belongs to the evening complex of the circadian clock consisting of *ELF3*, *ELF4* and *LUX ARRHYTHMO* (*LUX*). This complex has been described to be gating hypocotyl elongation under diurnal regulation of *PIF4* (Nusinow et al., 2011). Based on the *elf3-4* long hypocotyl phenotype, *ELF3* appears as a negative regulator of hypocotyl elongation, possibly by repressing *PIF4* (Nieto et al., 2015; Nusinow et al., 2011). Therefore, I decided to further study whether the differences in hypocotyl elongation between the different complementation lines could be correlated with differences in *PIF4* expression. It was expected that, as a positive regulator of thermomorphogenesis, *PIF4* expression at 28°C in *elf3-4* would be higher than Wt control due to a possible inability of *ELF3* protein to repress *PIF4* gene expression (Figure 13B). Seedlings carrying the constructs explained above were grown under long day conditions and constant ambient temperature (20°C). Seven days-old plants were shifted from 20°C to 28°C at the end of the day and plant material was harvested 4 hours after the shift. As Figure 14 shows, *PIF4* expression in the transgenic complementation lines that carry the Sha allele ($Pro_{Sha} : ELF3^{Sha}$) or the Sha mutation in the *ELF3*-Bay allele ($Pro_{Bay} : ELF3(A362V)_{Bay-0}$) exhibited higher expression of

PIF4 at 28°C than $Pro_{Bay-0}:ELF3^{Bay-0}$. Restoration of *PIF4* expression to Wt levels in the *elf3-4* background indicates the functionality of the constructs used in this assay.

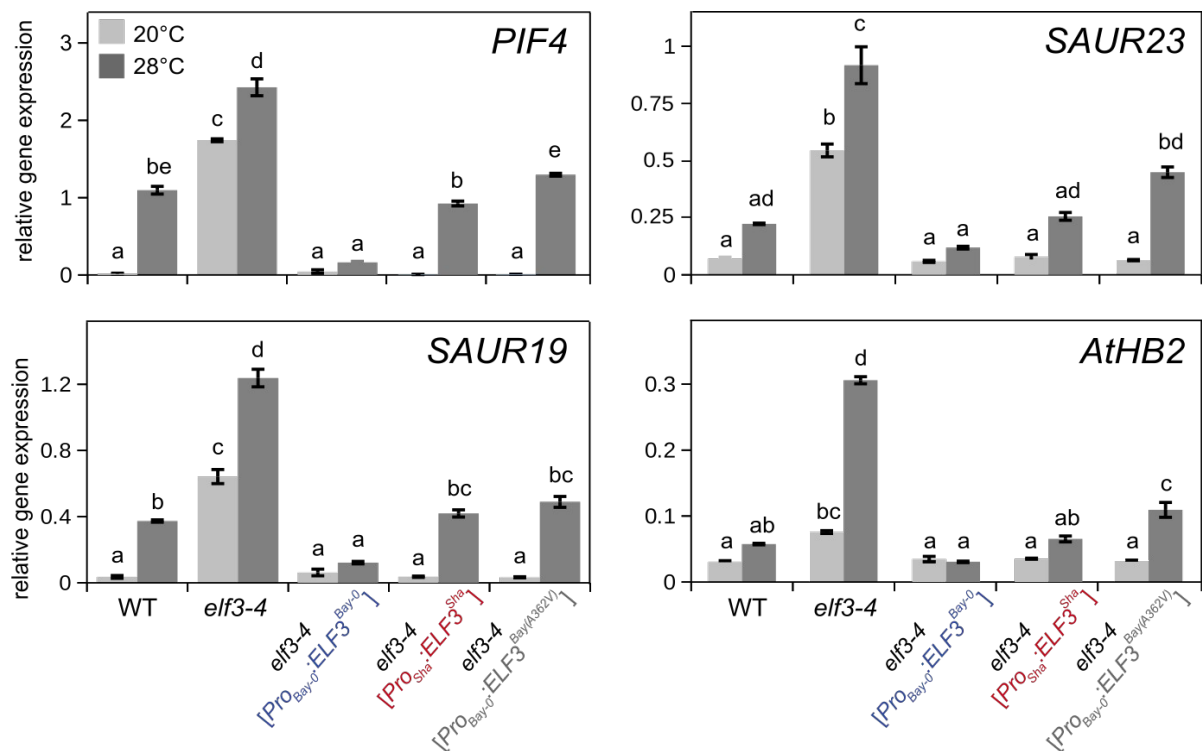


Figure 14. Transcription analysis of *ELF3* complementation lines. qRT-PCR analysis of *PIF4*, *SAUR23*, *SAUR19* and *ATHB2* in Wt, *elf3-4* and *ELF3* complementation lines. Seven days-old seedlings grown at 20°C (light gray) were shifted to 28°C (dark gray) at lights off. Samples were harvested 4 hours after shift. Different letters denote statistical differences as assessed by one-way ANOVA and Tukey HSD ($P < 0.05$).

As expected, *PIF4* was upregulated in *elf3-4* at both temperatures in comparison with Wt control plants, likely due to the lack of functional *ELF3* in this mutant and the inability to repress *PIF4* transcription.

In addition to this, known *PIF4* target genes from the *SMALL AUXIN UPREGULATED RNA* (*SAURs*) family (*SAUR19*, *SAUR23*) and the *ARABIDOPSIS THALIANA HOMEBOX PROTEIN2* (*ATHB2*), which are directly involved in growth were also observed to be significantly upregulated in Sha-derived lines, potentially triggered by a higher *PIF4* protein accumulation/functionality. The upregulation of these genes is once more reflecting the hypocotyl phenotype described in Figure 13.

In summary, I could identify *ELF3* as the candidate gene for *GIR2* QTL and confirm this by transgenic complementation. In addition, I could show that the QTN (QUANTITATIVE TRAIT NUCLEOTIDE) identified between Bay and Sha accessions (A362V) may trigger a malfunction in *ELF3* repression of *PIF4*. Altogether, my data demonstrates the essential role that *ELF3* has not only in light signaling but also in the regulation of thermomorphogenesis.

4.3 CHAPTER III. The *okapi (opi)*-EMS screen

In addition to quantitative genetics, classic mutagenesis approaches are a powerful option to identify signaling components. As shown in the first chapter, natural genetic variation in *Arabidopsis* is considerable for various phenotypic traits, and can be used as a source to identify new genes of interest. After identifying Rrs-7 as an extremely temperature-sensitive accession (Delker et al., 2010), ethyl methanesulfonate (EMS)-mutagenized Rrs-7 seedlings were screened for alterations in the extent of hypocotyl elongation in response to a moderate temperature increase from 20°C to 28°C.

4.3.1 Previous work

Before I joined the Quint Lab, screening of 45,000 M2 plants from 225 independent seed pools resulted in the isolation of 37 mutants that could be confirmed in the M3 generation. In contrast to the Wt, these mutants showed severe defects in their hypocotyl elongation in response to warmth (28°C). These mutants were named “*okapi*” (*opi*) (=short-necked giraffe species). Allelism tests among 20 mutants revealed the existence of at least seven independent complementation groups. These mutants were named *opi1*, *opi2*, *opi3*, *opi4*, *opi5*, *opi6* and *opi7*. All mutants showed a Wt etiolation response at 20°C, demonstrating that the TIHE phenotype was not due to a general elongation defect.

Mutants were back-crossed with Wt to allow segregating analysis and mapping by sequencing. A pool of DNA isolated from bulked segregants (BC1s) of *opi1*, *opi2*, *opi3*, *opi7* and Wt (Rrs-7) genomes were sequenced by Next generation sequencing (NGS). Mapping by sequencing established the target intervals based on SNP allele frequencies of ~1. A non-synonymous SNP (single nucleotide polymorphism) for *opi1* was identified in *DET1 (DE-ETIOLATED1)*. Complementation of the *opi1* mutant with a Wt *35S:DET1* construct restored the TIHE response and verified the causal mutation in *opi1* (Delker et al., 2014). DET1 is a subunit of an E3 ubiquitin ligase complex characterized to repress photomorphogenesis together with the COP1/SPA complex (Lau and Deng, 2012; Nixdorf and Hoecker, 2010). DET1 appeared here as a novel component of the temperature signaling pathway (Delker et al., 2014). COP1 (CONSTITUTIVE PHOTOMORPHOGENIC 1) and DET1 are considered positive regulators of PIF4 protein stability and activity by regulating one of its direct repressors, ELONGATED HYPOCOTYL 5 (HY5). Together with ELF3, HY5 is one of the major regulators of PIF4 (Delker et al., 2014). It has recently been further characterized to repress growth at low temperatures (17°C) by blocking PIF4 transcriptional activity (Gangappa and Kumar, 2017; Johansson et al., 2014).

4.3.2 *opi2*

4.3.2.1 Identification of the *opi2* causal mutation

Sequence information obtained for *opi2* established a candidate interval of 1.2 Mbp at the top of chromosome 3 (Figure 15A). I designed markers along the interval and tested then between Wt (Rrs-7) and *opi2*. Mapping using a population of 79 BC1s (F2) revealed co-segregants at the chromosomal position 440960, while 5 recombinant plants were found in the next marker position (666204). Based on that, *TRANSPORT INHIBITOR RESPONSE 3 (TIR3)* was considered as the potential candidate gene for the *opi2* mutation (Figure 15A). The finding that the *tir3* mutant phenocopied the *opi2* defect in hypocotyl elongation (Figure 15B) and that both mutants affected the same region within the gene (Figure 16) strengthened this hypothesis.

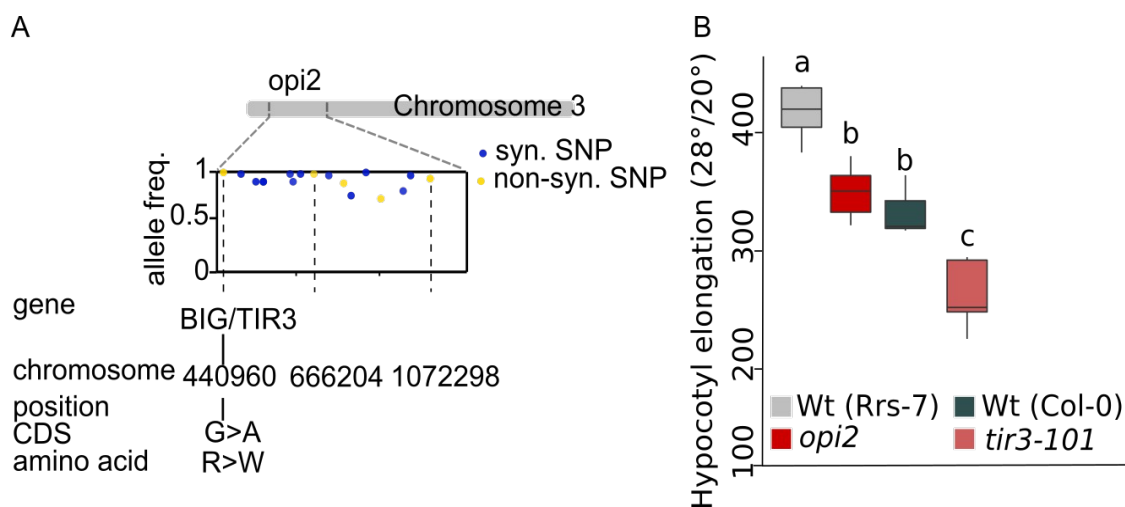


Figure 15. Mapping and characterization of the *opi2* mutant. Next generation sequencing (NGS) revealed a confidence interval at the top of chromosome 3. Mapping using CAPS markers revealed a non-synonymous SNP R>W at the position 440960 potentially responsible for the *opi2* phenotype. At this marker position *BIG/DOC1/TIR3* was located. (B) Temperature-induced hypocotyl elongation (TIHE) assay. The *tir3-101* mutant (in the Col-background) phenocopied the *opi2* defect in hypocotyl elongation. Different letters denote statistical differences as assessed by one-way ANOVA and Tukey HSD ($P < 0.05$).

DOC1/TIR3/BIG was initially isolated in a shade avoidance screen and described as a novel component in light signal transduction because of an overexpression of CAB genes in the dark (Li et al., 1994). Next, Ruegger et al. (1997) isolated *tir3* for exhibiting insensitivity to the auxin polar transport inhibitor 1-N-Naphthylphthalamic (NPA). In the last 20 years, this gene was isolated in at least another 8 screens and characterized for having alterations in vesicular trafficking, defects in cell expansion and division, and a mislocalization of the auxin efflux carrier PIN1 in presence of the vesicular trafficking inhibitor Brefeldin A (BFA; Gil, 2001; Guo et al., 2013; López-Bucio et al., 2005; Yamaguchi et al., 2007). BIG protein sequence is highly conserved among species and very complex. It is homologous to Ubr4 from mammals and the Calossin/Pushover (CaO) gene in *Drosophila*, where it is involved in the regulation of the circadian clock and synaptic transmission, respectively (Gil, 2001; Tasaki et al., 2013). Because

of its N-recogin domain (UBR, Figure 16), this protein has been characterized to be involved in the N-end rule pathway in mammals (Tasaki et al., 2013). Together, these data suggested *TIR3* as a very likely candidate for *OPI2*.

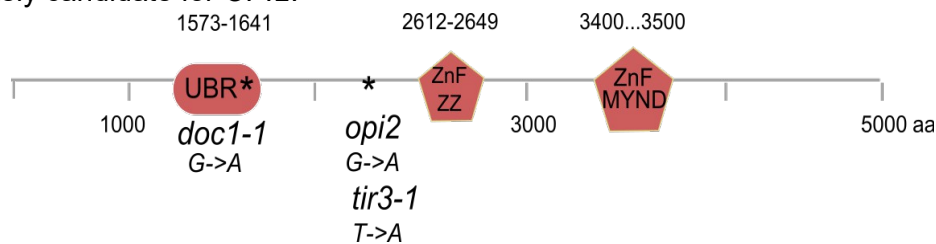


Figure 16. Predicted domains along TIR3/DOC1/BIG protein sequence. *doc1-1*, *opi2* and *tir3-1* mutations are marked with asterisk. Domains were predicted using Prosite (Expasy).

In the past, TIR3's role in temperature response was already highlighted because of the impairment of *tir3* mutants to elongate the hypocotyl at 28°C (Gray et al., 1998). However, characterization of protein function in plants has never been deeply followed up due to the large size of this gene. With a genomic sequence size of 17 Kb, BIG is exceptionally big. Its coding sequence (CDS) size of 15 Kb, encoding the second biggest CDS in *Arabidopsis*. Cloning and further characterization of the role this protein has in plants did not succeed so far. In order to confirm *TIR3/BIG* as candidate gene for *opi2* mutation and to further analyze its potential role in temperature response, cloning was initiated by the Golden Gate technique (Engler and Marillonnet, 2014) in collaboration with Sylvestre Marillonnet and as part of a bachelor thesis I supervised (Tanja Klause, 2014).

4.3.2.2 *BIG/TIR3* cloning by the Golden Gate technique

The Golden Gate cloning technique allows the directional and multiple assembly of several DNA fragments into a single clone module by the use of type II restriction enzymes (Engler and Marillonnet, 2014). As these enzymes cut DNA in a defined distance from its recognition site, they can be used for creating non-palindromic recognition sites. These sites allow to assemble DNA sequences by a directional ligation step. Due to the length of this gene, *BIG* was assembled in consecutive steps

(levels) starting with PCR fragments (level -3) which were fused in 3 consecutive steps (levels -2, -1, 0) to create a “Golden Gate entry vector” (Figure 18). In total, 30 PCR fragments were included in level -3; 19 modules formed the level -2 and 4 modules formed the level -1 (Figure 18).

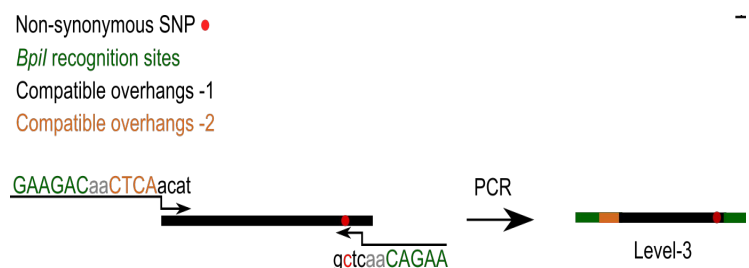


Figure 17. Example of level-3 creation by PCR. Up to 23 *BIG* cloning modules were designed and amplified from gDNA or cDNA. Each level-3 module contained *Bpil* recognition sites (green) and compatible overhangs for the consecutive levels -2 and -1 (orange and black). Non-synonymous SNPs (blue circle) introduced by PCR.

To ensure specific cloning procedure by the use of *Bsal-Bpil* enzymes, up to 21 synonymous mutations were introduced by PCR at the level -3 (PCR products) in the *BIG* coding sequence (Figure 17). These mutations removed extra *Bsal/Bpil* recognition sites which would have disturbed the cloning procedure. Together with *Bpil* recognition sites, compatible overhangs at the borders of those amplified products (Figure 17) were introduced. These overhangs provide specificity to the following assembly steps of the ligated modules.

Once all *BIG* fragments were amplified (level -3), they were cloned by a *Bpil/T4* restriction-ligation cycle into a level -2 vector. After antibiotic and blue-white selection, positive clones (level -2) were sent for sequencing to ensure no random mutations were introduced during the amplification step by PCR. Once it was confirmed that no mutation was introduced, the different level -2 modules were combined in a *Bsal/T4* restriction - ligation cycle to be assembled together in the pAGM1311 vector backbone (level -1) (Figure 18). Next, these 4 modules were used to create the final level 0 in a *Bpil/T4* restriction-ligation reaction (Figure 18). Antibiotic selection during the cloning procedure was alternating from spectinomycin to kanamycin; depending on the vector designated for each level. Level 0 was created with or without stop codon. Altogether, this method was used to build the different parts of the gene up to a full length of 17 Kb gDNA. Cloning of the cDNA was also done in parallel, but it will not be discussed here.

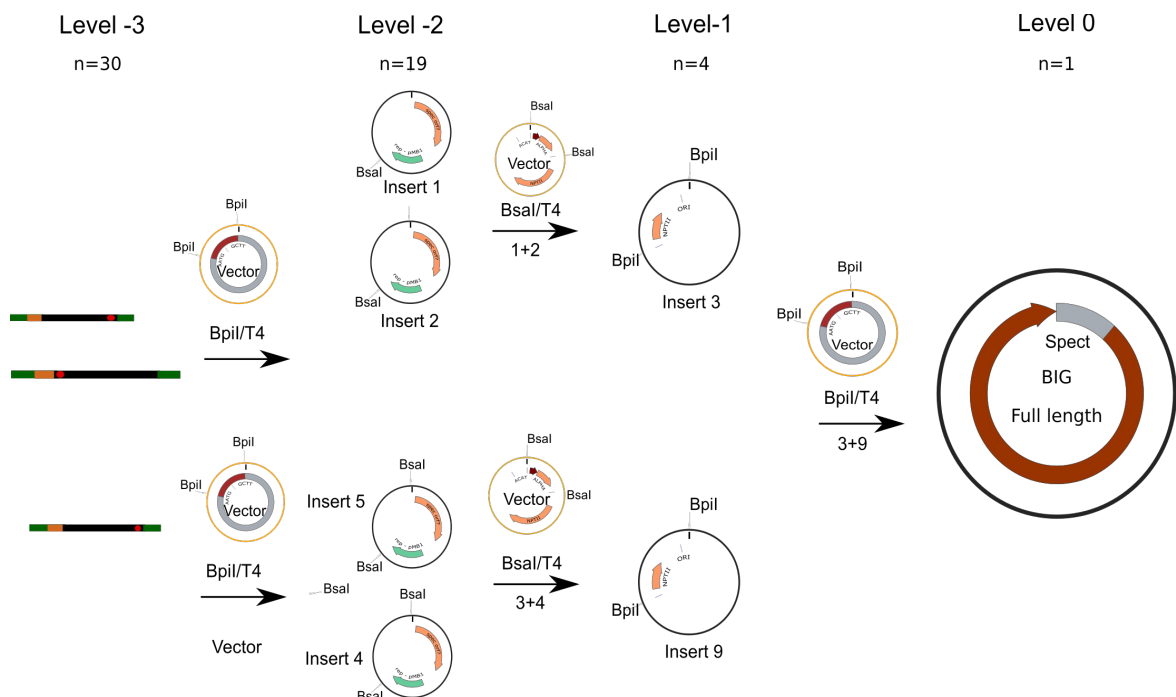


Figure 18. Example of the overall *BIG* cloning procedure from level -3 to level 0 (full length). Level-3 represents PCR products from *BIG* gDNA amplification. A *Bpil/T4* restriction ligation cycle was used to clone these fragments into level -2 vector. Combination of level-2 modules (#1,2) and (#4,5) are introduced by *Bsal/T4* restriction-ligation into level-1 vector, creating the modules #3 and #9 respectively. Combination of these modules by *Bpil/T4* restriction-ligation allowed the cloning of these fragments into a level 0 module (*BIG* full length).

Once level 0 was assembled, the next step was to build the level 1 binary plant expression vector by *Bsal* restriction-ligation. The design of level 1 done included a promoter 35SCAMV cassette (pICH41388) with or without a 5'UTR (TMB Ω); a terminator cassette (NOS) and a GFP-

tag in the N-terminal or C-terminal (Figure 19). However, none of these or other cassette combinations brought any positive result in the cloning of *BIG* into an expression vector.

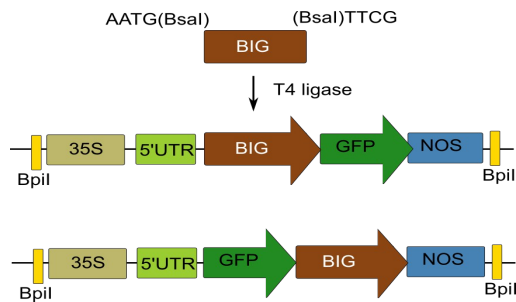


Figure 19.

Modules used for the assembly of the level 1 (*BIG* expression vector). Promoter 35SCAMV with or without a 5'UTR (TMB Ω); a terminator cassette (NOS) and a GFP-tag at the N-C terminal.

Because of the limitation we found in the creation of an expression vector by the Golden Gate technique, I decided to create a Golden Gate-Gateway compatible vector (pENTR-GG) that theoretically would allow to shift from the Golden Gate to the classical Gateway system. The pENTR/D-TOPO vector (Invitrogen) was modified to have *BsaI* recognition sites and level 1-*BIG* compatible overhangs next to the chloramphenicol/*ccdB* cassette by using *ccdB* survival cells (*E. coli* DB3).

After the creation of a pENTR-GG compatible vector I tried to assemble *BIG* into pENTR-GG. Theoretically, after a *BsaI*/*T4* restriction-ligation cycle, full length *BIG* should be cut out from the pICH41308 vector backbone (Golden Gate level 0) and be integrated into the compatible pENTR/GG vector where the *ccdB*/*chloramphenicol* cassette would be replaced. Cloned product was transformed into *E. coli* and kanamycin resistant cells were selected on LB agar plates. Colony-PCR covering the vector-gene junction revealed that *BIG* was present in those cells. This result was confirmed by restriction-digestion. Although mutations should not be introduced at this level, the pENTR-*BIG* clone was re-sequenced. Sequence information of pENTR-*BIG* revealed a foreign DNA insertion of ~200 bp in one of the exons. Exogenous DNA was confirmed to be genomic DNA from bacteria. The procedure was repeated several times, but in all cases, an exogenous DNA fragment was introduced at the same position. However, none *BsaI* recognition site was found along the sequence.

Because of the “impossibility” of cloning *BIG*, *opi2* mutant complementation and TIR3/*BIG* functional characterization in response to temperature could not be followed up. As consequence, I decided to focus on the characterization of two other mutants isolated from the screen: *opi3* and *opi7*.

4.3.3 *opi3* and *opi7*

4.3.3.1 Identification of the causal mutation

Next generation sequencing of a pool of 81 BC1-F3s and 260 BC1-F2s provided a candidate interval on chromosome 3 for *opi3* and on chromosome 4 for *opi7*, respectively (Figure 20). The *opi3* target interval covered a total of 3.2 Mbp and *opi7* sequence information predicted a confidence interval of 12 Mbp. CAPS markers were designed and tested along both intervals (Figure 20). Wt (Rrs-7) and M3s were used for this purpose.

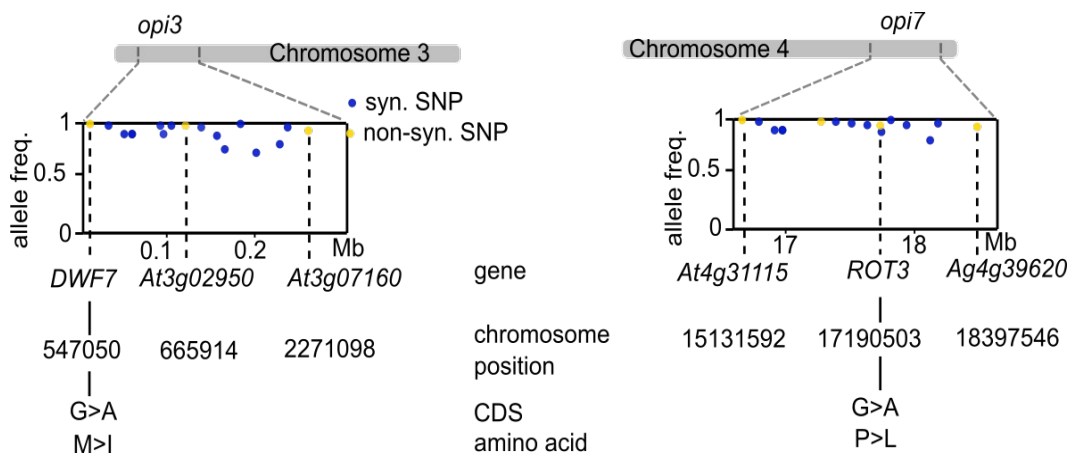


Figure 20. Identification of *opi3* and *opi7* potential mutations. (A) Next generation sequencing of a pool of 81 BC1-F3s provided a candidate interval on chromosomes 3 for *opi3*. Mapping identified *DWARF 7* as candidate gene for *opi3* mutation (M>I). (B) Next generation sequencing of a pool of 260 BC1-F2s provided a candidate interval on chromosomes 4 for *opi7*. Mapping of *opi7* identified *ROTUNDIFOLIA 3* as candidate gene for *opi7* (P>L).

Fine-mapping with CAPS markers on a BC1-F1 population, proposed a non-synonymous mutation (methionine to isoleucine) in the start codon of *DWARF 7/DWF7* (*AT3G02580*); which was therefore considered as the potential mutation responsible for the *opi3* phenotype. In the case of *opi7*, the second exon of *ROTUNDIFOLIA 3/ROT3* (*AT4G36380*) presented a non-synonymous mutation (proline to leucine) that was co-segregating with the *opi7* impairment in hypocotyl elongation (Figure 20). *DWF7* and *ROT3* are genes encoding for enzymes involved in the brassinosteroid biosynthesis pathway (Figure 21). Diverse alleles from *DWF7* (*STE1/BUL1*) and *ROT3* (*CYP90C1*) had been previously isolated during the study of the BR biosynthesis pathway. BR biosynthesis is composed of two major parts: the sterol-specific biosynthetic pathway (from squalene to campesterol) and the BR-specific biosynthetic pathway (from campesterol to the different bioactive forms of BRs). *DWF7/STE1/BUL1* encodes for a Δ^7 sterol C-5 desaturase involved in the conversion of episterol in the sterol-specific biosynthetic pathway (Figure 21). On the other hand, *ROT3/CYP90C1* is involved in the conversion of typhasterol to

castasterone, which has been deemed an activation step in the biosynthesis of BRs (Kim et al., 2005; Figure 21).

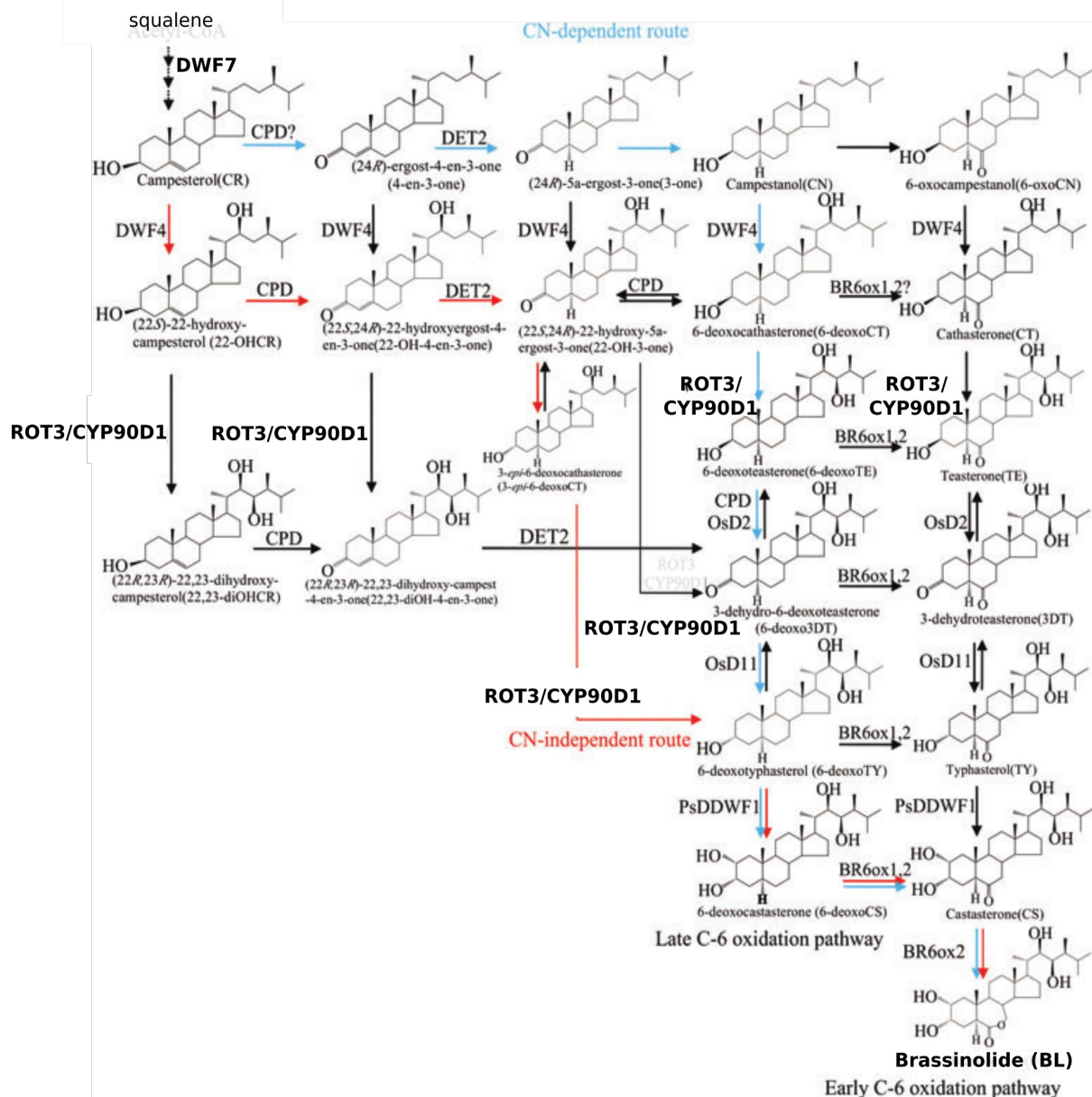


Figure 21. Simplified BR biosynthesis pathway with the enzymes involved in each step. Squalene is the precursor of the sterol-specific pathway that will result in campesterol as the end product. Campesterol will be the precursor used in the BR-specific biosynthesis pathway. At the end of the pathway, BR active compounds are produced, with brassinolide (BL) being the most active form. DWF7 and ROT3 catalyzing steps are marked in bold letters. Blue arrows represent the CN-dependent route. Red arrows represent the CN-independent route. Modified from Zhao and Li. (2012).

The *opi3* and *opi7* mutants isolated from the screen exhibited an impairment in hypocotyl elongation when they were exposed to high ambient temperature in comparison to Wt plants (Figure 22A). Because cell elongation defects had been previously described in BR mutants (Azpiroz et al., 1998), cell number and size of hypocotyl cells were analyzed in seven days-old seedlings. Cell length of hypocotyl cortical cells was visualized by staining the cell wall with propidium iodide. Confocal pictures were taken and analyzed by ImageJ. Measurements were

done from the top of the hypocotyl (petiole node – Cell number 1) to the bottom where the root-hypocotyl transition zone starts (collet area). While *opi3* and *opi7* cell length at 20°C was similar to Wt, as was also reflected in the hypocotyl length (Figure 22B,C), seedlings exposed to 28°C exhibited a strong defect in cell elongation, being more pronounced in the central elongation area of the hypocotyl (cells 6-18; Figure 22B,C).

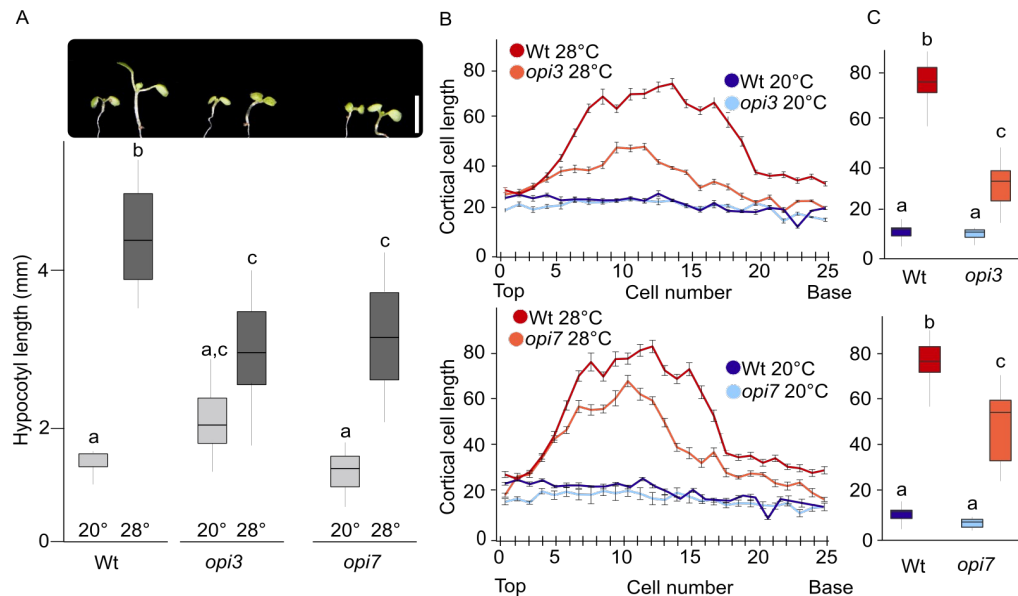


Figure 22. The *opi3* and *opi7* mutants exhibit a defect in hypocotyl elongation. (A) *opi3* and *opi7* mutants expose a defect in hypocotyl elongation at 28°C in comparison with Wt. Seven-days old seedlings grown at 20°C 3d + 28°C 4d (B) Hypocotyl cortical cell length (from top to base) of Wt, *opi3* and *opi7* at 20°C and 28°C of the seedlings quantified in A. (C) Box plots of hypocotyl elongation area (cells 6-18) shown in B. Different letters denote significant differences as assessed by 1-way ANOVA and Tukey-test ($p < 0.05$, $n > 8$).

In addition, the number of total hypocotyl cortical cell was also analyzed (Figure 23). Wild type plants exposed to 20°C and 28°C ambient temperature exhibited an increase in cell number, possibly caused by an increase in cell division. In contrast, *opi3* did not only show a defect in cell elongation at 28°C, but total cell number did not increase in response to high temperature as in Wt (Figure 23). Taken together, these results suggest that *opi3* and *opi7* defects in hypocotyl elongation were caused by a defect in cell elongation and cell division.

Together with hypocotyl elongation; petiole elongation and rosette size are among the traits more susceptible to changes in ambient temperature (Chapter I). To further study growth defects in these mutants, Wt, *opi3* and *opi7* seedlings grown on plates at 20° or 28°C were transferred to soil to allow further plant development. Rosette area and petiole length

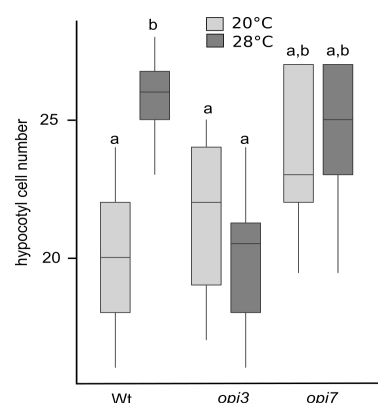


Figure 23. Total cortical cell number of Wt, *opi3* and *opi7* hypocotyls. Seedlings were grown at 20°C 3d + 28°C 4d (dark gray). Control seedlings at 20°C (light gray). Different letters denote significant differences as assessed by 1-way ANOVA and Tukey-test ($p < 0.05$, $n > 15$).

were measured in 14 days-old plants. Similar to what was observed at the seedling stage, rosette (Figure 24A,B) and petiole length (Figure 24C) of *opi3* and *opi7* plants were significantly smaller compared to Wt, indicating that the growth defect observed at the seedling stage affects also adult developmental stages.

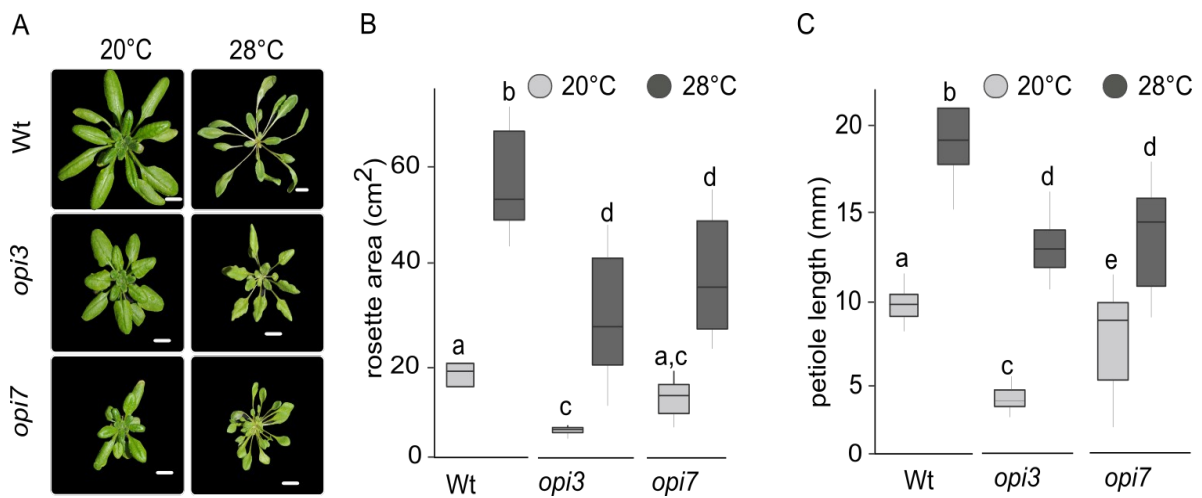
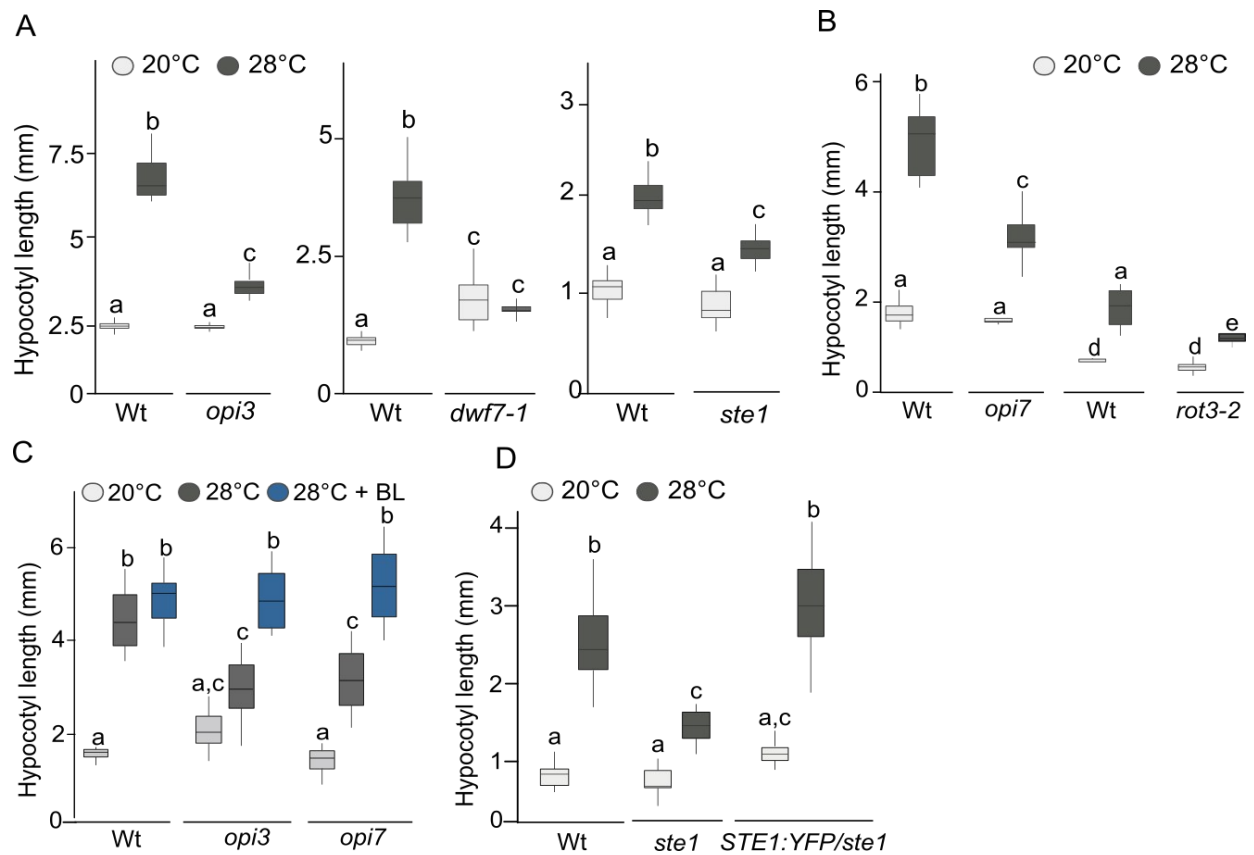


Figure 24. *opi3* and *opi7* exhibit additional cell elongation-associated phenotypes in later developmental stages. (A) Representative rosette pictures of 14-days old plants. (B) Quantification of rosette area and (C) Petiole elongation of Wt, *opi3* and *opi7* plants. Different letters denote significant differences as assessed by 1-way ANOVA and Tukey-test (p<0.05, n>8).

4.3.3.2 Pharmacological and transgenic complementation

opi3 and *opi7* sequence information and fine-mapping indicated that two BR biosynthesis enzymes, *DWF7* and *ROT3* could be the potential candidate genes for *OPI3* and *OPI7*. Because BR biosynthesis and signaling mutants exhibit a dwarf phenotype (Choe et al., 1999; Gray et al., 1998; Silvestro et al., 2013), I wanted to test if published mutant alleles for these genes were phenocopying the defect in hypocotyl elongation observed in *opi3* and *opi7*. Previously identified alleles of *opi3* (*dwf7-1* (Ws-2 background) and *ste1* (Col-0 background) and *rot3-2* (in Ler background) for *opi7* were tested in a TIHE assay. Seedlings were germinated at 20°C for three days and then transferred to 28°C. Pictures were taken in 7 days-old seedlings and hypocotyl length was measured. As Figure 25A,B shows, *dwf7-1*, *ste1* and *rot3-2* mutants exhibited a defect in hypocotyl elongation at 28°C in comparison to their respective Wt control plants, suggesting that a defect in these genes triggers the phenotype observed in *opi3* and *opi7* mutants. Since *DWF7* and *ROT3* encode for enzymes involved in the BR biosynthesis pathway, I next tested if active forms of BL added exogenously to the media could rescue the elongation defect in the hypocotyl, which could be potentially triggered by the lack of Brs. Epibrassinolide (BL) supplemented media was able to rescue the impairment of *opi3* and *opi7* hypocotyl elongation in response to temperature (Figure 25C). Furthermore, transgenic complementation

lines in the Col-0 background (*STE1p:STE1-YFP/ste1*) confirmed that the *opi3/dwf7/ste1* mutation is responsible for the TIHE defect observed in these alleles (Figure 25D).



Transgenic complementation of *opi7* was done by introducing Wt *35S:ROT3* in the *opi7* mutant background. T1 positive transformants were selected by kanamycin selection plates. Selection of homozygous T3s and complementation assay will be carried on in the near future.

4.3.3.3 Brassinosteroids are essential in temperature signaling

In contrast to auxin, the role of BRs in the temperature context is only poorly understood. As growth-associated hormones, it is expected that a lack of BRs in the plant triggers growth-associated defects such as impairment in cell elongation (Figure 22). Since growth-associated responses activated by high ambient temperature (e.g. hypocotyl and petiole elongation) are mainly caused by a process of elongation; lack of BRs are likely to trigger thermomorphogenic defects as the ones described for *opi3/dwf7* and *opi7*. Therefore, I addressed whether the role this hormone has in temperature response is dependent on the canonical PIF4 signaling pathway. To test that, a brassinosteroid biosynthesis inhibitor (propiconazole-PPZ) was used to block BR production in lines with a potential accumulation of PIF4 protein (*35S:PIF4*, *hy5* and *elf3*) causing a long hypocotyl phenotype. As Figure 26 shows, the hypersensitivity response to high ambient temperature of *35S:PIF4*, *hy5-51* and *elf3-4* present in the mock-grown samples was impaired when the seedlings were grown in presence of 1 μ M of PPZ, suggesting that BRs are essential for PIF4 promotion of hypocotyl elongation. Similar conclusions were established genetically due to the repression of the long hypocotyl phenotype in the *dwf7,elf3* double mutant (Figure 26B).

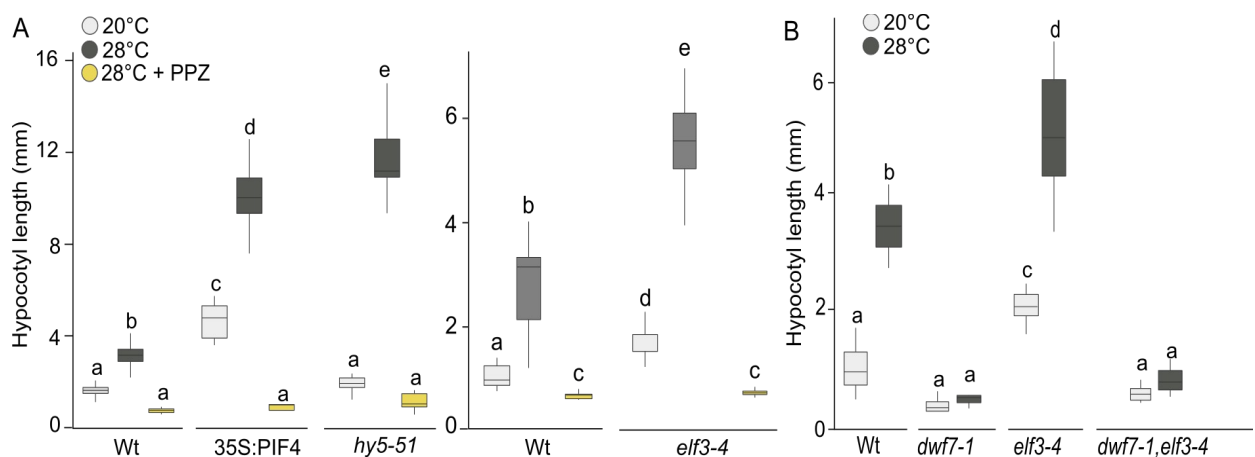


Figure 26. Brassinosteroids are essential for the temperature signal transduction. (A) Propiconazole (PPZ) (1 μ M) represses the hypocotyl elongation response to high temperature of *35S:PIF4*, *hy5-51* and *elf3-4* mutants. (B) *dwf7* is epistatic over *elf3* in the hypocotyl elongation in response to temperature. Different letters denote significant differences as assessed by 1-way ANOVA and Tukey-test ($p < 0.05$, $n > 8$).

While PPZ inhibition of PIF4-mediated elongation responses would suggest BR acting downstream of PIF4 in the temperature signaling pathway; another possibility that can not be neglected is that PIF4 protein accumulation/function requires an active BR signaling pathway. In both scenarios, lack of BRs would trigger the inhibition of hypocotyl elongation in PIF4-accumulated lines, but the molecular mechanism for that may be different. After having established the PIF4-dependent role on BRs presence, the next question to be addressed was the hierarchy between BRs and PIF4 in thermomorphogenesis. In order to test that, *pif4-2* loss-of-function defect in hypocotyl elongation was attempted to be rescued by grown on BL-

supplemented media at 28°C. As Figure 27A shows, BRs were able to rescue the *pif4-2* TIHE defect almost to Wt levels at 28°C, supporting the role of BRs downstream of PIF4. Furthermore, synthetic auxin (picloram) added to the media was also able to rescue the *pif4* defect, confirming published data about PIF4 involved in the activation of auxin biosynthesis (Stavang et al., 2009; Sun et al., 2012) and acting upstream of auxin. Inhibition of the *35S:PIF4* phenotype by a cocktail of auxin inhibitors (kynurenin + yucasin) supported this conclusion (Figure 27B). Whether or not a secondary role of BRs upstream of PIF4 may exist will be further study in the next chapters.

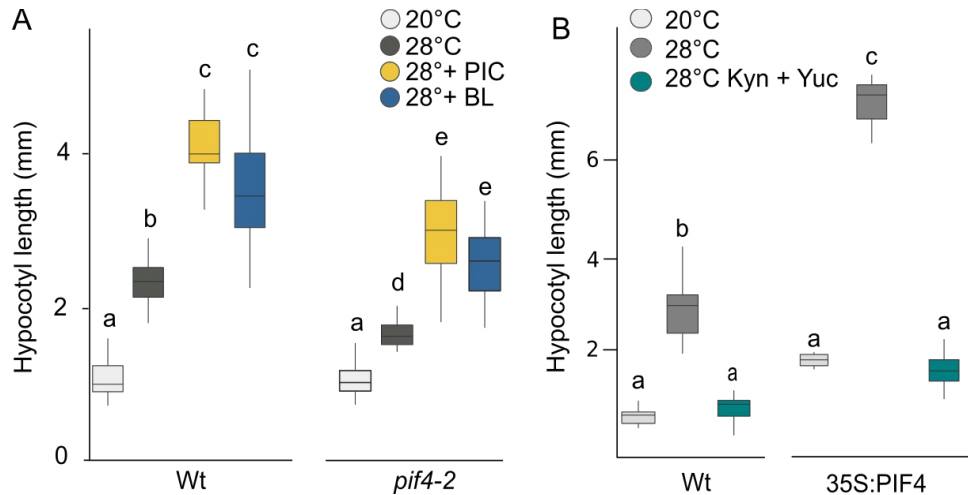


Figure 27. BR hierarchy on PIF4 function (A) *pif4-2* defect in hypocotyl elongation in response to temperature is partially rescued by epi-BL (100nM BL) and the synthetic auxin, picloram (5 μ M). (B) Hypersensitivity to high ambient temperature of *35S:PIF4* is repressed by auxin biosynthesis inhibitors (50 μ M Yucasin + 50 μ M Kynurenin). Different letters denote significant differences as assessed by 1-way ANOVA and Tukey-test ($p < 0.05$, $n > 8$).

4.3.4 The auxin-brassinosteroid hierarchy in temperature signal transduction

After have placed auxin and BRs downstream of PIF4, I aimed to elucidate the interdependency of both hormones in temperature-induced hypocotyl elongation. To test that, a combination of active forms of auxin (picloram), BR (epibrassinolide, BL) and biosynthesis inhibitors of both hormones (propiconazole-BR, yucasin-IAA and kynurenin-IAA) were used. Wt plants were exposed to the auxin picloram, the brassinosteroid inhibitor PPZ, and the combination of both components. As Figure 28A shows, the elongation effect triggered by picloram alone was blocked when BR inhibitor and picloram treatment were combined. In contrast, the BR effect on hypocotyl was able to overcome lack of auxin in the plant treated with the auxin inhibitors (Figure 28B). These results could be confirmed genetically by the use of auxin and BR mutants. As Figure 28C and 28D shows, impairment in hypocotyl elongation of auxin mutants was rescued by BL added exogenously to the media, while the hypocotyl elongation defect of BR mutants could not be restored by picloram. Together, my data demonstrates that in thermomorphogenesis auxin action depends on BR, which acts downstream of it.

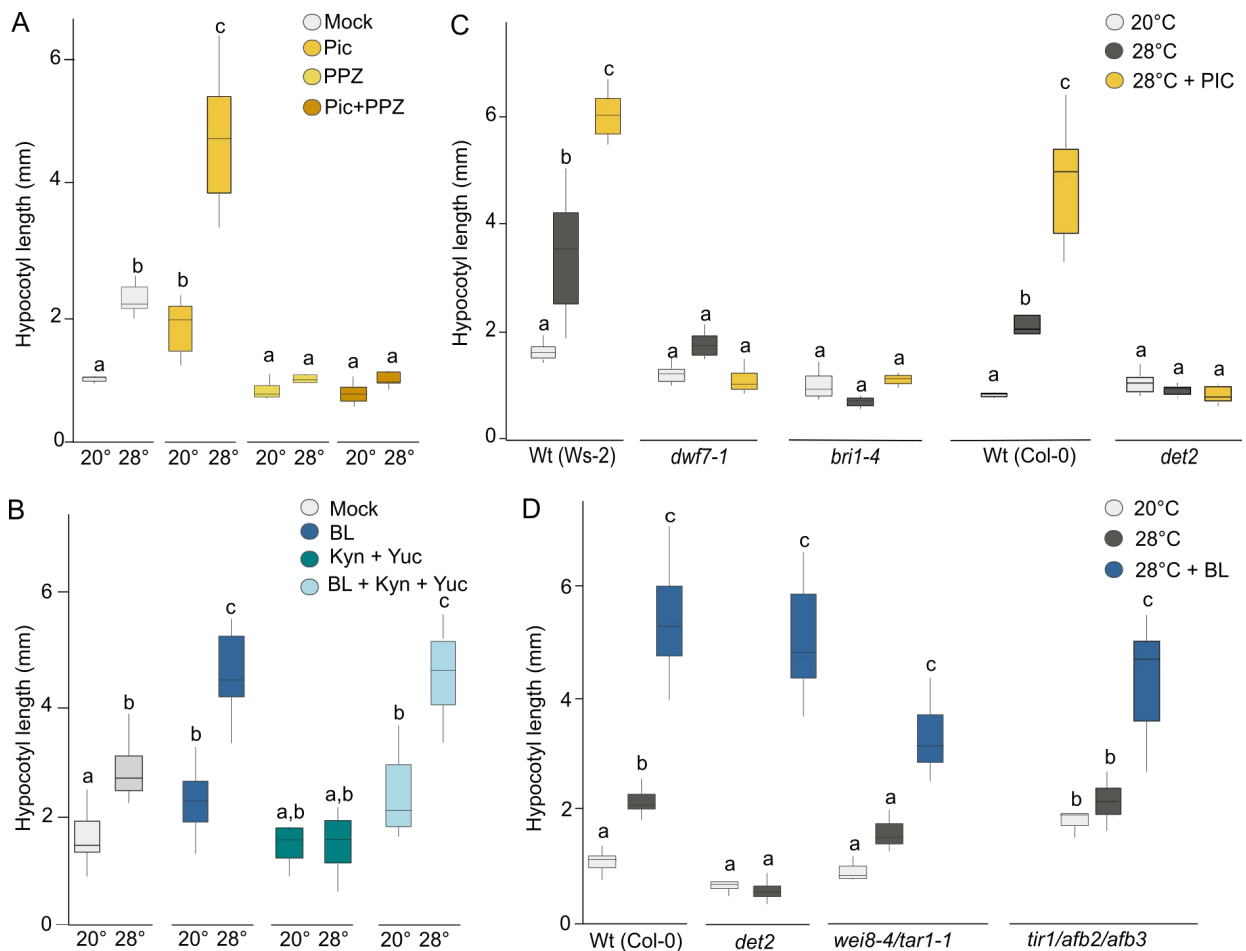


Figure 28. Brassinosteroids act downstream of auxin in the temperature signaling pathway. (A) TIHE assay of Wt (Col-0) seedlings exposed to picloram (5 μ M) or picloram combined with propiconazole-PPZ (1 μ M). (B) TIHE assay of Wt (Col-0) seedlings grown in presence of BL (100nM) or epi-BL combined with auxin biosynthesis inhibitors (50 μ M Yuc + 50 μ M Kyn). (C) BRs biosynthesis and signaling mutants defect in hypocotyl elongation cannot be rescued by picloram (5 μ M). (D) Auxin biosynthesis and signaling mutant defects can be rescued by BL (100nM). Different letters denote significant differences as assessed by 1-way ANOVA and Tukey-test ($p < 0.05$, $n > 8$).

4.3.5 The role of BRs in thermomorphogenesis: Gating PIF4

The impairment in hypocotyl elongation *35S::PIF4* exhibited in presence of PPZ (Figure 26A) and the rescue of *pif4-2* by BL (Figure 27) suggest BRs acting downstream of PIF4 in the temperature signaling. I next examined the relevance that lack of BRs may have on transcriptional regulation of growth-associated genes involved in the temperature response. Inactivated BR signaling triggers the brassinosteroid transcription factor BZR1, relocalization from the nucleus to the cytoplasm (Figure 4; Sun et al., 2010); therefore, the *dwf7/opi3* dwarf phenotype could be explained by the absence/inactivity of BZR1 in the nucleus. BZR1 has been described to act together with PIF4 in the regulation of growth-associated genes (Oh et al., 2012). Some of these genes, like *IAA19* and *SAUR19*, are auxin and temperature-induced genes known to be directly connected with growth promotion (Oh et al., 2012). Thus, expression of these genes in response to temperature was analyzed. To examine that, I made a 24h time-

course experiment where BZR1/PIF4 target gene expression in response to temperature was analyzed. Theoretically, if BZR1 remains inactive in the *dwf7* background, it should not activate these growth-associated genes in response to temperature. While such experiment should be carried out with stable BZR1-phosphorylated (inactive) or *bzr1*-loss of-function lines, these lines were not available when I designed this experiment. Therefore, I used *dwf7* to indirectly have a potential BZR1 inactive background by the lack of BRs in the plant. Samples were taken from 7 days-old seedlings at lights on (ZT:0) and every 4 hours for a 24 cycle.

As figure 29 shows, Wt seedlings exhibited an upregulation of both genes at 28°C in comparison to 20°C grown seedlings. In contrast, in the *dwf7* background, these genes did not respond to high temperature (Figure 29). In particular, the temperature-induced expression defect in *dwf7* was more prominent at noon, when growth occurs (Nozue et al., 2007). These data suggest that an active BR signaling pathway (assumed in Wt) is needed for the upregulation of BZR1/PIF4 growth-associated genes in response to temperature. As auxin-responsive genes are also present among BZR1-regulated genes suggests that a feed-back regulation of BRs to upstream components of the pathway may occur.

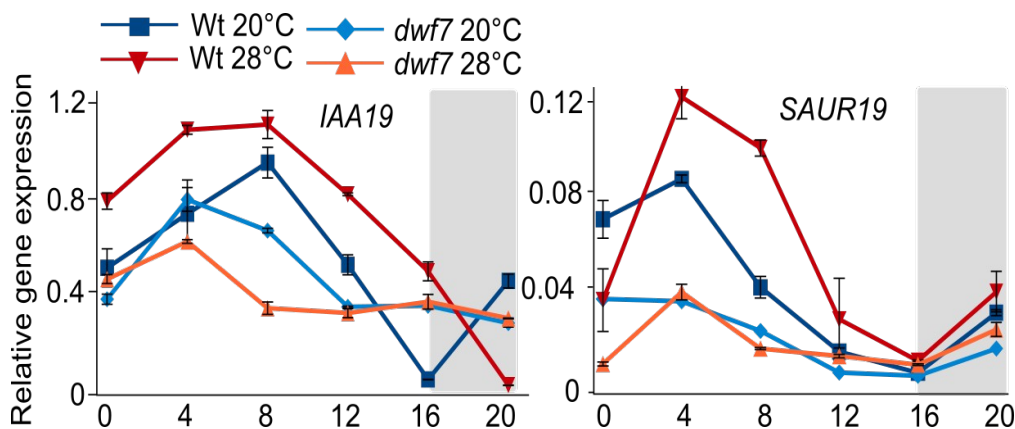


Figure 29. Expression analysis of IAA19 and SAUR19 in Wt and *dwf7*. Seedlings were grown at 20° or 28°C under long day photoperiods. Seven days after sowing, plant material was harvested at ZT:0 (lights on) and every four hours during a 24h-cycle. Shade area represents the night period.

The low expression levels of temperature-induced genes that *dwf7* exhibited (Figure 29) could be explained by two scenarios: In the first case, the results observed could be caused by the lack of active BZR1 in the nucleus, indicating that BZR1 is needed for the temperature-induced expression of these genes although PIF4 may be present. Under this scenario, a cooperative mechanism would be regulating the transcriptional response, and the presence of both transcription factors would be required. If that would be the case, BZR1 might have a positive function on temperature regulation as PIF4 has. Therefore, I tested the effect that BZR1 may have in thermomorphogenesis by performing a TIHE assay with *35S:BZR1* seedlings. As Figure 30A shows, *BZR1* overexpression exhibited a hyperelongation of the hypocotyl in a temperature-dependent manner, suggesting that BZR1 is a positive regulator of hypocotyl elongation under

high ambient temperature. Therefore, a cooperative regulation between these two transcription factors would be theoretically possible under high ambient temperature.

The second possibility would be that the lack of BRs in *dwf7* could affect not only BZR1 but also PIF4. While in the first scenario explained above, both proteins would independently be activated by temperature and come together in the regulation of specific genes in a cooperative manner, here PIF4 would strictly depend on BRs presence, thus a feed-back/forward regulation of BRs towards PIF4 would be expected. Indeed, PIF4 protein accumulates in response to BL, and post-translational regulations via BIN2 have been shown (Bernardo-García et al., 2014). However, transcriptional regulation of *PIF4* by BRs has never been reported. To test this hypothesis, *PIF4* gene expression was analyzed in *BZR1* overexpression lines. Material was grown at 20°C in long day conditions for 7 days and part of the seedlings were shifted to 28°C at lights off (ZT:16). Material was harvested after four hours and RNA was extracted. qRT-PCR of *PIF4* expression levels revealed that the lines overexpressing *BZR1* exhibited a temperature-dependent upregulation at 28°C in comparison to Wt plants (Figure 30B). In addition, I could observe that *PIF4*/BZR1 common target genes (*SAUR19* and *SAUR15*) were differentially upregulated at 28°C in *35S:BZR1* lines (Figure 30B). This suggests not only that BZR1 could be triggering the upregulation of these genes alone but also that this could be done via *PIF4* upregulation.

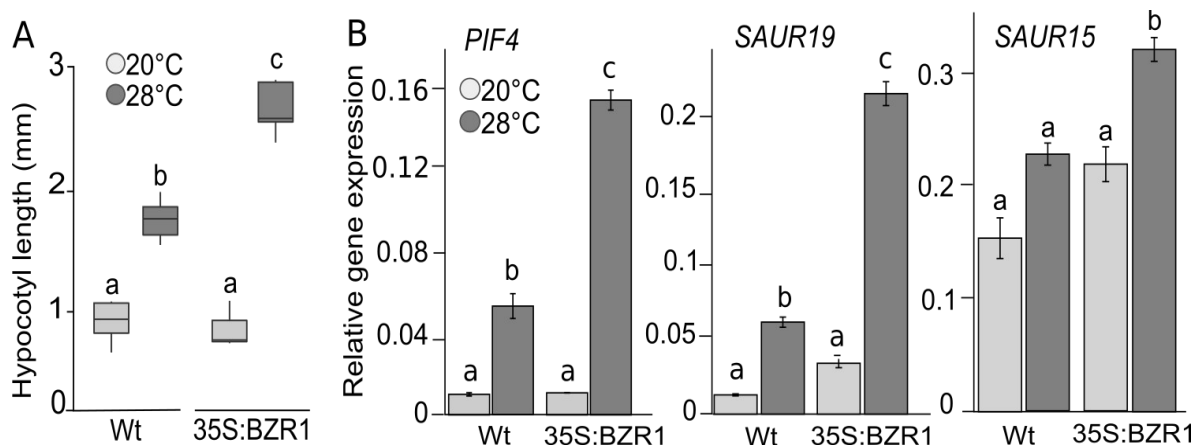


Figure 30. BZR1 is a positive regulator of hypocotyl elongation at high temperature. (A) TIHE assay of Wt and *BZR1* overexpression line. Seven days-old seedlings grown at 20°C for 3 days and shifted to 28°C for extra 4 days (dark grey) (B) Relative gene expression of *PIF4*, *SAUR19* and *SAUR15* in 7 days-old *35S:BZR1* seedlings grown at 20°C (light gray) and shifted to 28°C for 4 hours at the end of the light period (dark gray). Different letters denote significant differences as assessed by 1-way ANOVA and Tukey-test ($p < 0.05$, $n > 8$).

Since *PIF4* was differentially regulated in the *BZR1* overexpression line at 28°C (Figure 30), I hypothesized that BZR1 could be directly regulating *PIF4* in a temperature-dependent manner. BZR1 binds to the BR-response element (BRRE, CGTG [T/C] G) of BR-repressed genes (He, 2005). However, this transcription factor has also been described to bind E-box elements (CANNTG) when it is working as a transcriptional activator. Based on this information, the *PIF4* promoter (defined here as 2 Kb upstream from the start codon) was analyzed with the aim of

identifying potential BZR1 binding sites. As Figure 31 shows, the *PIF4* promoter region contains one BRRE element at position -1713 (dark red) and several E-box elements (light brown and orange boxes).

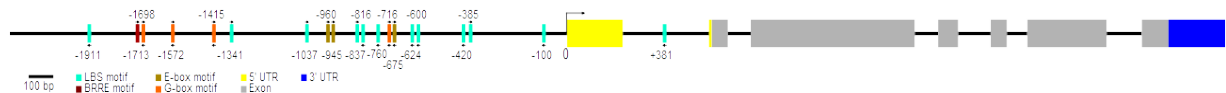


Figure 31. *PIF4* promoter region. Binding domains along 2 Kb upstream of *PIF4* start codon are marked: Lux-binding sites (LBS, light blue), G-box motifs (orange), BRRE motif (brown). Yellow and dark blue boxes represents 5' and 3'UTR. Gray boxes represent coding regions.

To test if BZR1 is directly regulating *PIF4*, the 2 Kb fragment upstream of *PIF4* start codon was cloned into a *pNH10:LUC* plasmid. In addition, *BZR1* was cloned under the control of a 35S promoter (*pGWB405*) to create a *BZR1* overexpression construct. Co-transfection of *PIF4pro:LUC* and CFP control constructs into *Arabidopsis* mesophyll protoplasts resulted in poor expression of *PIF4pro:LUC* (Figure 32A). However, when *PIF4pro:LUC* was co-transfected together with *35S:BZR1*, LUC was expressed at high levels (Figure 32A), indicating that BZR1 is

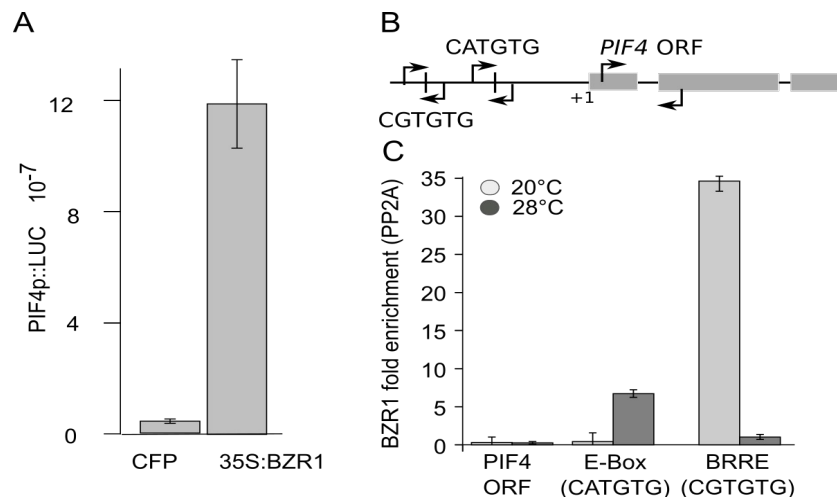


Figure 32. BZR1 activates *PIF4* promoter activity. (A) *PIF4* promoter fused to the luciferase reporter gene was co-transfected with *35S:BZR1* or *35S:CFP*. (B) *PIF4* promoter and coding region. Letters represent G-box, E-Box and BRRE domains present in *PIF4* promoter. Arrows represent the primers used in (C) ChIP-PCR on *35S:BZR1*-*CFP* seedlings. Marked regions of the promoter and ORF of *PIF4* were analyzed by qRT-PCR. Data were normalized with Wt control *PP2A* and *input*. Technical replicates of one representative experiment are shown.

able to regulate *PIF4* via the *PIF4* promoter. Nevertheless, the use of the protoplasts as expression system has the disadvantage of not being able to study the effect of temperature on *PIF4* expression. With the aim of further studying the interaction of the BZR1 transcription factor with the *PIF4* promoter *in vivo* a Chromatin Immunoprecipitation-PCR (ChIP-PCR) assay was performed. *GFP*-tagged *BZR1* overexpression lines (*35S:BZR1:GFP*) were used for this purpose. Wt plants (*Col-0*) were used as a negative control of the binding specificity to the transcription factor. Plants were grown under 20°C long day conditions for 7 days. At ZT:10

seedlings were shifted to 28°C and incubated for 8 hours. Plant material from 20°C and 28°C was harvested before lights switched on. Crosslinking, chromatin immunoprecipitation and reverse-crosslinking details are described in the Material and Methods section (3.4.7). After genomic DNA purification, quantitative PCRs were performed on the DNA isolated from both the *35S:BZR1* and the Wt samples. qRT-PCR primers were designed for amplifying the BRRE element (at position -1713) and an E-box element (at position -675). A *PIF4*-ORF between the first and second exon was used as a negative control of the binding (Figure 32B). After the qRT-PCR, the data obtained was normalized against the *PP2A* gene and input samples. As Figure 32C shows, BZR1 enrichment was found in the E-box element specifically at 28°C, while *PIF4* ORF (used as negative control) did not show any significant signal. The binding of BZR1 to *PIF4* E-box element occurred specifically at 28°C in spite of having used a *BZR1* overexpression line, suggesting a post-translational regulation of BZR1 specifically at high temperatures. My experiment also revealed that at 20°C BZR1 was enriched at the BRRE element but not at 28°C (Figure 32B) and meaning that high temperature causes association of BZR1 with growth promoting cis-elements rather than repressive BRREs. In that way, BZR1 may potentially upregulate *PIF4* expression at high ambient temperature to promote elongation/growth, and downregulate its expression when *PIF4* activity is less required (20°C).

Based on the higher activity that BZR1 may have at 28°C, I next wanted to analyze the potential regulation of this transcription factor at high ambient temperature. In accordance to published data (Li and He, 2016; Oh et al., 2012), analysis of *BZR1* expression levels over a 24h cycle showed no significant changes between 20° and 28°C (Figure 33A).

Since I observed a temperature-dependent transcriptional response in the ChIP experiment by BZR1 (Figure 32C), my data supports that BZR1 regulation by temperature is likely to occur at the post-translational level. Nevertheless, analysis of total protein extract in *35S:BZR1* lines did not show any obvious change between 20°C and 28°C, and the BZR1 phosphorylation status remained constant between both temperatures (Figure 33). Altogether, these data indicate that BZR1 regulation by temperature may be done by an unknown mechanism independent of the phosphorylation status or protein turn-over.

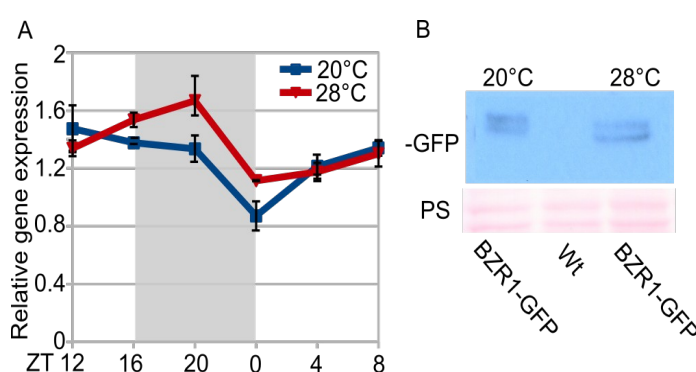


Figure 33. *BZR1* expression levels and protein accumulation at 20°C and 28°C. (A) *BZR1* expression levels in Wt seedlings over a 24h cycle. Plants were grown at 20°C or 28°C (LD). No significant differences were found with 1-way ANOVA and Tukey-test. (B) Western blot of total BZR1 protein in *35S:BZR1:GFP* seedlings grown at 20°C or shifted to 28°C at the end of the light period. Samples harvested before lights on. Wt was used as negative control. BZR1 was detected with anti-GFP antibody.

Surprisingly, the western blot of the protein extracts from the “unbound” and “eluted” (nuclear) fractions at 20° and 28°C from the ChIP showed a strong enrichment of BZR1 specifically at 28°C (Figure 34). Confocal microscopy on the same lines used for the ChIP supported the hypothesis that

at 20°C BZR1 is localized in nucleus and the cytoplasm, while at 28°C it strongly accumulates in the nucleus (Figure 35). However, the mechanism that may regulate BZR1 in this situation remains unknown and whether non-phosphorylated (active) forms are present in higher ratio than phosphorylated BZR1 should be examined. In summary, my data suggest that BZR1 may be able to activate and repress *PIF4* expression by binding to its different promoter elements in a temperature-dependent manner.

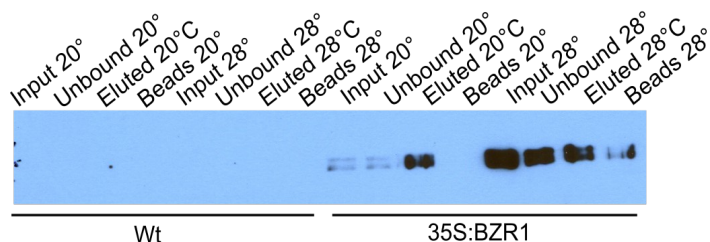


Figure 34. Western blot of nuclear BZR1. Protein fractions collected during the ChIP after chromatin immunoprecipitation at 20° and 28°C. anti-GFP antibody was used to detect BZR1. Wt was used as negative control.

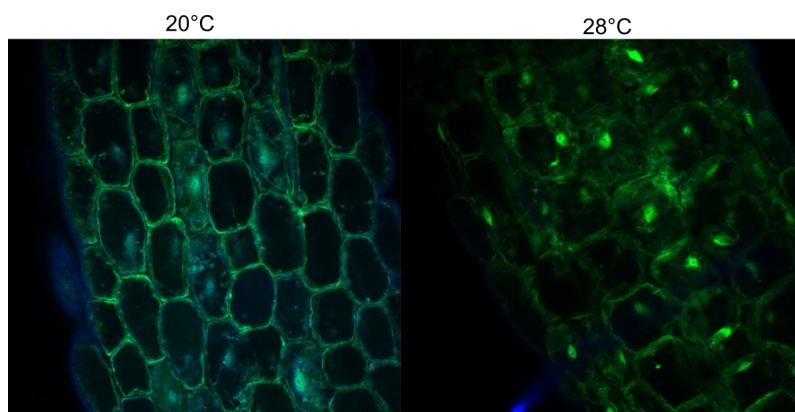


Figure 35. BZR1 accumulates in the nucleus at high ambient temperatures. *35S:BZR1:GFP* seedlings were grown at 20°C for 7 days and shifted to 28°C at the end of the light period. Material was harvested before lights on (ZT:8) and crosslinked.

4.3.6 PIF4 and BZR1 in thermomorphogenesis responses

So far my data suggest a dual role of BRs upstream and downstream of PIF4. Next I wanted to further study whether both transcription factors are needed to regulate this response, independently of the downstream or upstream role that BRs may have on PIF4 regulation.

As mentioned above, in the light signaling pathway PIF4 and BZR1 are able to interact at the promoters of common target genes, usually enhancing their expression. However, regarding my own data it remained unclear if the results obtained were product of a cooperative mechanism between BZR1 and PIF4 or if BZR1 acts through PIF4 in the activation of this response. If the latter would be the case, a *PIF4* overexpression line should theoretically be able to overcome the lack of BRs in the plant. Nevertheless, we know that BRs also control PIF4 activity via BIN2, thus lack of BRs would inactivate not only BZR1 by phosphorylation but also PIF4, independently of having an overexpression line of the latter one. Based on that, and to be able to study the interdependency of both transcription factors in the TIHE response, I used three published lines: *PIF4p:PIF41A*, *35S:PIF41A* (Bernardo-García et al., 2014) and *35S:Bzr1-D* (Oh et al., 2012). These lines carry point mutations in the BIN2 phosphorylation site, thus insensitive to the repressive effect of the BIN2 kinase. Using these lines I could study the relevance of each of these transcription factors in hypocotyl elongation. Theoretically, in the presence of PPZ, BR biosynthesis is blocked and BIN2 will be activated. Active BIN2 will phosphorylate and inactivate BZR1 and PIF4. Therefore, in the *PIF41A* line, PIF4 should remain stable while BZR1 would be inactivated. Same situation would be for *Bzr1-D*.

If the upregulation of one of these factors can overcome the lack of the other (triggered by the presence of PPZ) at high temperature, these lines should still elongate in presence of PPZ at 28°C, meaning that there is no cooperative binding mechanism needed to trigger growth

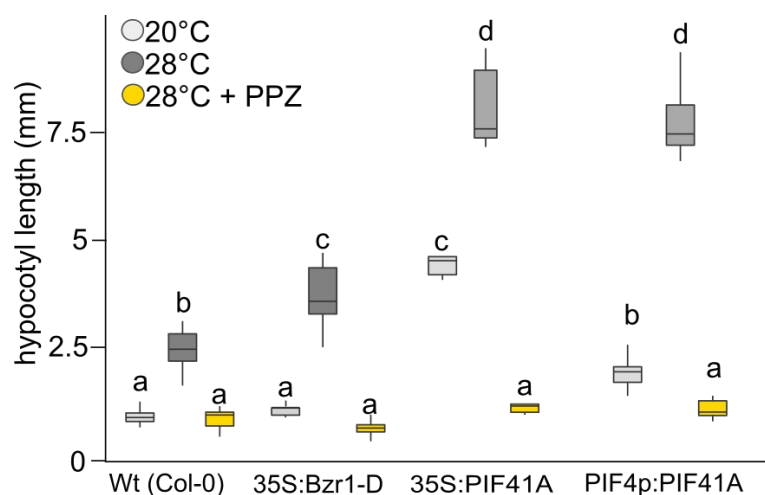


Figure 36. BZR1 and PIF4 are needed for hypocotyl elongation in response to temperature. Hypocotyl length (mm) of Wt, *35S:Bzr1-D*, *35S:PIF41A* and *PIF4p:PIF41A* grown at 20°C (light gray) or shifted to 28°C for 4 days in the presence (yellow) or absence (dark gray) of PPZ grown at 20°C (light gray) and shifted to 28°C for 4 hours at the end of the light period (dark gray). Different letters denote significant differences as assessed by 1-way ANOVA and Tukey-test ($p < 0.05$, $n > 8$).

responses. To test that, these lines were grown in the presence of PPZ at 20°C for 3 days and shifted to 28°C for additional 4 days. As Figure 36 shows, hypersensitivity to high ambient temperature of *35S:Bzr1-D*, *PIF4p:PIF41A* and *35S:PIF41A* in the mock-grown plants was repressed by PPZ in the media. This indicates that both transcription factors may be needed for a proper response to high ambient temperature. However, further assays should be done to confirm this result, such as TIHE response of *35S:BZR1* in the *pif4* mutant background or *35S:PIF4* response in *bzr1*. Interestingly, *PIF4p:PIF41A* exhibited a hyperelongation of the hypocotyl at 28°C similar to *35S:PIF41A* levels. While the latter exhibited already longer hypocotyls at 20°C, *PIF4p:PIF41A* elongation occurred specifically at 28°C (Figure 36), which mimics the temperature-dependent phenotype observed in *BZR1* overexpression lines (Figure 30). This observation is being further studied in more detail.

In summary, the data collected so far suggests a cooperative regulatory mechanism between PIF4 and BZR1, where both transcription factors are required for the regulation of temperature-induced hypocotyl elongation,

5. Discussion

As sessile organisms, plants have to activate proper responses that will help them to offset detrimental effects caused by increases in growth temperature. These adjustments are caused by numerous changes occurring at molecular and phenotypic levels, aiming to help the plant to cope with these conditions. Different morphological and novel molecular responses to warmth are highlighted in this work, and their potential implications in plant adaptation are discussed here.

5.1 Thermomorphogenic responses in plant adaptation

Based on the detrimental effects that temperature increases have on plant production, it becomes crucial to further study the mechanisms that plants use to overcome the exposition to warm environments. Understanding phenotypic plasticity, defined as the range of phenotypes a single genotype can express as a function of its environment (Nicotra et al., 2010), may provide hints for increasing plant fitness. Plants have a remarkable capacity to sense and respond to changes in ambient temperature and the extensive characterization of *Arabidopsis thaliana* morphology presented in Chapter I allowed the identification of traits and accessions highly sensitive to warm environments.

All the traits analyzed in this study were significantly affected by temperature, while the impact that this stimulus had on individual traits differed. In accordance with published data, quantitative morphometric traits associated with vegetative development such as hypocotyl or petiole elongation increased their trait value with temperature, while vegetative timing of development, flowering time and seed production decreased at high temperatures (Figure 7). Within the different responses observed, variability in the sensitivity among the traits was also observed. For instance, as shown in Figure 7, petiole angle, hypocotyl elongation and silique length showed high sensitivity to ambient temperature, gradually increasing its value with temperature ($16^{\circ}>20^{\circ}>24^{\circ}>28^{\circ}$). In contrast, some seed-associated traits like seeds/plant exhibited a strong decrease between lower temperatures (16° - 20° C), while higher temperatures (24° - 28° C) showed a saturated response (Figure 37). Further study of this observation revealed a non-linear response in several traits.

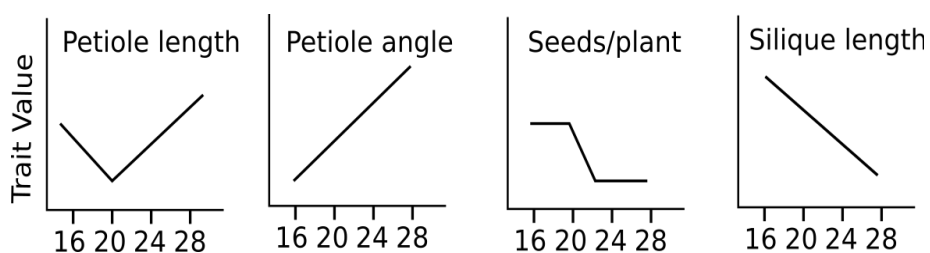


Figure 37. Traits scored exhibited different sensitivity to warm temperature. Curves of the overall response are represented with a solid line. X-axis represents ambient temperature ($^{\circ}$ C), y-axis represents the specific trait value scored.

In particular, only few traits exhibited a gradual change by temperature in all accessions, while most of them showed different response curves (Figure 37). For example, petiole length and petiole angle exhibited both an increase to high ambient temperature, while the response curves differed (Figure 37). A similar scenario was observed for negative responses such as seeds per plant or silique length (Figure 37). The different type of responses identified within these traits may suggest different roles during plant acclimation or adaptation. In addition, this could indicate an early or late saturation of the response in a trait-dependent manner. Whether the different susceptibility of those traits may contribute to plant adaptation should be further study. Hypocotyl elongation was also highly susceptible towards ambient temperature, but so far the role this response has in the adaptation process remains poorly understood.

To account for the differences in the response patterns, Q_{10} is a common estimate to quantify changes occurring in the plant in response to temperature fluctuations. Using this parameter as a quantifiable unit to measure temperature impact on each specific trait, I could observe that high ambient temperature accelerated general growth of the plant, triggering classical temperature-associated phenotypes like early flowering (Figure 6B, Figure 7). Interestingly, the data obtained showed that the overall response in all traits analyzed was significantly affected by increases in ambient temperature (data not shown), while the impact that the genotypic background exhibited on those traits differed. This could be seen in vegetative development, which was highly conserved among accessions, exhibiting low impact from the genetic background (Figure 9). In contrast, flowering time was highly affected by temperature and the genetic background of the plant (Figure 9), and some accessions were even able to overcome the impact that high temperature has on flowering time. Interestingly, these accessions exhibited also higher elongation rates under warm temperatures (Figure 7).

The observation that the genetic background could overcome the effect of high temperature was further studied. Interestingly accessions in which temperature had a neutral effect in flowering time (meaning no changes across temperatures) showed better fitness (understood here as better seed production; Figure 10). Those accessions were defined as high capacity accessions (Figure 38). This suggested that the duration of the vegetative phase and the strength in the response of some quantitative traits may influence in the acclimation process across generations. In fact, low capacity accessions presented weaker response to high ambient temperature and stronger reduction in yield production.

Based on that, the extent of a phenotypic change in response to temperature may be further analyzed by individual accessions as exemplified in Figure 38 for hypocotyl elongation and yield production. In summary, the morphometric and developmental data obtained highlight the tolerance of Got-7 and Rrs-7 towards high ambient temperature (Figure 7, Figure 8) by having more plastic

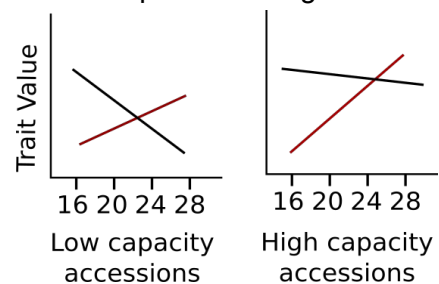


Figure 38. Phenotypic plasticity between different accessions. Red and black lines represent the reaction norms of hypocotyl elongation and yield respectively.

phenotypic responses than other accessions and transgenerational effects should be further studied. While *Got-7* has vernalization requirements that could make the work more inconvenient, *Rrs-7* was proposed as useful accession to perform further screens in temperature response. In contrast, one of the commonly used accessions, *Col-0*, seemed not to be the most promising genetic background due to its low plasticity to warm temperature (Figure 7). Among the temperature-responsive phenotypes, the hypocotyl elongation was one of the most sensitive traits. Due to its strong genetic variation among accessions, this trait was established as a model response to high ambient temperature and used to identify molecular players underlying this response. The Bay-Sha hypocotyl variation was exploited in a QTL analysis to identify the gene/s responsible for that genetic variation (Chapter II). In parallel, *Rrs-7* was used in a forward-genetic screen with the aim of identifying novel players in the temperature signaling pathway (Chapter III). Relevance and impact of both projects will be discussed next.

5.2 Temperature vs. light crosstalk

Light and temperature are two of the most important signals regulating plant growth. Plants exposed to high ambient temperature and shade exhibit what is typically named “shade avoidance syndrome” characterized for long hypocotyls and upward leaf movement (Casal, 2012). Similarly, densely packed trichomes and hyponastic growth have been observed in the leaves of plants exposed to high light or warmth, as a mechanism of keeping leaves cooler by increased transpiration or avoiding radiation respectively (Crawford et al., 2012). Furthermore, light signaling mutants exhibit alterations in flowering time similarly to high temperature conditions (Franklin et al., 2014). The observation that low light/shade and high temperature grown seedlings exhibit similar phenotypical responses suggests that at the molecular level both pathways may share similar players. In fact, in the last 10 years, several light signaling components have been described to be regulated by high temperature. For instance, *PIF4* was originally isolated in a screen for mutants displaying hypersensitivity to red light (Huq and Quail, 2002). Another example is the isolation of the light signaling component *DET1* as the causal gene for the *opi1* mutation (Delker et al., 2014), which became a novel player in the temperature signaling pathway. *DET1* appears to stabilize *PIF4* protein in the dark (Bauer et al., 2004) and contribute to *PIF4* expression regulation under high ambient temperature (Delker et al., 2014). While *DET1* activity is needed for maintaining *PIF* stability, the *COP/SPA* complex regulates also *PIF4* at transcriptional level via *HY5*; which appeared as a negative regulator of the pathway by repressing *PIF4* expression in a temperature dependent manner (Delker et al., 2014). With the characterization of *DET1* and *HY5*, an additional temperature-light signaling crosstalk was established (Figure 39)

In addition, the red and far-red light photoreceptors, phytochrome A and B have an essential role in repressing skotomorphogenesis and shade avoidance responses. *phyb* loss-of-function mutants exhibit hyperelongation of the hypocotyl in the light. The observation that *phyb* mutants

do not exhibit a TIHE response (Jung et al., 2016) suggested that these proteins may be involved not only in light but also in temperature sensing. Activity of these proteins has been described to be highly affected by ambient temperature (Franklin et al., 2014). Recently, PhyB has been proposed as a novel temperature sensor and highlighted as a crucial integrator of temperature and light signaling pathways by associating with PIF4 target genes in a temperature-dependent manner blocking their transcriptional activation (Jung et al., 2016; Legris et al., 2016). However, a *phyabcde* pentuple mutant still shows a transcriptomic response to high ambient temperature, indicating that additional players may be translating the temperature response independently or in addition to phytochromes.

The blue light photoreceptors, CRYPTOCHROME1 and CRYPTOCHROME2, act redundantly with phytochromes in regulating plant architecture at warmer temperatures (Devlin and Kay, 1999; Mazzella et al., 2000). For instance, CRY1 and PHYB buffer the impact of warm temperatures together with HFR1 (Foreman et al., 2011), which mediates PHYB- and CRY1-mediated repression of PIF4 activity to control plant growth at high temperatures (Foreman et al., 2011) by forming PIF4-HFR1 heterodimers. In *Arabidopsis*, this blue light receptor has been shown to be involved in the regulation of the circadian period (Franklin et al., 2014; Pedmale et al., 2016). Recently, CRY1 has been described as a negative regulator of high temperature-mediated hypocotyl elongation by interacting with PIF4 under blue light conditions and preventing PIF4 association to its target promoters (Ma et al., 2016); similar to PHYB. My inability to detect temperature-induced *PIF4* expression during the day in LD photoperiods, might reflect the strong repressive function of PhyB and other light components on *PIF4* expression and function (Figure 39). The external coincidence mechanism proposed by Nomoto et al.

(2012) provides a scenario where photoperiod and temperature fluctuations are equally integrated by the circadian clock and light signaling. In this model, both external factors are able to control the rhythmic expression of PIF4 independently, but integrated into the same signaling modules (PIFs and hormone balance). In that manner, long day photoperiods inhibit hypocotyl elongation as low temperature does. In contrast, short day photoperiods and high ambient temperature trigger similar phenotypic responses in the plant (Nomoto et al., 2012; Yamashino et al., 2013).

In summary, different signals perceived by the clock and other light signaling components will be integrated and growth responses will be fine-tuned accordingly. Nevertheless, most of the published studies have been done in short day photoperiods, where PIF4 mRNA and protein peaks at the end of the night together with maximum growth rates. In long day conditions, the PIF4 peak shifts to the light phase, and is strongly repressed during the night (Nomoto et al.,

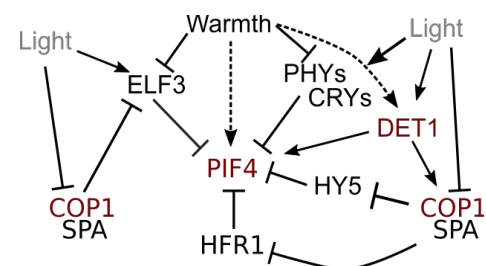


Figure 39. Influence of light signaling components in the temperature signaling pathway. Red-labeled denote positive players involved in temperature signal regulation.

2012). These observations suggest that different mechanisms of regulation may occur between short and long day conditions, although similar players may be involved (Figure 39).

5.3 ELF3 as a negative regulator of temperature signaling

Due to the strong overlaps between light and temperature, players acting in both pathways were expected to be identified. Based on the phenotypic variability among accessions (Chapter I), hypocotyl elongation seemed a promising phenotype for quantitative genetic analyses. We used a segregating population derived from two *Arabidopsis thaliana* accessions (Bay x Sha RIL population; Loudet et al., 2002) to investigate the phenotypic variation in response to warmth. We identified three chromosomal regions (*GIR1*, *GIR2* and *GIR5*) directly involved in temperature-induced hypocotyl elongation (Figure 11). Due to its large contribution to the phenotype (23%), the region on chromosome 2 (*GIR2*) was further mapped, and *ELF3* (*AT2G25930*) was proposed as a likely candidate for the gene underlying the variation observed. I could confirm *ELF3* as the gene underlying *GIR2.1* by using Bay-*ELF3* and Sha-*ELF3* transgenic complementation lines (Figure 13B; Raschke et al., 2015). Furthermore, the *elf3* mutant photocopied a high temperature phenotype, suggesting a negative role of this protein in the regulation of thermomorphogenesis (Figure 13B).

While *ELF3* had been identified in shade avoidance QTL studies (*SAR2*, (Jiménez-Gómez et al., 2010); *EODINDEX1*, Coluccio et al., 2011) and circadian clock periodicity (Anwer et al., 2014), *GIR2*-QTL (Raschke et al., 2015) was the first QTL analysis that focused on temperature-induced variation of hypocotyl elongation. Despite the differences in light and temperature growth conditions used in the other analyses, the isolation of *ELF3* from four independent QTL studies highlights this factor as a core plant growth regulator in shade and warmth. Simultaneously to our approach, a Genome-wide association study (GWAS) was performed for hypocotyl elongation in response to high ambient temperature (Box et al., 2015), with similar results to the ones we obtained for *GIR2*, which strengthened the importance of *ELF3* in the regulation of thermomorphogenesis. *ELF3* was first identified through a mutation (*elf3*) causing early flowering under both long day and short day photoperiods (Zagotta et al., 1996). *ELF3* encodes a protein of 695 amino acids without any previously characterized functional domains with the exception of the presence of a proline-rich region, an acidic region, and a threonine/glutamine-rich region that could potentially play a role in transcriptional activation (Hicks et al., 1996, 2001). Later on, *ELF3* was described as a component of the Evening Complex (EC; LUX-*ELF3*-*ELF4*) with transcription regulatory activities (Nusinow et al., 2011). Specifically, one of the functions described for the EC is repressing growth during the day by inhibiting *PIF4* expression under short photoperiods (Nusinow et al., 2011). In support to its potential function, *ELF3* is a nuclear localized protein (Liu et al., 2001) and barely detectable under continuous darkness, suggesting a role for light in *ELF3* nuclear stabilization (Liu et al., 2001). In fact, *ELF3* protein levels are regulated by the light signaling components COP1

(CONSTITUTIVE PHOTOMORPHOGENIC 1) and PHYB (PHYTOCHROME B). Specifically, the N-terminal part of ELF3 interacts with the C-terminal region of PHYB, probably acting also as a co-factor in the PHYB repression of hypocotyl elongation during the day (Liu et al., 2001). During the night, after COP1/SPA stabilization, ELF3 is dissociated from the EC by COP1 ubiquitination and degraded by the 26S proteasome, allowing growth by PIF4 accumulation. In addition to this, recent studies have suggested that ELF3 repression of PIF4 can occur also during the night in an EC-independent manner by ELF3-PIF4 protein interaction (Nieto et al., 2015). The finding that the A362V point mutation is located in the ELF4, COP1, PHYB interaction region (Li et al., 2001; Nusinow et al., 2011) could potentially impede the correct association with some of its co-regulators or protein localization.

Bay-0 and Sha alleles of *ELF3* have been shown to differentially regulate developmental timing and circadian clock period length in *Arabidopsis* (Anwer et al., 2014). In all cases, ELF3^{Sha} was identified as the allele responsible for the hyperelongation phenotype under both shade and warm conditions (Coluccio et al., 2011; Jiménez-Gómez et al., 2010; Raschke et al., 2015). In Anwer et al. (2014) this phenotype was related with an acceleration of the circadian oscillations in a light-dependent manner, due to a single encoded amino acid change A362V, usually found in high latitudinal stripes in Central Asia (Anwer et al., 2014). Quantification of ELF3-YFP revealed that the nuclear–cytoplasmic ratio of ELF3^{Sha} was four times less than that of ELF3^{Bay} (Anwer et al., 2014), suggesting that the amino acid exchange described in Sha could be compromising ELF3 nuclear localization. If the same scenario holds for warmth conditions, then ELF3^{Sha} might fail to accumulate in the nucleus during the day, allowing higher *PIF4* levels and therefore a longer hypocotyl response at 28°C as observed in the Sha accession. Another possibility not discussed so far is that the ELF3^{Sha} allele could be more unstable or exhibit higher turn-over rates, which may ultimately result in less ELF3 protein in the nucleus to repress PIF4.

In addition to the natural non-synonymous SNP A362V, a difference in the length of the polyglutamine (polyQ) tail was also detected between Bay and Sha (Figure 40; Coluccio et al., 2011). While in mammals, these tandem repeats have been associated with chronic diseases, a role of the polyQ tail in plants

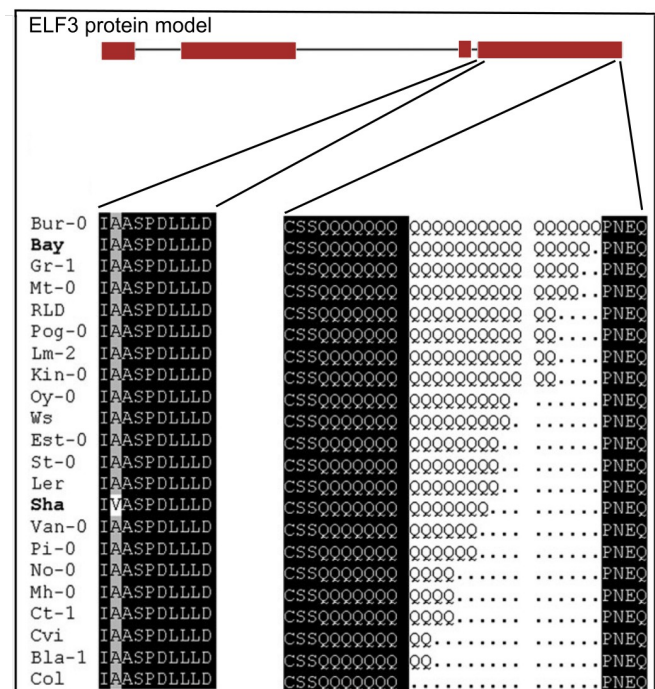


Figure 40. Comparison of ELF3 protein sequences among accessions. A schematic representation of the protein shows a substitution of the conserved alanine (A) by valine (V) in Sha at amino acid position 362 and a variable number of glutamines at amino acid position 544. Red boxes represent the exons along the DNA sequence. Modified from Coluccio et al. (2011).

remains unknown. In *Arabidopsis*, the extent of variation in the C-terminal region of the protein differs between accessions and a role in the control of circadian rhythms, period and phase was proposed (Tajima et al., 2007). Nevertheless, in that study no direct correlation between the length of the polyQ repeats and hypocotyl elongation as found (Tajima et al., 2007). Another study suggested that the alterations in the ELF3 polyQ tail could trigger variations in ELF3-dependent flowering time (Undurraga et al., 2012). In this study, differences in flowering time were observed, but no clear correlation could be established between the copy number of glutamines and the phenotype analyzed. A recent study from Press et al. (2016) managed to show an influence of the polyQ tail on plant thermomorphogenesis. Here, the authors stated that deleting the entire polyQ tract eliminated thermoresponsive hypocotyl elongation. However, variations in the number of glutamines did not show any significant difference (Press et al., 2016). Based on these results, only minor differences on hypocotyl elongation between Bay and Sha depend on their polyQ tail would be expected. Altogether, this supports the idea that the major differences observed in this trait (Figure 12) are caused by the non-synonymous SNP present in the ELF3 coding region between these two accessions.

In addition to *GIR2.1 (ELF3)*, the QTL analysis by multiple testing revealed a second peak in the *GIR2* region (Raschke et al., 2015). As both genes could be separated by mapping, this peak was considered a new gene (*GIR2.2*) that significantly contributes to the phenotypic variation. Such a “Ghost QTL” phenomenon was described for first time by Haley and Knott (Haley and Knott, 1992). Since a “Ghost QTL” is frequently a result of the QTL method used, generally a single QTL analysis method may cause problems in positioning two QTLs that are closely linked; and tend to position only one in between two real QTL positions. Indeed, a similar result was described in Jimenez-Gómez et al. (2010) with the existence of a second gene underlying *SAR2*. Although *GIR2.1* and *GIR2.2* were separated, I could not reconfirm *GIR2.2* by mapping. Nevertheless, the initial confidence interval for *GIR2.2* included PhyB and COP1 chromosomal positions, two major players involved in the regulation of hypocotyl elongation (Huq and Quail, 2002; Wang et al., 2015).

Based on the data presented in this chapter, I can conclude that the circadian clock, specifically ELF3, has an essential role in plant thermomorphogenesis. While ELF3 may buffer temperature fluctuations at normal growth conditions, at high ambient temperatures, ELF3 may be re-localized into the cytoplasm or degraded, allowing *PIF4* expression and protein activity. PIF4 protein accumulation will trigger upregulation of growth-associated genes involved in cell elongation and plant thermomorphogenesis. Recently, another clock component, TOC1, has been characterized to have similar ELF3 mechanistic regulation on PIF4 protein by avoiding its activity in the late evening (Zhu et al., 2016). While ELF3 function is more relevant in the early evening, the function of both proteins on PIF4 repression may overlap. This study highlights

again the importance of the circadian clock in gating growth and hypocotyl elongation under high ambient temperature.

5.4 Brassinosteroids are essential for thermomorphogenesis

Brassinosteroids (BRs) are a group of polyhydroxylated steroid hormones that regulate growth and development. Brassinolide (BL), the most active form of BRs, plays pivotal roles in the hormonal regulation of these processes. However, in contrast to the five classic phytohormones which were characterized in the first half of the 20th century, BL was isolated for first time at the end of the 1970s from *Brassica napus* L. pollen extracts (Grove et al., 1979), and described as a novel steroid growth-promoting compound. In the 1980s, an important role of BRs in cell elongation was shown in different tissue types (Mandava, 1988), reinforcing the important role this hormone has in plant growth and development and specifically on hypocotyl elongation. However, only in the 1990s, when BR mutants started to be characterized, it was considered as a phytohormone involved in the regulation of plant growth (Clouse, 1998). BR biosynthesis and signaling mutants (e.g. *det2*, *cpd*, *bri1*) expose general defects in growth, with dwarfed statures, reduced petiole and leaf length, shorter inflorescence stems and small flowers with reduced male fertility (Clouse, 1998).

Based on the dwarf phenotype of BR mutants, it is not surprising that *dwf7* and *rot3* were isolated from our temperature screen. The observation that these mutants showed a defect in thermomorphogenic responses strongly suggests that BRs are essential for this response. The first evidence for an involvement of BRs in thermomorphogenesis was provided by Gray et al. (1998), who showed a TIHE defect of a BR biosynthesis mutant. Almost 10 years later, BRs were again pointed out to be essential for elongation responses (Stavang et al., 2009). However, in this study, only a general role of phytohormones in seedling thermomorphogenesis was assessed.

One of the common characteristics in BR deficient mutants is a reduction in longitudinal growth, due to a reduced number of cells or failure in cell elongation (Asami et al., 2000). Accordingly, among the phenotypes found in *opi3* and *opi7* mutants a reduction in longitudinal growth was identified. This defect has been previously associated with an impairment in cell elongation in *dwf7* and other BRs mutants (Choe et al., 1999b) it is potentially caused by an impairment in microtubule organization (Catterou et al., 2001).

Despite the role that BRs may have in the control of cell elongation, I could show that the defect *opi3* and *opi7* showed in hypocotyl elongation was not only triggered by a defect in cell elongation, but also cell division (Figure 23). The difference between my data and the data published by Choe et al. (1999) can be due to the difference in the growth conditions used and the organ analyzed. In the study published by Choe et al. (1999), plants were grown at constant 20°C, where indeed Wt and *dwf7/opi7* also had the same number of cells (see Figure 23). In addition to the variation in the growth conditions, Choe et al. (1999) measured cell elongation in

gynoecia and stamens of flowers, while I analyzed seedling development (hypocotyl). Together, these data does not seem contradictory, but the defect that BR mutants display in cell division at high temperatures was unlikely to be visible at standard growth temperatures (20°C). Recent publications have shown that BR mutants exhibit a decrease in mitotic activity and reduced meristem size in roots (Vilarrasa-Blasi et al., 2014). In addition to this, Cheon et al. (2010) reported that the *dwf7-1* mutant exhibited slower cell division rates in roots, which is in agreement with the defect I observed at 28°C. The short root phenotype of the null BR receptor mutant *bri1-116* has also been reported to be caused by defects in both cell expansion and division (González-García et al., 2011). Together, my observations are supported by previous analyses of BR's role in cell elongation and division. In addition, it demonstrates the essential role that this hormone has in response to high ambient temperature.

Plants have multiple pathways for biosynthesis of BL, which are all derived from the steroid specific biosynthetic pathway. In plants, the sterol pathway represents a sequence of more than 30 enzyme-catalyzed reactions. Specifically, *DWF7/STE1/BUL1* encodes for a Δ^7 sterol C-5 desaturase involved in the conversion of episterol in the sterol-specific biosynthetic pathway. After sterol biosynthesis, a mixture of sterols are produced: campesterol, sitosterol and stigmasterol. Since campesterol is not only the end product of this route but the precursor of the BR biosynthesis specific pathway, it is difficult to rule out the possibility that the *opi3/dwf7* phenotype can be caused directly or indirectly by the lack of sterols. The molecular genetic and biochemical analysis of sterol-deficient mutants in *Arabidopsis* strongly suggests an essential role for sterols in regulating multiple events in plant development, independent of their conversion to BRs. Sterols are isoprenoid-derived lipids that have diverse and essential functions in all eukaryotes. Bulk sterols are integral components of the membrane lipid bilayer, where, in conjunction with phospholipids, they regulate membrane permeability and fluidity. In addition, sterols are critical for the formation of liquid-ordered (*lo*) membrane states (lipid "rafts") that are supposed to play an important role in maintaining membranes in a state of fluidity adequate for function (Dufourc, 2008). Taking into account that one of the potential sensing mechanism that plants may have to perceive temperature fluctuations is the change in membrane fluidity; the potential role that the lack of campesterol in *opi3* may have in membrane composition should be considered. Nevertheless, Chung et al. (2010) described that triple mutants on early steps of the BR biosynthesis pathway (*det2, dwf4, smt2*) exhibited a dwarf phenotype inspite of accumulating > 400% more campesterol than Wt plants. This result would suggest that the lack of BRs and not campesterol is the reason for the phenotype observed. Additionally, the pharmacological rescue of *opi3* with epibrassinolide (Figure 25C) strongly suggests that BRs and not sterol deficiency are responsible for the *opi3* phenotype. In any case, a quantification of BR precursors and active forms in *opi3*, and a quantification of the sterol composition would be required to confirm this hypothesis.

Following steroid biosynthesis, campesterol (C28, a total of 28 carbon atoms in the compound) and sitosterol (C29) will be used in the BL biosynthesis specific pathway which produces BL active forms (28-norbrassinolide, brassinolide and 28-homobrassinolide) (Fujioka and Yokota, 2003). This route is based on triterpenoid pathways composed by hydroxylation, reduction, epimerization and oxidation reactions initially thought to follow two parallel pathways: the early C-6 and late C-6 oxidation pathways (Fujioka et al., 1998). The two pathways converge at castasterone (CS), which ultimately leads to the biosynthesis of BL by lactonization of the B ring (Figure 21). The BR biosynthesis enzyme *ROT3* encodes a heme-thiolate protein, CYP90C1 (Kim et al., 1998, 2005). *ROT3*/CYP90C1 and its homolog CYP90D1 catalyze different C-23 hydroxylation steps in the BR-specific biosynthesis pathway (Kim et al., 2005; Ohnishi et al., 2012; Figure 21). *ROT3* has been shown to have a positive role in the elongation of the hypocotyl in response to different light conditions (Kim et al., 2005). Because *ROT3*/CYP90C1 has a homologue, this could explain the difference in the strength of the phenotype between *dwf7* and *rot3* (Figure 24). In addition to this, the BR biosynthesis is composed of redundant steps in the downstream part of the pathway. Based on that, there is only one enzyme that converts episterol (DWF7) but possible shortcuts could be taken if *ROT3* is defective (Figure 21). In any case, the transgenic complementation of *opi7* by *35S:ROT3* will be the confirmation that this gene is underlying the *opi7* mutation. Taken together, the isolation of two BR biosynthesis enzymes (DWF7 and *ROT3*) from this screen and its complementation strengthens the role of BR biosynthesis in thermomorphogenesis.

In addition to the already described role of BRs in cell elongation, BRs have also been described to be involved in carbon fixation. Studies realized in cucumber revealed that plants pre-treated with epibrassinolide exhibited higher a CO₂ assimilation and carboxylation rate of rubisco, as well as a higher quantum efficiency of photosystem II (PSII) in comparison to control non-treated plants (Xia et al., 2009; Yu et al., 2004). Additionally, pre-treated plants exhibited higher concentration of soluble sugars and starch as a consequence of higher photosynthesis efficiency (Xia et al., 2009; Yu et al., 2004). Taking into consideration the sensitivity of the photosynthesis machinery to high ambient temperature, a BR-deficient background may settle more difficulties to offset these environmental conditions. Supporting this hypothesis, a study by Singh and Shono (2005) found epibrassinolide-treated tomato plants as more tolerant to high temperature than untreated plants as a result of high accumulation of heat shock proteins and improvement in photosynthetic efficiency. Similarly, BL treatment to tomato plants prior to high temperature exposure protects rubisco enzyme and RuBP regeneration to provide better protection against warmth (Ogweno et al., 2008). Based on these data, the predicted lack of this hormone in *opi3* and *opi7* could not only affect cell elongation-associated responses at high ambient temperature, but other physiological processes like photosynthesis efficiency, which may ultimately affect plant fitness.

With regard to growth-associated responses, BRs are not controlling plant development alone but tightly coordinated with gibberellin (GA) and auxin (IAA) signaling pathways. Crosstalk regulation between these hormones has been extensively studied in different contexts. However, most of the knowledge is concentrated in light-dependent responses. For instance, BR and GA signaling interactions have been studied extensively in the control of cell expansion during photomorphogenesis (Li et al., 2012), and the molecular role of auxin in thermomorphogenesis has been approached only recently (Wang et al., 2016).

5.5 Auxin-brassinosteroid crosstalk in temperature response

Most of the crosstalk studies performed in recent years between auxin and BRs have been restricted to light responses. While Stavang et al. (2009) had previously described a synergistic interaction of both hormones in hypocotyl elongation in response to warmth, this study together with mine are the only ones approaching this question in a temperature context. My results regarding the auxin and BRs hierarchy show the essential role that BRs have in the temperature response, and highlight the positioning of BR downstream of auxin in this signaling pathway (Chapter III, Figure 28). In line with my data (Figure 28) Nemhauser et al. (2004) showed that the long hypocotyl of *Yucca-D* mutants (which have an overproduction of auxin) is repressed by the *bri1* mutation (BR receptor), suggesting that both hormones are needed for proper organ elongation and BRs act downstream of auxin.

The impairment in hypocotyl elongation of auxin mutants could be rescued by epibrassinolide (Figure 28C), indicating that BRs can overcome the defect of auxin biosynthesis/signaling in response to warmth. While my data confirmed a clear hierarchy at the phenotypical level (IAA → BR) under high ambient temperature, several studies have highlighted the crosstalk between IAA and BR at the transcriptional level in both directions. Studies in *Arabidopsis* and rice have shown that auxin can increase the expression of the BR receptor (BRI1) and BR response genes (Sakamoto and Fujioka, 2013; Sakamoto et al., 2013). In addition, auxin induces BR biosynthesis by activating *DWF4* expression (Chung et al., 2011) and BRs are able to coordinate auxin transport by controlling the expression and localization of PIN1 and PIN2 (Lanza et al., 2012). While most of these data come from standard growth conditions (20°C), we could assume that similar responses would appear also in warm environments. Altogether, this would suggest that the transcriptional cross-regulation observed from BRs towards auxin is probably part of a feed-back/forward mechanism in the regulation of the growth-associated responses. With regard to auxin transport, the candidate gene for the *opi2* mutation, *BIG*, has been described as a putative ubiquitin ligase and a role in regulating PIN1 re-cycling has been suggested (Gil, 2001). However, as PIN1 stabilization in the plasma membrane is mainly regulated by phosphorylation of its hydrophilic loop (Huang et al., 2010) and the absence of N-degron recognition sites in the PIN1 sequence, a direct regulation of PIN1 by *BIG* is unlikely. Another more likely scenario is that *BIG* may be controlling general subcellular trafficking

mechanisms and PIN1 mislocalization in *tir3* is a consequence of it. In any case, the defect of PIN1 recycling in *tir3* could also involve other vesicular trafficking components such as GNOM/ARF, direct targets of BFA which are directly involved in polar distribution of PIN auxin efflux carriers. Due to the essential role of auxin transport in thermomorphogenesis (Chapman et al., 2012; Gray et al., 1998), the potential defect of auxin transport in the *opi2* background may trigger the phenotype observed in this mutant (Figure 15). In contrast to auxin, BRs are not transported along the plant. Because of that, BR synthesis and signaling are tightly regulated in a local (spatio/temporal) manner, and auxin may be needed for it. Indeed, IAA and BR seem to have a cooperative role in the shoot, while recent studies in the root have shown that both hormones act antagonistically in the regulation of cell elongation/ division ratios (Chaiwanon and Wang, 2015; González-García et al., 2011). There, BRs may be tightly controlling intracellular auxin levels to allow elongation in a cell-specific manner, and a primary and secondary response via IAA and BRs respectively could also be hypothesized. For instance, auxin responsive genes are activated within the first hour after exposition to shade, while BR responsive genes have been reported to peak after 4-5 hours (Labusch et al., 2016). Recently, a tripartite regulatory network BZR1-ARF6-PIF4 (BAP) was proposed between PIF4, auxin and BRs signaling pathways (Oh et al., 2012) to act cooperatively in the regulation of growth-associated genes (Figure 41A). Indeed, Auxin (ARFs) and BR transcription factors (BZR1/BZR2) have more than 40% common targets involved in growth processes (Oh et al., 2014). These genes are mainly regulating cell elongation and auxin response (*PINs* and *SAURs*; Oh et al., 2014). While the BAP module was described to participate in growth regulation under different light conditions, no evidence exists (although likely) that

it works also under temperature responses. The observation that the loss-of-function *arf6/arf8* exhibited a Wt response in the TIHE assay (Figure 41A) suggests that BZR1 and PIF4 but not ARF6/8 are essential for a proper response to high ambient temperature. Nevertheless, some ARFs target genes still respond to auxin in *pif4pif5* mutants (Chapman et al., 2012; Nozue et al., 2011), which may suggest that auxin activates independent responses from BZR1-PIF4 by using other ARFs (Figure 41B).

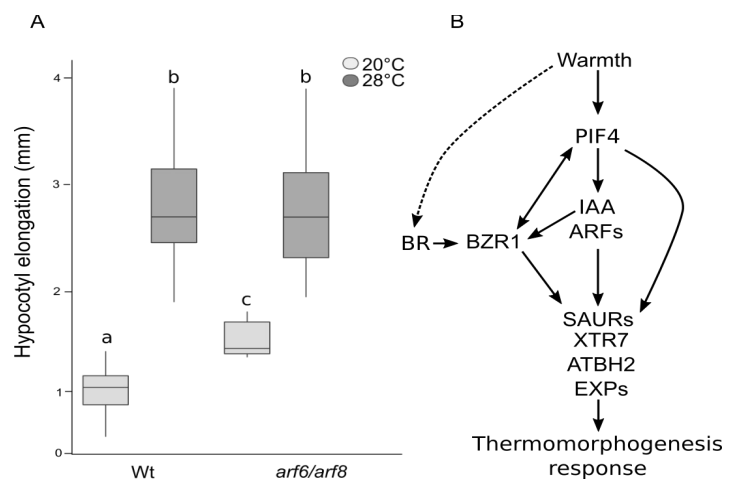


Figure 41. Auxin and brassinosteroids in the regulation of thermomorphogenesis. (A) TIHE response of *arf6/arf8* to high ambient temperature. Hypocotyl elongation of 7 day-old seedlings grown at 20°C (light gray) or shifted to 28°C (3d 20°C +4d 28°C). (B) Predicted transcriptional regulation in response to warm temperature. BZR1 and PIF4 control the expression of temperature induced genes involved in thermomorphogenesis. Auxin, upstream of brassinosteroids may regulate transcriptional expression dependent and independently of the BZR1/PIF4 module. Whether BR biosynthesis and PIF4 are directly regulated by temperature remains unknown (dashed lines).

5.6 BZR1 regulates temperature signaling by gating PIF4

PIF4 was initially described to act upstream of auxin (Sun et al., 2012) and my data confirmed BRs being downstream of both in the temperature signaling pathway (Figure 28). Based on that, a linear signaling cascade could be speculated. Nevertheless, the *pif4* elongation defect at 28°C could not be fully rescued by BL or picloram exogenously supplemented into the media (Figure 27), suggesting that these hormones can partially offset the lack of *pif4* but do not fully overcome its function. Hence, a cooperative mechanism becomes a more likely scenario. Due to the crucial role that PIF4 has in temperature response, a tight regulation at transcriptional and post-translational levels is expected. I presented ELF3 (Chapter II; Raschke et al., 2015) and HY5/DET1 (Chapter III; Delker et al., 2014) as negative regulators controlling *PIF4* transcription and activity in the temperature response. Recently, a study by Gangappa and Kumar (2017) highlighted the role of DET1 and COP1 in temperature-induced *PIF4* expression and hypocotyl elongation. In addition, upregulation of *PIF4* expression in *BZR1* overexpression lines (Figure 30) suggested BZR1 as a novel positive regulator of *PIF4*. Based on protoplast transient expression assays and ChIP-PCR results (Figure 32) I could confirm that this regulation directly is associated to BZR1 interacting with E-box elements on *PIF4* promoter region.

Based on binding-association studies using genome-wide chromatin immunoprecipitation, E-boxes (CANNTG) are predominantly distributed in BR-induced genes while BRRE sites are preferentially found on the promoters of BR repressed genes (Sun et al., 2010). Hence, BZR1 was suggested to have a dual role in the regulation of gene expression (He, 2005). BZR1 can work as heterodimer or homodimer, suggesting that it may change its recognition site depending on its co-regulator. In fact, TOPLESS mediates BR-induced transcriptional repression through interaction with the BZR1-EAR domain (Oh et al., 2014), BZR1-WRKY40 association leads to repression of defense genes (Zhu et al., 2013), and BZR1 association with PIFs and ARFs trigger the upregulation of growth-associated genes (Oh et al., 2014). Furthermore, BZR1 is able to repress BR biosynthesis genes when BR signals are activated by BZR1-BZR1 homodimers on the promoter of target genes. Under this scenario, where BZR1 can regulate its activity depending on its “associated partner”, a likely hypothesis is that BZR1 activates *PIF4* expression by PIF4-BZR1 heterodimerization. Indeed, it has been suggested that PIF4 may regulate its own expression but whether this is done alone or together with BZR1 is unknown. In this work I could show *in vitro* and *in vivo* that BZR1 may be regulating *PIF4* expression. To further study if this regulation relies on PIF4 association, protoplast assays co-expressing 35S:BZR1 and PIF4p:LUC in the *pif4/pifq* mutant backgrounds could be realized. Moreover, to test if BZR1 is strictly required for temperature-induced *PIF4* expression, analysis of *PIF4* in a *bzr1* knock out should ideally be carried on. However, no real knock out has been so far characterized.

In addition to BZR1 enrichment in E-box elements in the *PIF4* promoter (Figure 32C), I could also observe an enrichment of BZR1 on the BRRE element at 20°C (Figure 32C). This may suggest that BZR1 is able to activate and repress *PIF4* expression to regulate plant growth in a temperature-dependent manner. Whether BZR1 is able to repress *PIF4* expression by its own or whether it needs another binding co-factor is unknown. BZR1-HY5 interact in response to light (Li and He, 2016) and I could also detect accumulation of ELF3 protein levels in presence of BL (*Appendix V*), which suggests that these proteins could be involved directly or indirectly in *PIF4* regulation together with BZR1. While *PIF4* expression increases under high ambient temperature (Figure 30; Oh et al., 2012), the mechanism underlying this observation remains unknown. Based on my results, BZR1 may be involved in temperature-induced *PIF4* expression. Due to the high temperature-specific response observed in BZR1 overexpression lines (Figure 30, Figure 32), this transcription factor could be one of the ways for *PIF4* to sense ambient temperature and BZR1 may be involved in the control of this process by *PIF4*/BZR1 heterodimerization. However, I did not detect transcriptional regulation of *BZR1* by temperature (Figure 33A), suggesting that BZR1 regulation may occur at the post-transcriptional level (Li and He, 2016; Oh et al., 2012). In fact, BZR1 has been reported to be regulated post-transcriptionally by BIN2 phosphorylation (He et al., 2002). In low BR levels, BZR1 is phosphorylated by BIN2 and thereby inactivated. After inactivation, BZR1 may remain in the nucleus or be moved out to the cytoplasm by the 14-3-3 kinases, where it will be degraded by the 26S proteasome. In darkness, there is an increase of BZR1 dephosphorylated forms and consequently higher activity (Li and He, 2016). While we could assume a similar scenario under high ambient temperatures, Oh et al. (2012) reported no changes in phosphorylation status between 20°C and 28°C nor changes in protein abundance and we could confirm that under our experimental conditions (Figure 33). However, analysis of protein abundance and phosphorylation status were performed with total protein extract. Eluted and bound nuclear protein fractions obtained from the ChIP assay (Figure 34) revealed a stronger accumulation of BZR1 at 28°C than at 20°C in the nucleus, and this observation could be confirmed by confocal microscopy (Figure 35). This correlates with a potential higher activity of BZR1 at 28°C.

Thus, I could not detect changes on BZR1 phosphorylation status nor changes in the expression levels, the regulatory mechanism underlying BZR1 stabilization in the nucleus remains so far unknown. Prior to BZR1 phosphorylation, BIN2 interacts with the C-terminal region of BZR1 and phosphorylates its N-terminal which is potentially involved in DNA binding and *PIF4* interaction (Ryu et al., 2007; Wang et al., 2012). Therefore, a potential *PIF4*-BIN2 competitive mechanism could be regulating BZR1 activity or nuclear localization. If that would be the case, after *PIF4* protein stabilization by high temperature, BIN2 inactivation and BZR1/*PIF4* dimer formation, BZR1-*PIF4* association could retain BZR1 in the nucleus. Indeed, BZR1 has 25 Ser/Thr residues potentially involved in its subcellular distribution, but the mutation of the two BIN2

phosphorylation sites present in the DNA binding domain are enough to retain BZR1 in the nucleus (Ryu et al., 2007). Interestingly, that domain is also involved in PIF4-BZR1 protein interaction. Based on this, another possibility could be that PIF4 is sensing temperature cues independently of BZR1 and then translates this information to BZR1 in order to activate the expression of growth-associated genes. If that would be the case, PIF4 may trigger BZR1 accumulation in the nucleus to upregulate its own expression as part of a feed-forward mechanism.

Taking into account that BIN2 not only phosphorylates BZR1 but also PIF4 and that both transcription factors appear to respond to temperature increases, the next question to be addressed was whether the presence of both transcription factors is strictly necessary for temperature-induced hypocotyl elongation. I therefore performed additional experiments to address this issue. For that purpose, I used the activator effect of PPZ towards the BIN2 kinase that will phosphorylate PIF4 and BZR1 under low BR and therefore repressing hypocotyl elongation. The PIF41A mutant which has a mutation in the BIN2 phosphorylation site, and is insensitive to PPZ (Bernardo-García et al., 2014), lost its temperature-induced-hypocotyl elongation phenotype in the presence of PPZ (Figure 36). This result indicates that under our growth conditions, PIF4 alone can not overcome the lack of BZR1 (triggered by the presence of PPZ), and that both transcription factors are needed for the TIHE response. This confirms published data showing that the *bri1* mutant (with inactive BZR1) represses the long hypocotyl phenotype of *35S:PIF4* (Oh et al., 2012). In contrast, the observation that PIF41A showed PPZ insensitivity under red light (Bernardo-García et al., 2014) suggests that BZR1 may not be strictly necessary for hypocotyl elongation under these light conditions.

5.7 BZR1 and ELF3 as antagonistic regulators of *PIF4* expression and activity

BZR1 and ELF3 are highlighted in this work as factors involved in regulating *PIF4* expression levels and thereby also protein activity in a light- and temperature-dependent manner. In accordance with published data, during the day PhyB is translocated to the nucleus where it promotes ELF3 accumulation by disrupting COP1-ELF3 interaction (Liu et al., 2001; Nieto et al., 2015; Reed et al., 2000). Stabilized ELF3 will bind to the PIF4 bHLH domain and block its transcriptional activity (Nieto et al., 2015). Additionally, the EC represses *PIF4* expression by binding to LUX-Binding-Sites on the *PIF4* promoter. During the night, COP1 stabilization triggers ubiquitination and degradation of ELF3 (Wang et al., 2015), allowing PIF4 protein accumulation and induction of temperature-responsive genes. As mentioned before, I could not observe temperature-dependent induction of *PIF4* expression during the day, suggesting that light components are tightly regulating growth during the day (in long day photoperiods) by overcoming temperature cues (see external coincidence mechanism, described above). The observation that *ELF3* overexpression lines exhibit a short hypocotyl (Nieto et al., 2015) and *elf3*

loss-of-function a “temperature-induced phenotype” (=long hypocotyl; Figure 13), confirms the negative role of ELF3 in the regulation of hypocotyl elongation. The short hypocotyl phenotype of *ELF3* overexpression lines could be rescued by adding epiBL to the media (data not shown), suggesting that BR signaling is acting downstream of ELF3 and is able to overcome PIF4 protein repression of this negative regulator. In that regard, hormones have been described to impact on the circadian clock. Specifically, BR affects periodicity of the clock (Hanano et al., 2006), which could potentially reflect higher growth rates observed in BL-treated plants or plants exposed to high ambient temperature.

In addition, I could observe nuclear ELF3 accumulation in BL-treated seedlings in darkness (*Appendix V*). This suggests that BL may be able to offset potential regulatory mechanisms in ELF3 protein stability. However, no visual changes in COP1:GFP protein accumulation was observed between epiBL pre-treated and mock control samples (data not shown). As mentioned before, ELF3 regulatory function on *PIF4* expression and protein activity can be dependent or independent on the EC. Hence, whether ELF3 accumulation in response to BL is EC-dependent should be further studied. Given the fact that ELF3 does not repress *PIF4* expression directly but through LUX, elucidating this question would give more information about the role of ELF3 under high BL conditions. Theoretically, if the accumulation of ELF3 by BL occurs independently of the EC, the function of ELF3 towards PIF4 may be exclusively in the regulation of PIF4 protein activity. The observation that BL triggers the accumulation of a negative regulator of growth while being at the same time a strong growth promoter was already reported for the DELLAs (Li et al., 2012). Stewart Lilley and colleagues (2013) revealed RGA accumulation in the nucleus in BL pre-treated seedlings. While this initially appears to be a contradictory response due to role of DELLAs in repressing growth, also it indicates that BRs may have a strong potential in fine-tuning growth by activating and repressing different mechanisms in order to ensure a moderate physiological response at the phenotypic level. For instance, PhyA represses PIF1 to prevent over-activation of photomorphogenesis (Krzymuski et al., 2014; Shen et al., 2008). A similar case was reported for HFR1, which accumulates to repress PIF4 protein activity under high temperatures (Foreman et al., 2011). In any case, the temperature influence on ELF3 accumulation by BL should be further studied.

5.8 The current model of temperature signal transduction

The model I propose for the temperature signal transduction pathway supports the major role of PIF4 in the regulation of thermomorphogenesis and highlights the BR signaling component BZR1 as a novel positive regulator of the pathway. In addition, ELF3 appears here as a negative regulator of temperature-induced plant morphology by regulating PIF4 not only under shade conditions but also in a temperature-dependent manner (Chapter II).

In warm environments, the negative regulators HY5 and PHYB will become inactive or degraded by COP1 and DET1 activities, allowing PIF4 protein stabilization (Delker et al., 2014; Legris et

al., 2016). Additionally, ELF3 and PHYB will be released (probably triggered by conformational changes) from the promoter region of *PIF4* and temperature-induced genes, respectively (Box et al., 2015; Jung et al., 2016). High BR conditions are presumed under high ambient temperature, which will inactivate BIN2 and stabilize BZR1 in the nucleus. After nuclear stabilization, PIF4 may also trigger BZR1 accumulation in the nucleus by PIF4-BZR1 dimer formation. BZR1/PIF4 heterodimers will upregulate *PIF4* expression as part of a feed-forward mechanism by binding to its cis-elements present on the *PIF4* promoter. Additionally, PIF4/BZR1 will induce common target genes involved in cell elongation and growth responses. Activation of these genes will mainly involve SAURs and cell wall modifiers, which will ultimately trigger the thermomorphogenesis response observed. As a feed-back mechanism, BRs may enhance ELF3 and DELLA protein accumulation to repress PIF4 and moderate the physiological response (Figure 42).

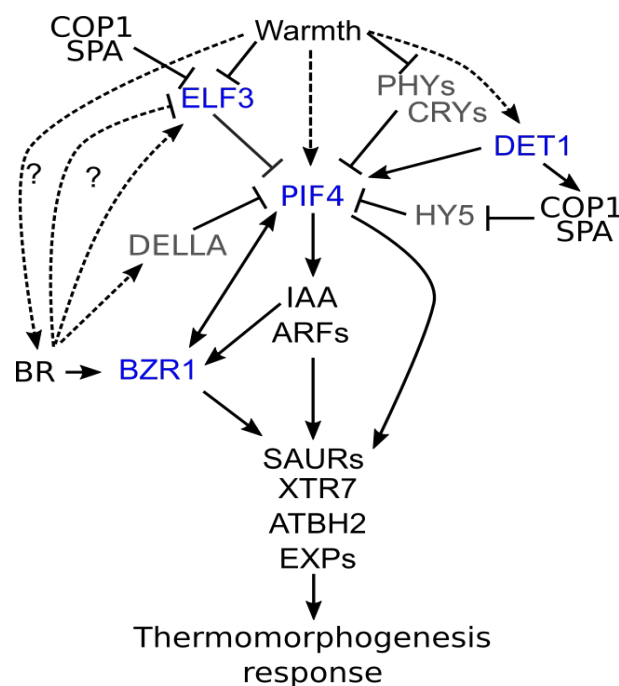


Figure 42. Simplified model proposed for temperature signal transduction. Increase in ambient temperature is perceived and integrated by PHB, CRY1 and the EC (ELF3-ELF4-LUX), that will be re-localized or inactivated. De-phosphorylated BZR1 will form heterodimers with PIF4 to induce *PIF4* and BZR1/PIF4 common target genes expression triggering thermal growth. As part of a feed-back mechanism, BL could potentially trigger the accumulation of ELF3 and DELLA proteins in the nucleus to fine-tune the elongation response. Dashed-arrows represent predicted regulatory mechanisms not shown so far at high ambient temperature. Temperature-induced destabilization components are gray-colored. Blue-colored players represent the main contributions of my work to the model.

6. Conclusions

While plants show a remarkable plasticity to survive a continuously changing environment, exposition to increased high ambient temperature is projected to threaten future crop yields and food security. This work is focused on trying to better understand the morphological and molecular changes plants activate in response to warmth. Comprehensive profiling of *Arabidopsis thaliana* growth and development in response to different ambient temperatures have revealed profound effects of temperature on plant morphology and highlighted optimal accessions for further screens. In addition, using hypocotyl elongation as a model phenotype, forward-genetic screens identified ELF3 and the brassinosteroids as novel components of the temperature signal transduction pathway, with an essential thermostat function. Specifically, I found strong evidence that ELF3 and BZR1 may control *PIF4* expression in order to regulate thermomorphogenesis. In light of these discoveries, the study of BZR1 regulation under high ambient temperature would add valuable information to the current temperature signal transduction. In summary, BRs are shown here to regulate three different levels of the temperature signal transduction downstream, upstream and at the level of PIF4, which highlights the relevance of this phytohormone in controlling the temperature signaling cascade.

7. Bibliography

- Anwer, M.U., Boikoglou, E., Herrero, E., Hallstein, M., Davis, A.M., James, G.V., Nagy, F., and Davis, S.J. (2014). Natural variation reveals that intracellular distribution of ELF3 protein is associated with function in the circadian clock. *eLife* 3, e02206.
- Asami, T., Min, Y.K., Nagata, N., Yamagishi, K., Takatsuto, S., Fujioka, S., Murofushi, N., Yamaguchi, I., and Yoshida, S. (2000). Characterization of Brassinazole, a Triazole-Type Brassinosteroid Biosynthesis Inhibitor. *Plant Physiol.* 123, 93–100.
- Asseng, S., Ewert, F., Martre, P., Rotter, R.P., Lobell, D.B., Cammarano, D., Kimball, B.A., Ottman, M.J., Wall, G.W., White, J.W., et al. (2015). Rising temperatures reduce global wheat production. *Nat. Clim Change* 5, 143–147.
- Athanasίου, K., Dyson, B.C., Webster, R.E., and Johnson, G.N. (2010). Dynamic Acclimation of Photosynthesis Increases Plant Fitness in Changing Environments. *Plant Physiol.* 152, 366–373.
- Azpiroz, R., Wu, Y., LoCascio, J.C., and Feldmann, K.A. (1998). An Arabidopsis brassinosteroid-dependent mutant is blocked in cell elongation. *Plant Cell* 10, 219–230.
- Balasubramanian, S., and Weigel, D. (2006). Temperature Induced Flowering in Arabidopsis thaliana. *Plant Signal. Behav.* 1, 227–228.
- Bauer, D., Viczián, A., Kircher, S., Nobis, T., Nitschke, R., Kunkel, T., Panigrahi, K.C.S., Adám, E., Fejes, E., Schäfer, E., et al. (2004). Constitutive photomorphogenesis 1 and multiple photoreceptors control degradation of phytochrome interacting factor 3, a transcription factor required for light signaling in Arabidopsis. *Plant Cell* 16, 1433–1445.
- Belkhadir, Y., and Jaillais, Y. (2015). The molecular circuitry of brassinosteroid signaling. *New Phytol.* 206, 522–540.
- Bernardo-García, S., de Lucas, M., Martínez, C., Espinosa-Ruiz, A., Davière, J.-M., and Prat, S. (2014). BR-dependent phosphorylation modulates PIF4 transcriptional activity and shapes diurnal hypocotyl growth. *Genes Dev.* 28, 1681–1694.
- Bertani, G. (1951). Studies on lysogenesis. I. The mode of phage liberation by lysogenic Escherichia coli. *J. Bacteriol.* 62, 293–300.
- Box, M.S., Huang, B.E., Domijan, M., Jaeger, K.E., Khattak, A.K., Yoo, S.J., Sedivy, E.L., Jones, D.M., Hearn, T.J., Webb, A.A.R., et al. (2015). ELF3 Controls Thermoresponsive Growth in Arabidopsis. *Curr. Biol.* 25, 194–199.
- Casal, J.J. (2012). Shade Avoidance. *Arab. Book Am. Soc. Plant Biol.* 10.
- Catterou, M., Dubois, F., Schaller, H., Aubanelle, L., Vilcot, B., Sangwan-Norreel, B.S., and Sangwan, R.S. (2001). Brassinosteroids, microtubules and cell elongation in Arabidopsis thaliana. I. Molecular, cellular and physiological characterization of the Arabidopsis bull mutant, defective in the delta 7-sterol-C5-desaturation step leading to brassinosteroid biosynthesis. *Planta* 212, 659–672.
- Chaiwanon, J., and Wang, Z.-Y. (2015). Spatiotemporal Brassinosteroid Signaling and Antagonism with Auxin Pattern Stem Cell Dynamics in Arabidopsis Roots. *Curr. Biol.* 25, 1031–1042.

- Chapman, E.J., Greenham, K., Castillejo, C., Sartor, R., Bialy, A., Sun, T., and Estelle, M. (2012). Hypocotyl Transcriptome Reveals Auxin Regulation of Growth-Promoting Genes through GA-Dependent and -Independent Pathways. *PLoS ONE* 7, e36210.
- Cheon, J., Park, S.-Y., Schulz, B., and Choe, S. (2010). Arabidopsis brassinosteroid biosynthetic mutant dwarf7-1 exhibits slower rates of cell division and shoot induction. *BMC Plant Biol.* 10, 270.
- Choe, S., Dilkes, B.P., Gregory, B.D., Ross, A.S., Yuan, H., Noguchi, T., Fujioka, S., Takatsuto, S., Tanaka, A., Yoshida, S., et al. (1999a). The Arabidopsis dwarf1 mutant is defective in the conversion of 24-methylenecholesterol to campesterol in brassinosteroid biosynthesis. *Plant Physiol.* 119, 897–907.
- Choe, S., Noguchi, T., Fujioka, S., Takatsuto, S., Tissier, C.P., Gregory, B.D., Ross, A.S., Tanaka, A., Yoshida, S., Tax, F.E., et al. (1999b). The Arabidopsis dwarf7/ste1 mutant is defective in the delta7 sterol C-5 desaturation step leading to brassinosteroid biosynthesis. *Plant Cell* 11, 207–221.
- Christin, P.-A., and Osborne, C.P. (2014). The evolutionary ecology of C4 plants. *New Phytol.* 204, 765–781.
- Chung, H.Y., Fujioka, S., Choe, S., Lee, S., Lee, Y.H., Baek, N.I., and Chung, I.S. (2010). Simultaneous suppression of three genes related to brassinosteroid (BR) biosynthesis altered campesterol and BR contents, and led to a dwarf phenotype in Arabidopsis thaliana. *Plant Cell Rep.* 29, 397–402.
- Chung, Y., Maharjan, P.M., Lee, O., Fujioka, S., Jang, S., Kim, B., Takatsuto, S., Tsujimoto, M., Kim, H., Cho, S., et al. (2011). Auxin stimulates DWARF4 expression and brassinosteroid biosynthesis in Arabidopsis: Auxin-induced expression of DWF4. *Plant J.* 66, 564–578.
- Clouse, S.D., and Sasse, J.M. (1998). BRASSINOSTEROIDS: Essential Regulators of Plant Growth and Development. *Annu. Rev. Plant Physiol. Plant Mol. Biol.* 49, 427–451.
- Coluccio, M.P., Sanchez, S.E., Kasulin, L., Yanovsky, M.J., and Botto, J.F. (2011). Genetic mapping of natural variation in a shade avoidance response: ELF3 is the candidate gene for a QTL in hypocotyl growth regulation. *J. Exp. Bot.* 62, 167–176.
- Crawford, A.J., McLachlan, D.H., Hetherington, A.M., and Franklin, K.A. (2012). High temperature exposure increases plant cooling capacity. *Curr. Biol.* 22, R396–R397.
- Delker, C., Pöschl, Y., Raschke, A., Ullrich, K., Ettingshausen, S., Hauptmann, V., Grosse, I., and Quint, M. (2010). Natural variation of transcriptional auxin response networks in Arabidopsis thaliana. *Plant Cell* 22, 2184–2200.
- Delker, C., Sonntag, L., James, G.V., Janitza, P., Ibañez, C., Ziermann, H., Peterson, T., Denk, K., Mull, S., Ziegler, J., et al. (2014). The DET1-COP1-HY5 pathway constitutes a multipurpose signaling module regulating plant photomorphogenesis and thermomorphogenesis. *Cell Rep.* 9, 1983–1989.
- Delker, C., van Zanten, M., and Quint, M. (2017). Thermosensing Enlightened. *Trends Plant Sci.*
- Devlin, P.F., and Kay, S.A. (1999). Cryptochromes--bringing the blues to circadian rhythms. *Trends Cell Biol.* 9, 295–298.
- Dufourc, E.J. (2008). Sterols and membrane dynamics. *J. Chem. Biol.* 1, 63–77.
- Engler, C., and Marillonnet, S. (2014). Golden Gate cloning. *Methods Mol. Biol. Clifton NJ* 1116, 119–131.

- Erwin, J.E., Heins, R.D., and Karlsson, M.G. (1989). Thermomorphogenesis in *Lilium longiflorum*. *Am. J. Bot.* **76**, 47–52.
- Foreman, J., Johansson, H., Hornitschek, P., Josse, E.-M., Fankhauser, C., and Halliday, K.J. (2011). Light receptor action is critical for maintaining plant biomass at warm ambient temperatures. *Plant J. Cell Mol. Biol.* **65**, 441–452.
- Franklin, K.A., Lee, S.H., Patel, D., Kumar, S.V., Spartz, A.K., Gu, C., Ye, S., Yu, P., Breen, G., Cohen, J.D., et al. (2011). PHYTOCHROME-INTERACTING FACTOR 4 (PIF4) regulates auxin biosynthesis at high temperature. *Proc. Natl. Acad. Sci.* **108**, 20231–20235.
- Franklin, K.A., Toledo-Ortiz, G., Pyott, D.E., and Halliday, K.J. (2014). Interaction of light and temperature signalling. *J. Exp. Bot.*; **65**(11):2859-2871.
- Franklin, K.A. and Wigge, P., (2014). *Temperature and Plant development*. John Wiley & Sons. N. p.
- Fujioka, S., and Yokota, T. (2003). Biosynthesis and metabolism of brassinosteroids. *Annu. Rev. Plant Biol.* **54**, 137–164.
- Fujioka, S., Noguchi, T., Yokota, T., Takatsuto, S., and Yoshida, S. (1998). Brassinosteroids in *Arabidopsis thaliana*. *Phytochemistry* **48**, 595–599.
- Gampala, S.S., Kim, T.-W., He, J.-X., Tang, W., Deng, Z., Bai, M.-Y., Guan, S., Lalonde, S., Sun, Y., Gendron, J.M., et al. (2007). An Essential Role for 14-3-3 Proteins in Brassinosteroid Signal Transduction in *Arabidopsis*. *Dev. Cell* **13**, 177–189.
- Gangappa, S.N., and Kumar, S.V. (2017). DET1 and HY5 Control PIF4-Mediated Thermosensory Elongation Growth through Distinct Mechanisms. *Cell Rep.* **18**, 344–351.
- Gay, L., Neubauer, G., Zagalska-Neubauer, M., Pons, J.-M., Bell, D.A., and Crochet, P.-A. (2008). Speciation with gene flow in the large white-headed gulls: does selection counterbalance introgression? *Heredity* **102**, 133–146.
- Gentile, C., Sehadova, H., Simoni, A., Chen, C., and Stanewsky, R. (2013). Cryptochrome antagonizes synchronization of *Drosophila*'s circadian clock to temperature cycles. *Curr. Biol. CB* **23**, 185–195.
- Gil, P. (2001). BIG: a calossin-like protein required for polar auxin transport in *Arabidopsis*. *Genes Dev.* **15**, 1985–1997.
- González-García, M.-P., Vilarrasa-Blasi, J., Zhiponova, M., Divol, F., Mora-García, S., Russinova, E., and Caño-Delgado, A.I. (2011). Brassinosteroids control meristem size by promoting cell cycle progression in *Arabidopsis* roots. *Development* **138**, 849–859.
- Gould, P.D., Ugarte, N., Domijan, M., Costa, M., Foreman, J., Macgregor, D., Rose, K., Griffiths, J., Millar, A.J., Finkenstädt, B., et al. (2013). Network balance via CRY signalling controls the *Arabidopsis* circadian clock over ambient temperatures. *Mol. Syst. Biol.* **9**, 650.
- Gray, W.M., Östin, A., Sandberg, G., Romano, C.P., and Estelle, M. (1998). High temperature promotes auxin-mediated hypocotyl elongation in *Arabidopsis*. *Proc. Natl. Acad. Sci. U. S. A.* **95**, 7197–7202.
- Grove, M.D., Spencer, G.F., Rohwedder, W.K., Mandava, N., Worley, J.F., Warthen, J.D., Steffens, G.L., Flippen-Anderson, J.L., and Cook, J.C. (1979). Brassinolide, a plant growth-promoting steroid isolated from *Brassica napus* pollen. *Nature* **281**, 216–217.

- Guo, X., Lu, W., Ma, Y., Qin, Q., and Hou, S. (2013). The BIG gene is required for auxin-mediated organ growth in *Arabidopsis*. *Planta* 237, 1135–1147.
- Haley, C.S., and Knott, S.A. (1992). A simple regression method for mapping quantitative trait loci in line crosses using flanking markers. *Heredity* 69, 315–324.
- Hanano, S., Domagalska, M.A., Nagy, F., and Davis, S.J. (2006). Multiple phytohormones influence distinct parameters of the plant circadian clock. *Genes Cells* 11, 1381–1392.
- Harrison, S.J., Mott, E.K., Parsley, K., Aspinall, S., Gray, J.C., and Cottage, A. (2006). A rapid and robust method of identifying transformed *Arabidopsis thaliana* seedlings following floral dip transformation. *Plant Methods* 2, 19.
- He, J.-X. (2005). BZR1 Is a Transcriptional Repressor with Dual Roles in Brassinosteroid Homeostasis and Growth Responses. *Science* 307, 1634–1638.
- He, J.-X., Gendron, J.M., Yang, Y., Li, J., and Wang, Z.-Y. (2002). The GSK3-like kinase BIN2 phosphorylates and destabilizes BZR1, a positive regulator of the brassinosteroid signaling pathway in *Arabidopsis*. *Proc. Natl. Acad. Sci.* 99, 10185–10190.
- Hicks, K.A., Millar, A.J., Carre, I.A., Somers, D.E., Straume, M., Meeks-Wagner, D.R., and Kay, S.A. (1996). Conditional Circadian Dysfunction of the *Arabidopsis* early-flowering 3 Mutant. *Science* 274, 790–792.
- Hicks, K.A., Albertson, T.M., and Wagner, D.R. (2001). EARLY FLOWERING3 encodes a novel protein that regulates circadian clock function and flowering in *Arabidopsis*. *Plant Cell* 13, 1281–1292.
- Hoffmann, A.A., and Sgrò, C.M. (2011). Climate change and evolutionary adaptation. *Nature* 470, 479–485.
- Huang, F., Kemel Zago, M., Abas, L., van Marion, A., Galván-Ampudia, C.S., and Offringa, R. (2010). Phosphorylation of Conserved PIN Motifs Directs *Arabidopsis* PIN1 Polarity and Auxin Transport[W][OA]. *Plant Cell* 22, 1129–1142.
- Huq, E., and Quail, P.H. (2002). PIF4, a phytochrome-interacting bHLH factor, functions as a negative regulator of phytochrome B signaling in *Arabidopsis*. *EMBO J.* 21, 2441–2450.
- Ibanez, C., Poeschl, Y., Peterson, T., Bellstaedt, J., Denk, K., Gogol-Doering, A., Quint, M., and Delker, C. (2015). Developmental and phenotypic plasticity of *Arabidopsis thaliana* accessions across an ambient temperature range. *BioRxiv*
- IPCC. Climate change 2014: Impacts, adaptation and vulnerability
- Jiménez-Gómez, J.M., Wallace, A.D., and Maloof, J.N. (2010). Network analysis identifies ELF3 as a QTL for the shade avoidance response in *Arabidopsis*. *PLoS Genet.* 6, e1001100.
- Johansson, H., Jones, H.J., Foreman, J., Hemsted, J.R., Stewart, K., Grima, R., and Halliday, K.J. (2014). *Arabidopsis* cell expansion is controlled by a photothermal switch. *Nat. Commun.* 5, 4848.
- Jung, J.-H., Domijan, M., Klose, C., Biswas, S., Ezer, D., Gao, M., Khattak, A.K., Box, M.S., Charoensawan, V., Cortijo, S., et al. (2016). Phytochromes function as thermosensors in *Arabidopsis*. *Science*.
- Kim, G.T., Tsukaya, H., and Uchimiya, H. (1998). The ROTUNDIFOLIA3 gene of *Arabidopsis thaliana* encodes a new member of the cytochrome P-450 family that is required for the regulated polar elongation of leaf cells. *Genes Dev.* 12, 2381–2391.

- Kim, G.-T., Fujioka, S., Kozuka, T., Tax, F.E., Takatsuto, S., Yoshida, S., and Tsukaya, H. (2005). CYP90C1 and CYP90D1 are involved in different steps in the brassinosteroid biosynthesis pathway in *Arabidopsis thaliana*. *Plant J. Cell Mol. Biol.* *41*, 710–721.
- Kim, T.-W., Guan, S., Sun, Y., Deng, Z., Tang, W., Shang, J.-X., Sun, Y., Burlingame, A.L., and Wang, Z.-Y. (2009). Brassinosteroid signal transduction from cell-surface receptor kinases to nuclear transcription factors. *Nat. Cell Biol.* *11*, 1254–1260.
- Koini, M.A., Alvey, L., Allen, T., Tilley, C.A., Harberd, N.P., Whitelam, G.C., and Franklin, K.A. (2009). High Temperature-Mediated Adaptations in Plant Architecture Require the bHLH Transcription Factor PIF4. *Curr. Biol.* *19*, 408–413.
- Krzymuski, M., Cerdán, P.D., Zhu, L., Vinh, A., Chory, J., Huq, E., and Casal, J.J. (2014). Phytochrome A antagonizes PHYTOCHROME INTERACTING FACTOR 1 to prevent over-activation of photomorphogenesis. *Mol. Plant* *7*, 1415–1428.
- Kumar, S.V., and Wigge, P.A. (2010). H2A.Z-containing nucleosomes mediate the thermosensory response in *Arabidopsis*. *Cell* *140*, 136–147.
- Lanza, M., Garcia-Ponce, B., Castrillo, G., Catarecha, P., Sauer, M., Rodriguez-Serrano, M., Páez-García, A., Sánchez-Bermejo, E., Tc, M., Leo del Puerto, Y., et al. (2012). Role of Actin Cytoskeleton in Brassinosteroid Signaling and in Its Integration with the Auxin Response in Plants. *Dev. Cell* *22*, 1275–1285.
- Lau, O.S., and Deng, X.W. (2012). The photomorphogenic repressors COP1 and DET1: 20 years later. *Trends Plant Sci.* *17*, 584–593.
- Lee, H.-J., Jung, J.-H., Cortés Llorca, L., Kim, S.-G., Lee, S., Baldwin, I.T., and Park, C.-M. (2014). FCA mediates thermal adaptation of stem growth by attenuating auxin action in *Arabidopsis*. *Nat. Commun.* *5*, 5473.
- Lee, H.-S., Kim, Y., Pham, G., Kim, J.W., Song, J.-H., Lee, Y., Hwang, Y.-S., Roux, S.J., and Kim, S.-H. (2015). Brassinazole resistant 1 (BZR1)-dependent brassinosteroid signalling pathway leads to ectopic activation of quiescent cell division and suppresses columella stem cell differentiation. *J. Exp. Bot.* *66*, 4835–4849.
- Legris, M., Klose, C., Burgie, E.S., Costigliolo, C., Neme, M., Hiltbrunner, A., Wigge, P.A., Schäfer, E., Vierstra, R.D., and Casal, J.J. (2016). Phytochrome B integrates light and temperature signals in *Arabidopsis*. *Science*. Vol 354, Issue 6314, pp.897-900
- Leinonen, T., Cano, J.M., Mäkinen, H., and Merilä, J. (2006). Contrasting patterns of body shape and neutral genetic divergence in marine and lake populations of threespine sticklebacks. *J. Evol. Biol.* *19*, 1803–1812.
- Li, Q.-F., and He, J.-X. (2016). BZR1 Interacts with HY5 to Mediate Brassinosteroid- and Light-Regulated Cotyledon Opening in *Arabidopsis* in Darkness. *Mol. Plant* *9*, 113–125.
- Li, H.M., Altschmied, L., and Chory, J. (1994). *Arabidopsis* mutants define downstream branches in the phototransduction pathway. *Genes Dev.* *8*, 339–349.
- Li, Q.-F., Wang, C., Jiang, L., Li, S., Sun, S.S.M., and He, J.-X. (2012). An interaction between BZR1 and DELLAs mediates direct signaling crosstalk between brassinosteroids and gibberellins in *Arabidopsis*. *Sci. Signal.* *5*, ra72.
- Lincoln, C., Britton, J.H., and Estelle, M. (1990). Growth and development of the *axr1* mutants of *Arabidopsis*. *Plant Cell* *2*, 1071–1080.

- Liu, X.L., Covington, M.F., Fankhauser, C., Chory, J., and Wagner, D.R. (2001). ELF3 encodes a circadian clock-regulated nuclear protein that functions in an Arabidopsis PHYB signal transduction pathway. *Plant Cell* *13*, 1293–1304.
- Lobell, D.B., and Field, C.B. (2007). Global scale climate–crop yield relationships and the impacts of recent warming. *Environ. Res. Lett.* *2*, 14002.
- Logemann, E., Birkenbihl, R.P., Ülker, B., and Somssich, I.E. (2006). An improved method for preparing *Agrobacterium* cells that simplifies the Arabidopsis transformation protocol. *Plant Methods* *2*, 16–16.
- López-Bucio, J., Hernández-Abreu, E., Sánchez-Calderón, L., Pérez-Torres, A., Rampey, R.A., Bartel, B., and Herrera-Estrella, L. (2005). An auxin transport independent pathway is involved in phosphate stress-induced root architectural alterations in Arabidopsis. Identification of BIG as a mediator of auxin in pericycle cell activation. *Plant Physiol.* *137*, 681–691.
- Loudet, O., Chaillou, S., Camilleri, C., Bouchez, D., and Daniel-Vedele, F. (2002). Bay-0 x Shahdara recombinant inbred line population: a powerful tool for the genetic dissection of complex traits in Arabidopsis. *TAG Theor. Appl. Genet. Theor. Angew. Genet.* *104*, 1173–1184.
- Loveys, B.R., Atkinson, L.J., Sherlock, D.J., Roberts, R.L., Fitter, A.H., and Atkin, O.K. (2003). Thermal acclimation of leaf and root respiration: an investigation comparing inherently fast- and slow-growing plant species. *Glob. Change Biol.* *9*, 895–910.
- Lutz, U., Posé, D., Pfeifer, M., Gundlach, H., Hagmann, J., Wang, C., Weigel, D., Mayer, K.F.X., Schmid, M., and Schwechheimer, C. (2015). Modulation of Ambient Temperature-Dependent Flowering in Arabidopsis thaliana by Natural Variation of FLOWERING LOCUS M. *PLOS Genet.* *11*, e1005588.
- Ma, D., Li, X., Guo, Y., Chu, J., Fang, S., Yan, C., Noel, J.P., and Liu, H. (2016). Cryptochrome 1 interacts with PIF4 to regulate high temperature-mediated hypocotyl elongation in response to blue light. *Proc. Natl. Acad. Sci. U. S. A.* *113*, 224–229.
- Mandava, N.B. (1988). Plant Growth-Promoting Brassinosteroids. *Annu. Rev. Plant Physiol. Plant Mol. Biol.* *39*, 23–52.
- Martínez, O., and Curnow, R.N. (1992). Estimating the locations and the sizes of the effects of quantitative trait loci using flanking markers. *Theor. Appl. Genet.* *85*, 480–488.
- Mazzella, M.A., Bertero, D., and Casal, J.J. (2000). Temperature-dependent internode elongation in vegetative plants of Arabidopsis thaliana lacking phytochrome B and cryptochrome 1. *Planta* *210*, 497–501.
- McClung, C.R., and Davis, S.J. (2010). Ambient Thermometers in Plants: From Physiological Outputs towards Mechanisms of Thermal Sensing. *Curr. Biol.* *20*, R1086–R1092.
- Nemhauser, J.L., Mockler, T.C., and Chory, J. (2004). Interdependency of brassinosteroid and auxin signaling in Arabidopsis. *PLoS Biol.* *2*, e258.
- Nicotra, A.B., Atkin, O.K., Bonser, S.P., Davidson, A.M., Finnegan, E.J., Mathesius, U., Poot, P., Purugganan, M.D., Richards, C.L., Valladares, F., et al. (2010a). Plant phenotypic plasticity in a changing climate. *Trends Plant Sci.* *15*, 684–692.
- Nieto, C., López-Salmerón, V., Davière, J.-M., and Prat, S. (2015). ELF3-PIF4 Interaction Regulates Plant Growth Independently of the Evening Complex. *Curr. Biol.* *25*, 187–193.
- Nixdorf, M., and Hoecker, U. (2010). SPA1 and DET1 act together to control photomorphogenesis throughout plant development. *Planta* *231*, 825–833.

- Nomoto, Y., Kubozono, S., Miyachi, M., Yamashino, T., Nakamichi, N., and Mizuno, T. (2012). A Circadian Clock- and PIF4-Mediated Double Coincidence Mechanism is Implicated in the Thermosensitive Photoperiodic Control of Plant Architectures in *Arabidopsis thaliana*. *Plant Cell Physiol.* *53*, 1965–1973.
- Nozue, K., Covington, M.F., Duek, P.D., Lorrain, S., Fankhauser, C., Harmer, S.L., and Maloof, J.N. (2007). Rhythmic growth explained by coincidence between internal and external cues. *Nature* *448*, 358–361.
- Nozue, K., Harmer, S.L., and Maloof, J.N. (2011). Genomic Analysis of Circadian Clock-, Light-, and Growth-Correlated Genes Reveals PHYTOCHROME-INTERACTING FACTOR5 as a Modulator of Auxin Signaling in *Arabidopsis*. *PLANT Physiol.* *156*, 357–372.
- Nusinow, D.A., Helfer, A., Hamilton, E.E., King, J.J., Imaizumi, T., Schultz, T.F., Farré, E.M., and Kay, S.A. (2011). The ELF4-ELF3-LUX complex links the circadian clock to diurnal control of hypocotyl growth. *Nature* *475*, 398–402.
- Ogwen, J.O., Song, X.S., Shi, K., Hu, W.H., Mao, W.H., Zhou, Y.H., Yu, J.Q., and Nogués, S. (2008). Brassinosteroids Alleviate Heat-Induced Inhibition of Photosynthesis by Increasing Carboxylation Efficiency and Enhancing Antioxidant Systems in *Lycopersicon esculentum*. *J. Plant Growth Regul.* *27*, 49–57.
- Oh, E., Zhu, J.-Y., and Wang, Z.-Y. (2012). Interaction between BZR1 and PIF4 integrates brassinosteroid and environmental responses. *Nat. Cell Biol.* *14*, 802–809.
- Oh, E., Zhu, J.-Y., Bai, M.-Y., Arenhart, R.A., Sun, Y., and Wang, Z.-Y. (2014). Cell elongation is regulated through a central circuit of interacting transcription factors in the *Arabidopsis* hypocotyl. *eLife* *3*.
- Ohnishi, T., Godza, B., Watanabe, B., Fujioka, S., Hategan, L., Ide, K., Shibata, K., Yokota, T., Szekeres, M., and Mizutani, M. (2012). CYP90A1/CPD, a brassinosteroid biosynthetic cytochrome P450 of *Arabidopsis*, catalyzes C-3 oxidation. *J. Biol. Chem.* *287*, 31551–31560.
- Parent, B., and Tardieu, F. (2012). Temperature responses of developmental processes have not been affected by breeding in different ecological areas for 17 crop species. *New Phytol.* *194*, 760–774.
- Pedmale, U.V., Huang, S.-S.C., Zander, M., Cole, B.J., Hetzel, J., Ljung, K., Reis, P.A.B., Sridevi, P., Nito, K., Nery, J.R., et al. (2016). Cryptochromes Interact Directly with PIFs to Control Plant Growth in Limiting Blue Light. *Cell* *164*, 233–245.
- Penfield, S., Kendall, S., and MacGregor, D. (2012). Temperature perception and signal transduction - mechanisms across multiple organisms. In *Temperature Adaptation in a Changing Climate: Nature at Risk*, K.B. Storey, and K.K. Tanino, eds. (Wallingford: CABI), pp. 6–23.
- Peng, S., Huang, J., Sheehy, J.E., Laza, R.C., Visperas, R.M., Zhong, X., Centeno, G.S., Khush, G.S., and Cassman, K.G. (2004). Rice yields decline with higher night temperature from global warming. *Proc. Natl. Acad. Sci. U. S. A.* *101*, 9971–9975.
- Porra, R.J., Thompson, W.A., and Kriedemann, P.E. (1989). Determination of accurate extinction coefficients and simultaneous equations for assaying chlorophylls a and b extracted with four different solvents: verification of the concentration of chlorophyll standards by atomic absorption spectroscopy. *Biochim. Biophys. Acta BBA - Bioenerg.* *975*, 384–394.
- Press, M.O., Lanctot, A., and Queitsch, C. (2016). PIF4 and ELF3 Act Independently in *Arabidopsis thaliana* Thermoresponsive Flowering. *PLOS ONE* *11*, e0161791.

- Quint, M., Delker, C., Franklin, K.A., Wigge, P.A., Halliday, K.J and van Zanten, M. (2016). Molecular and genetic control of plant thermomorphogenesis. *Nature Plants* 2, 15190
- Raschke, A., Ibañez, C., Ullrich, K.K., Anwer, M.U., Becker, S., Glöckner, A., Trenner, J., Denk, K., Saal, B., Sun, X., et al. (2015). Natural variants of ELF3 affect thermomorphogenesis by transcriptionally modulating PIF4-dependent auxin response genes. *BMC Plant Biol.* 15, 197.
- Reed, J.W., Nagpal, P., Bastow, R.M., Solomon, K.S., Dowson-Day, M.J., Elumalai, R.P., and Millar, A.J. (2000). Independent action of ELF3 and phyB to control hypocotyl elongation and flowering time. *Plant Physiol.* 122, 1149–1160.
- Ruegger, M., Dewey, E., Hobbie, L., Brown, D., Bernasconi, P., Turner, J., Muday, G., and Estelle, M. (1997). Reduced naphthylphthalamic acid binding in the tir3 mutant of Arabidopsis is associated with a reduction in polar auxin transport and diverse morphological defects. *Plant Cell* 9, 745–757.
- Ryu, H., Kim, K., Cho, H., Park, J., Choe, S., and Hwang, I. (2007). Nucleocytoplasmic Shuttling of BZR1 Mediated by Phosphorylation Is Essential in Arabidopsis Brassinosteroid Signaling. *Plant Cell* 19, 2749–2762.
- Saidi, Y., Finka, A., Muriset, M., Bromberg, Z., Weiss, Y.G., Maathuis, F.J.M., and Goloubinoff, P. (2009). The heat shock response in moss plants is regulated by specific calcium-permeable channels in the plasma membrane. *Plant Cell* 21, 2829–2843.
- Sakamoto, T., and Fujioka, S. (2013). Auxins increase expression of the brassinosteroid receptor and brassinosteroid-responsive genes in *Arabidopsis*. *Plant Signal. Behav.* 8, e23509.
- Sakamoto, T., Morinaka, Y., Inukai, Y., Kitano, H., and Fujioka, S. (2013). Auxin signal transcription factor regulates expression of the brassinosteroid receptor gene in rice. *Plant J.* 73, 676–688.
- Sambade, A., Pratap, A., Buschmann, H., Morris, R.J., and Lloyd, C. (2012). The Influence of Light on Microtubule Dynamics and Alignment in the Arabidopsis Hypocotyl. *Plant Cell* 24, 192–201.
- Schmuths, H., Bachmann, K., Weber, W.E., Horres, R., And Hoffmann, M.H. (2006). Effects of Preconditioning and Temperature During Germination of 73 Natural Accessions of Arabidopsis thaliana. *Ann. Bot.* 97, 623–634.
- Shen, H., Zhu, L., Castillon, A., Majee, M., Downie, B., and Huq, E. (2008). Light-induced phosphorylation and degradation of the negative regulator PHYTOCHROME-INTERACTING FACTOR1 from Arabidopsis depend upon its direct physical interactions with photoactivated phytochromes. *Plant Cell* 20, 1586–1602.
- Silvestro, D., Andersen, T.G., Schaller, H., and Jensen, P.E. (2013). Plant sterol metabolism. $\Delta(7)$ -Sterol-C5-desaturase (STE1/DWARF7), $\Delta(5,7)$ -sterol- $\Delta(7)$ -reductase (DWARF5) and $\Delta(24)$ -sterol- $\Delta(24)$ -reductase (DIMINUTO/DWARF1) show multiple subcellular localizations in Arabidopsis thaliana (Heynh) L. *PLoS One* 8, e56429.
- Singh, I., and Shono, M. (2003). Effect of 24-epibrassinolide on pollen viability during heat-stress in tomato. *Indian J. Exp. Biol.* 41, 174–176.
- Stavang, J.A., Gallego-Bartolomé, J., Gómez, M.D., Yoshida, S., Asami, T., Olsen, J.E., García-Martínez, J.L., Alabadí, D., and Blázquez, M.A. (2009). Hormonal regulation of temperature-induced growth in Arabidopsis: Hormones and modulation of growth by temperature. *Plant J.* 60, 589–601.

- Stewart Lilley JL, Gan Y, Graham IA, Nemhauser JL. (2013) The effects of *DELLA* s on growth change with developmental stage and brassinosteroid levels. *Plant J.* 76, 165-173.
- Storz, J.F. (2002). Contrasting patterns of divergence in quantitative traits and neutral DNA markers: analysis of clinal variation. *Mol. Ecol.* 11, 2537–2551.
- Sun, J., Qi, L., Li, Y., Chu, J., and Li, C. (2012). PIF4–Mediated Activation of YUCCA8 Expression Integrates Temperature into the Auxin Pathway in Regulating Arabidopsis Hypocotyl Growth. *PLoS Genet.* 8, e1002594.
- Sun, Y., Fan, X.-Y., Cao, D.-M., Tang, W., He, K., Zhu, J.-Y., He, J.-X., Bai, M.-Y., Zhu, S., Oh, E., et al. (2010). Integration of Brassinosteroid Signal Transduction with the Transcription Network for Plant Growth Regulation in Arabidopsis. *Dev. Cell* 19, 765–777.
- Sureshkumar, S., Dent, C., Seleznev, A., Tasset, C., and Balasubramanian, S. (2016). Nonsense-mediated mRNA decay modulates FLM-dependent thermosensory flowering response in Arabidopsis. *Nat. Plants* 2, 16055.
- Taiz, Lincoln and Eduardo Zeiger. (2015). *Plant physiology and Development*. Sunderland, MA: Sinauer Associates.
- Tajima, T., Oda, A., Nakagawa, M., Kamada, H., and Mizoguchi, T. (2007). Natural variation of polyglutamine repeats of a circadian clock gene ELF3 in Arabidopsis. *Plant Biotechnol.* 24, 237–240.
- Tasaki, T., Kim, S.T., Zakrzewska, A., Lee, B.E., Kang, M.J., Yoo, Y.D., Cha-Molstad, H.J., Hwang, J., Soung, N.K., Sung, K.S., et al. (2013). UBR box N-recognin-4 (UBR4), an N-recognin of the N-end rule pathway, and its role in yolk sac vascular development and autophagy. *Proc. Natl. Acad. Sci. U. S. A.* 110, 3800–3805.
- Team R Core (2012). *R: A language and environment for statistical computing*. R Foundation for Statistical Computing, Vienna, Austria, 2012 (ISBN 3-900051-07-0).
- Toledo-Ortiz, G., Huq, E., and Quail, P.H. (2003). The Arabidopsis basic/helix-loop-helix transcription factor family. *Plant Cell* 15, 1749–1770.
- Tuinstra, M.R., Ejeta, G., and Goldsbrough, P.B. (1997). Heterogeneous inbred family (HIF) analysis: a method for developing near-isogenic lines that differ at quantitative trait loci. *Theor. Appl. Genet.* 95, 1005–1011.
- Uleberg, E., Widerøe, I.S., Grindflek, E., Szyda, J., Lien, S., and Meuwissen, T.H.E. (2005). Fine mapping of a QTL for intramuscular fat on porcine chromosome 6 using combined linkage and linkage disequilibrium mapping. *J. Anim. Breed. Genet. Z. Tierzuchtung Zuchtungsbiologie* 122, 1–6.
- Undurraga, S.F., Press, M.O., Legendre, M., Bujdoso, N., Bale, J., Wang, H., Davis, S.J., Verstrepen, K.J., and Queitsch, C. (2012). Background-dependent effects of polyglutamine variation in the Arabidopsis thaliana gene ELF3. *Proc. Natl. Acad. Sci.* 109, 19363–19367.
- Vilarrasa-Blasi, J., González-García, M.-P., Frigola, D., Fàbregas, N., Alexiou, K.G., López-Bigas, N., Rivas, S., Jauneau, A., Lohmann, J.U., Benfey, P.N., et al. (2014). Regulation of Plant Stem Cell Quiescence by a Brassinosteroid Signaling Module. *Dev. Cell* 30, 36–47.
- Wang, X. (2006). Brassinosteroids Regulate Dissociation of BKI1, a Negative Regulator of BRI1 Signaling, from the Plasma Membrane. *Science* 313, 1118–1122.

- Wang, C.-Q., Sarmast, M.K., Jiang, J., and Dehesh, K. (2015). The Transcriptional Regulator BBX19 Promotes Hypocotyl Growth by Facilitating COP1-Mediated EARLY FLOWERING3 Degradation in Arabidopsis. *Plant Cell* 27, 1128–1139.
- Wang, R., Zhang, Y., Kieffer, M., Yu, H., Kepinski, S., and Estelle, M. (2016). HSP90 regulates temperature-dependent seedling growth in Arabidopsis by stabilizing the auxin co-receptor F-box protein TIR1. *Nat. Commun.* 7, 10269.
- Wang, Z.-Y., Wang, Q., Chong, K., Wang, F., Wang, L., Bai, M., and Jia, C. (2006). The brassinosteroid signal transduction pathway. *Cell Res.* 16, 427–434.
- Wang, Z.-Y., Bai, M.-Y., Oh, E., and Zhu, J.-Y. (2012). Brassinosteroid signaling network and regulation of photomorphogenesis. *Annu. Rev. Genet.* 46, 701–724.
- Whitlock, M.C. (2008). Evolutionary inference from QST. *Mol. Ecol.* 17, 1885–1896.
- Whitman, D., and Agrawal, A. (2009). What is Phenotypic Plasticity and Why is it Important? In *Phenotypic Plasticity of Insects*, (Science Publishers), p.
- Whittle, C.A., Otto, S.P., Johnston, M.O., and Krochko, J.E. (2009). Adaptive epigenetic memory of ancestral temperature regime in *Arabidopsis thaliana*. This paper is one of a selection of papers published in a Special Issue from the National Research Council of Canada – Plant Biotechnology Institute. *Botany* 87, 650–657.
- de Wit, M., Lorrain, S., and Fankhauser, C. (2014). Auxin-mediated plant architectural changes in response to shade and high temperature. *Physiol. Plant.* 151, 13–24.
- Woodward, A., Smith, K.R., Campbell-Lendrum, D., Chadee, D.D., Honda, Y., Liu, Q., Olwoch, J., Revich, B., Sauerborn, R., Chafe, Z., et al. (2014). Climate change and health: on the latest IPCC report. *The Lancet* 383, 1185–1189.
- Wu, F.-H., Shen, S.-C., Lee, L.-Y., Lee, S.-H., Chan, M.-T., and Lin, C.-S. (2009). Tape-Arabidopsis Sandwich - a simpler Arabidopsis protoplast isolation method. *Plant Methods* 5, 16.
- Xia, X.-J., Huang, L.-F., Zhou, Y.-H., Mao, W.-H., Shi, K., Wu, J.-X., Asami, T., Chen, Z., and Yu, J.-Q. (2009). Brassinosteroids promote photosynthesis and growth by enhancing activation of Rubisco and expression of photosynthetic genes in *Cucumis sativus*. *Planta* 230, 1185–1196.
- Yamaguchi, N., Suzuki, M., Fukaki, H., Morita-Terao, M., Tasaka, M., and Komeda, Y. (2007). CRM1/BIG-mediated auxin action regulates Arabidopsis inflorescence development. *Plant Cell Physiol.* 48, 1275–1290.
- Yamashino, T., Nomoto, Y., Lorrain, S., Miyachi, M., Ito, S., Nakamichi, N., Fankhauser, C., and Mizuno, T. (2013). Verification at the protein level of the PIF4-mediated external coincidence model for the temperature-adaptive photoperiodic control of plant growth in *Arabidopsis thaliana*. *Plant Signal. Behav.* 8, e23390.
- Yin, Y., Vafeados, D., Tao, Y., Yoshida, S., Asami, T., and Chory, J. (2005). A New Class of Transcription Factors Mediates Brassinosteroid-Regulated Gene Expression in Arabidopsis. *Cell* 120, 249–259.
- Yoo, S.-D., Cho, Y.-H., and Sheen, J. (2007). Arabidopsis mesophyll protoplasts: a versatile cell system for transient gene expression analysis. *Nat. Protoc.* 2, 1565–1572.
- Yu, J.Q., Huang, L.F., Hu, W.H., Zhou, Y.H., Mao, W.H., Ye, S.F., and Nogués, S. (2004). A role for brassinosteroids in the regulation of photosynthesis in *Cucumis sativus*. *J. Exp. Bot.* 55, 1135–1143.

Zagotta, M.T., Hicks, K.A., Jacobs, C.I., Young, J.C., Hangarter, R.P., and Meeks-Wagner, D.R. (1996). The Arabidopsis ELF3 gene regulates vegetative photomorphogenesis and the photoperiodic induction of flowering. *Plant J.* 10, 691–702.

Zhao, B., and Li, J. (2012). Regulation of Brassinosteroid Biosynthesis and Inactivation. *J. Integr. Plant Biol.* 54, 746–759.

Zhu, J.-Y., Sae-Seaw, J., and Wang, Z.-Y. (2013). Brassinosteroid signalling. *Dev. Camb. Engl.* 140, 1615–1620.

Zhu, J.-Y., Oh, E., Wang, T., and Wang, Z.-Y. (2016). TOC1–PIF4 interaction mediates the circadian gating of thermoresponsive growth in Arabidopsis. *Nature Communications* 7, 13692.

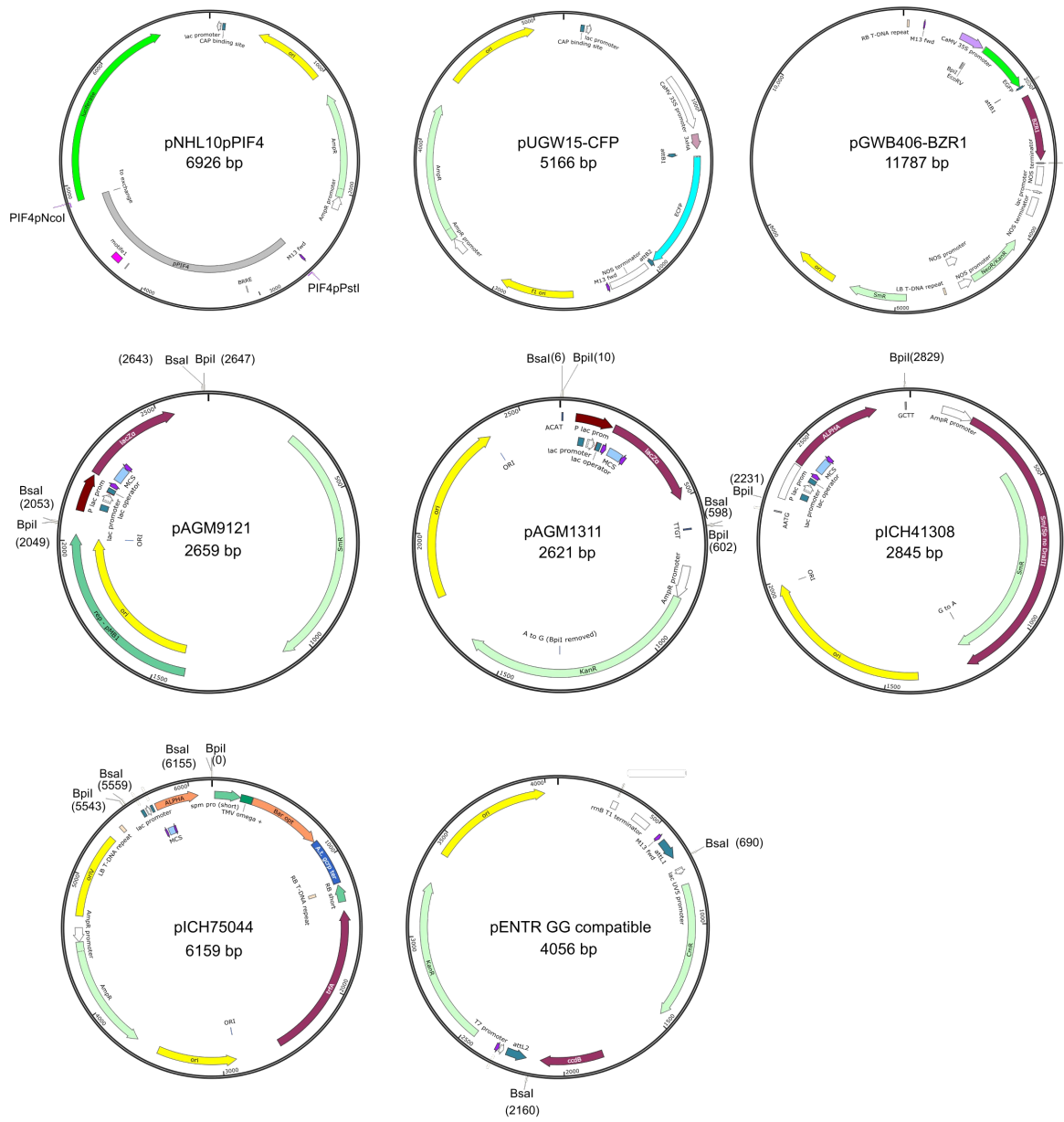
Appendix I

Line	Description	NASC/source	Background	Chapter
Bay-0	Wt	N57923		I
C24	Wt	N906/183AV		I
Col-0	Wt	N1092		I;III
Cvi-0	Wt	CS22682		I
Got-7	Wt	Cs22685		I
Ler-1	Wt	Cs22686		I;III
No-0	Wt	CS28564		I
Rrs-7	Wt	CS22688		I;III
Sha	Wt	N929/236AV		I
Ws-2	Wt	N28827		I;III
Bay-0	Wt	41AV		II
Sha	Wt	236AV		II
HIFs lines	heterogeneous inbred families	33HV84		II
HIFs lines	heterogeneous inbred families	33HV194		II
Pro _{Sha} :ELF3 ^{Sha}	Transgenic complementation line	Anwer et al., 2014	<i>elf3-4</i>	II
Pro _{Bay} :ELF3(A362V) _{Bay-0}	Transgenic complementation line	Anwer et al., 2014	<i>elf3-4</i>	II
Pro _{Bay} :ELF3(A362V) _{Bay-0}	Transgenic complementation line	Anwer et al., 2014	<i>elf3-4</i>	II
<i>hy5-51</i>	light/temperature signaling	N596651	Col-0	III
<i>elf3-4</i>	light/temperature signaling	N3790	Ws-2	III
<i>br1-4</i>	Brassinosteroid biosynthesis	N3953	Ws-2	III
<i>det2</i>	Brassinosteroid biosynthesis	N6159	Col-0	III
<i>rot3-2</i>	Brassinosteroid biosynthesis	N3728	Ler	III
<i>pif4-2</i>	Phytocrome interactor factor; TF	N66043	Col-0	III
<i>wei8-4/tar1-1</i>	Auxin biosynthesis	N16412	Col-0	III
<i>ste1</i>	Brassinosteroid biosynthesis	Silvestro et al., 2013	Col-0	III
35S:STE1:YFP	Brassinosteroid biosynthesis	Silvestro et al., 2013	<i>ste1</i> (Col-0)	III
35S:PIF4	Phytocrome interactor factor; TF	Van Zanten, Martijn	<i>pif4</i> (Col-0)	III
35S:Bzr1-D	Brassinosteroid signaling; TF	Oh et al., 2014	Col-0	III
<i>dwf7-1</i>	Brassinosteroid biosynthesis	Choe et al., 1999	Ws-2	III
<i>tir1/afb2/afb3</i>	Auxin signaling	Luz Irina Calderón Villalobos	Col-0	III
35S:PIF41A	Phytocrome interactor factor; TF	Salomé Prat	<i>pif,pif5</i> (Col-0)	III
pPIF4:PIF41A	Phytocrome interactor factor; TF	Salomé Prat	<i>pif,pif5</i> (Col-0)	III

Appendix II

Oligonucleotides	Sequence	Use
<i>ELF3_F</i>	TCAATATCACCCCGGCATGG	qRT PCR
<i>ELF3_R</i>	CCACTTGGACTGCTTCCTGT	
<i>PIF4_F</i>	AGATGCAGCCGATGGAGATG	qRT PCR
<i>PIF4_R</i>	GCTCACCAACCTAGTGGTCC	
<i>SAUR19_F</i>	CTTCAAGAGCTTCATAATAATTCAAACTT	qRT PCR
<i>SAUR19_R</i>	GAAGGAAAAAATGTTGGATCATCTT	
<i>IAA19_F</i>	GGTGACAACTGCGAATACGTTACCA	qRT PCR
<i>IAA19_R</i>	CCCGGTAGCATCCGATCTTTTCA	
<i>DWF7_F</i>	TGGCGGCGGATAATGCTT	qRT PCR
<i>DWF7_R</i>	TTTCGGAGCCATGTCTGGAG	
<i>DWF4_F</i>	CGGTGATCTCAGCCGTACAT	qRT PCR
<i>DWF4_R</i>	AGTTGTTTCCCCACGTCGAA	
<i>BRRE_F</i>	GGCTAAATTAGTTAGACTGTC	qRT PCR
<i>BRRE_R</i>	TACCAGGTAATTGGAGTGGT	
<i>REG2_F</i>	CCGTATGGTCAAATTATAT	qRT PCR
<i>REG2_R</i>	TCCTGAAATGTATATCATTAA	
<i>REG1_F</i>	CTTCACTTGTATGTGTCCCCT	qRT PCR
<i>REG1_R</i>	CTCTAGGGACAACAGTACTG	
<i>SAUR15_F</i>	AAG AGG ATT CAT GGC GGT CTA TG	qRT PCR
<i>SAUR15_R</i>	GTA TTG TTA AGC CGC CCA TTG G	
<i>ELF3_F_BbVI</i>	CTTCTCGAGCTGAAACAAACCT	CAPS
<i>ELF3_R_BbVI</i>	GACGACAACATGTGGTAGAGGA	
<i>dwf7_HaeIII F</i>	TGG TCT CGG ACT GAT TGG AA	CAPS
<i>dwf7_HaeIII R</i>	TGG GCA TTC TCA CTC TGC TT	
<i>4g18470_ApoIF</i>	GTT GAC GAG GTA CTT GTT ACA AAA	CAPS
<i>4g18470_ApoIR</i>	TCT GAT TCC TCA GAC TCA TTA ACT C	
<i>4G33945_BseMIIF</i>	ACA TTC AGA GCA CAG AGA GAC TCA	CAPS
<i>4G33945_BseMIIR</i>	GGG AAG CAA CAA CAC GGA AG	
<i>ROT3_DdeIF</i>	TTCTCCAAGTAGTTCCGTAATTGATCTA	CAPS
<i>ROT3_DdeIR</i>	ACGAACATAATAGGGACACCAA	
<i>elf3-4dCAPS3F</i>	AGGGCCTAGAGCTCCTCCTA	CAPS
<i>elf3-4dCAPS3R</i>	CCAGGATGAACCAAAGTGCT	
<i>PIF4pStI</i>	CTAGCGCTGCAGATTTACATTTATGAATTTCCACATTTATC	Cloning
<i>PIF4pNcoI</i>	CCATGGTGCATGGTCAGATCTCTGGAGACATTTCA	
<i>BZR1_1F</i>	CAC CAT GAC TTC GGA TGG AGC TAC G	Cloning
<i>BZR1_1011rWS</i>	TCA ACC ACG AGC CTT CCC AT	
<i>ROT3_f1CACC</i>	CAC CAT GCA ACC TCC GGC AAG CGC	Cloning
<i>ROT3_r</i>	ATG ATC TTC AAG TGA GAT CGG AG	

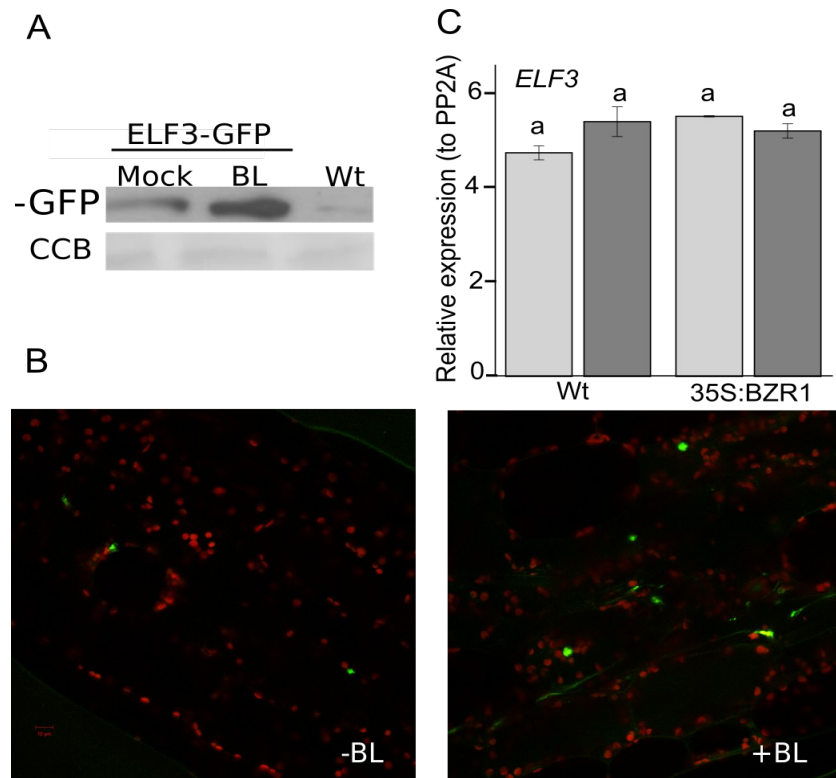
Appendix III



Appendix IV

Developmental data			
Juvenile vegetative stage			
Germination time	radicle emergence	days	1
Seeding establishment	cotyledons opened fully	days	2
2 rosette leaves	rosette leaves >1 mm in length	days	3
3 rosette leaves	rosette leaves >1 mm in length	days	4
4 rosette leaves	rosette leaves >1 mm in length	days	5
5 rosette leaves	rosette leaves >1 mm in length	days	6
6 rosette leaves	rosette leaves >1 mm in length	days	7
7 rosette leaves	rosette leaves >1 mm in length	days	8
Adult vegetative stage			
8 rosette leaves	rosette leaves >1 mm in length	days	9
9 rosette leaves	rosette leaves >1 mm in length	days	10
10 rosette leaves	rosette leaves >1 mm in length	days	11
11 rosette leaves	rosette leaves >1 mm in length	days	12
12 rosette leaves	rosette leaves >1 mm in length	days	13
13 rosette leaves	rosette leaves >1 mm in length	days	14
14 rosette leaves	rosette leaves >1 mm in length	days	15
Adult reproductive phase			
Inflorescence emergence	First flower buds visible	days	16
Flowering time_days	Bolt>1cm	days	17
Flowering time_n leaves	Bolt>1cm	n° leaves	18
Flowering time_first flower	First flower full opened	days	19
Siliques production	First silique appear	days	20
morphometric phenotypes			
Hypocotyl length	7 days old seedlings	pixels	21
Petiole angle	7 days old seedlings	°	22
Length of primary root	7 days old seedlings	pixels	23
Petiole length	20 days old seedlings	pixels	24
Chlorophyll content	14 days old seedlings	µg/mg leave	25
Foliar surface	Bolt>1cm	mm ²	26
Senescence-associated phenotypes			
Total number of siliques per p	First silique shattered	Count	27
Max. Plant height	First silique shattered	cm	28
Gametophytic phase			
Seed area		pixels	29
Seed length		pixels	30
Seed weight		µgr.	31
Total number of seeds per plant		Count	32
Total number of seeds per silique		Count	33
Silique length		mm	34

Appendix V



ELF3 is accumulated in response to BL. (A) Western blot of ELF3 detected using GFP antibody. Wt is used as negative control. CCB shows the total protein after blotting. (B) *ELF3* mRNA levels at 20° (light gray) or 28°C (dark gray) in Wt and *35S:BZR1* (C) Confocal images of ELF3 protein localization under mock or BL pre-treated samples. In A and B, 7 days-old pELF3:ELF3:YFP seedlings were grown at 20°C (LD) and shifted to 28°C at the end of the day (ZT:16). Samples were harvested 3 hours after shift. No significant differences was assessed by 1-way ANOVA and Turkey-test ($p < 0.05$, $n > 8$).

Appendix IV

Solutions: always fresh Mannitol stock, the other stock solutions can last for months.

Enzyme solution, W5, MMG, PEG, W1 must be prepared fresh every time.

Enzyme solution	Stock solutions	final concentration	20 ml
Mannitol	0.8 M	0.4 M	10 ml
KCl	0.1 M	20 mM	4 ml
Water			3.8 ml
MES pH 5.7	0.2 M	20 mM	2 ml
		Heat up at 55°C	
Cellulase (SERVA cat-16419)	solid	1%	200 mg
Macerozyme (SERVA cat-28302)	solid	0.25%	50 mg
		Mix and incubate 10min at 55°C	
		Cool down on ice	
BSA	solid	0.10%	20 mg
CaCl₂	1 M	10 mM	200 ul
W5 solution	Stock solutions	final concentration	100 ml
NaCl	5 M	154 mM	3.08 ml
CaCl₂	1 M	125 mM	12.5 ml
KCl	0.1 M	5 mM	2.5 ml
Glucose		5 mM	90mg
MES	0.2 M	2 mM	1 ml
MMG	Stock solutions	final concentration	20 ml
Mannitol	0.8 M	0.4 M	10 ml
MgCl₂	0.15 M	15 mM	2 ml
Mes pH 5.7	0.2 M	4 mM	0.4 ml
Water			7.6 ml
PEG (on the rotation shaker until the PEG is dissolved)			
	Stock solutions	final concentration	20 ml
Mannitol	0.8 M	0.2 M	5 ml
CaCl₂	1 M	0.1 M	2 ml
PEG (MW 4000; Fluka cat-81242)	solid		8 g
Water			6 ml
W1	Stock solutions	final concentration	20 ml
Mannitol	0.8 M	0.5 M	12.6 ml
KCl	0.1 M	20 mM	4 ml
Mes pH 5.7	0.2 M	4 mM	0.4 ml
Water			3 ml

Acknowledgments

I would like to thank Professor Marcel Quint and Dr. Carolin Delker for their extraordinary support, advice and active discussions through my thesis; as well as for teaching excellent scientific practice and keeping positive and pleasant atmosphere in the group. I would like to thank Professor Stephan Abel, Professor Bettina Hause, Professor Klaus Humbeck, Dr. Selma Gago and Dr. Katharina Bürstenbinder for their support and useful advices. In addition, I would like to thank Dr. Sylvestre Marillonnet for his expertise with the Golden Gate technique.

Because a good project can only be managed with good people around, I would like to thank Philipp Janitza, Kathrin Denk, Jana Trenner, Usman Anwer, Julia Bellstädt, and Steve Babben for their help at professional and personal level. Special mention to Julia and Philipp for the great time together outside the lab. In addition, this project would have been impossible without the funding support of the DFG, the Leibniz-Association and the EMBO organization.

To conclude, I would like to thank my parents for their endless emotional support during these years. Therefore, I would like to dedicate this work to them. In addition, I would like to thank my international Halle friends for emotional well-being throughout the completion of the project at hand and the good moments we spent together. Specially, I would like to thank to Maria Klecker, Maria Santo, Markus Franzén, Montserrat Solé, Frederik Faden, Giulia Furlan, Pavel Reichman and George Chezha.

Curriculum Vitae

Personal information

Born in Valencia, Spain (1988)

Email: caribrob@gmail.com

Telephone: +4917657736257

Research experience:

Confocal microscopy, mutant characterization, protoplast transient expression, LUC assay, gateway and Golden Gate cloning techniques, ChIP-PCR, Elisa's Technique, *Arabidopsis* work, molecular biology, R statistical program, ImageJ, microbiological and chemical analysis

Positions and projects:

2013-current

PhD student in Natural Sciences; "Regulation of phenotypic plasticity in high ambient temperature: ELF3 and BZR1 as major thermostats gating PIF4 signaling"

Supervisors : Prof. Dr. Marcel Quint and Dr. Carolin Delker
Leibniz Institute for plantbiochemistry (IPB), Halle - Germany
Martin Luther University (MLU), Halle - Germany

2012

Master's Final Project

"RSL1-1D, an ubiquitin ligase that confers abscisic acid insensitivity and seed longevity"

Ion Homeostasis, Cellular Stress and Genomics.

Supervisor: Dr. Ramón Serrano, Dr. Eduardo Bueso
IBMCP(UPV-CSIC); Valencia, Spain

2011

Fellowship – Erasmus Grant

MERIT program-Sugar signaling; Utrecht University. The Netherlands

Molecular Plant Physiology. Sjef Smeekens. Supervisor: Dr. Johannes Hanson, Dr. Jeroen Lastdrager

Internship

Plant cIRES Biotech, Dr.Mar Castellano Moreno
CBGP (Biotechnology and Plant Genomics Center)
Madrid, Spain

2010

Bachelor's final project "Identification of sulfate starvation responsive proteins in different tissues of *Brassica napus* by 2D- gel electrophoresis"

Proteomics Department

Supervisors: Dr.Julia Kehr, Dr. Anja Buhtz
CBGP (Biotechnology and Plant Genomics Center)
Madrid, Spain

2009

Technical assistant: Food Laboratory
Manufacturas Ceylan S.L
Valencia, Spain

Performed chemical and microbiological analysis, immunotests with Elisa's Technique
Wrote procedures Handbook on Elisa's Technique and beat established targets

Education and training:

2011-2012

Master's Degree in Plant Biotechnology (Average mark: 3.2)
IBMCP-CSIC (Valencia, Spain)

2006-2011

Bachelor's Degree in Biotechnology (Average mark: 1.59)
Specialized in Biomedical Science
Francisco de Vitoria University (Madrid, Spain)

Master's Degree in Management of Biotechnology Companies (Average mark: 1.83)
Francisco de Vitoria University (Madrid, Spain)

Supervision:

Alexandra Grossjohan – Bachelor thesis (2016)
Tanja Klause – Bachelor thesis (2014)

Conferences:

2007 - Inter University Convention II Biotechnology; Sevilla, Spain
2008 - Inter University Convention on Biotechnology and Company; Salamanca, Spain
2011 - Summer School on Environmental Signalling; Utrecht University, The Netherlands
2013 - Plant science student conference; Halle, Germany
2015 - International Conference of *Arabidopsis* Research (ICAR); Paris, France
2016 - Molecular biology of plants; Drabringhausen, Germany

Research Grants:

2011 - Erasmus Grant
2016 - EMBO short fellowship (ASTF- 593 – 2016)
Visiting researcher, EMBO short time fellowship - Salomé Prat, Madrid (Spain)

Personal skills:

social, team work, hard worker
Spanish: mother tongue; English B2, German A1

Peer-review of scientific journals:

BMC

Publication list

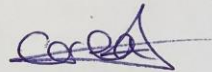
1. **Ibañez, C.**, Poeschl, Y., Peterson, T., Bellstädt, J., Denk, K., Gogol-Döring, A., Quint, M., and Delker, C. (2015). *Developmental plasticity of Arabidopsis thaliana accessions across an ambient temperature range*. BioRxiv 17285.
2. Raschke, A.*, **Ibañez, C.***, Ullrich, K.K., Anwer, M.U., Becker, S., Glöckner, A., Trenner, J., Denk, K., Saal, B., Sun, X., et al. (2015). *Natural variants of ELF3 affect thermomorphogenesis by transcriptionally modulating PIF4-dependent auxin response genes*. BMC Plant Biol. 15, 197.
3. Delker, C., Sonntag, L., James, G.V., Janitza, P., **Ibañez, C.**, Ziermann, H., Peterson, T., Denk, K., Mull, S., Ziegler, J., et al. (2014). *The DET1-COP1-HY5 pathway constitutes a multipurpose signaling module regulating plant photomorphogenesis and thermomorphogenesis*. Cell Rep 9, 1983–1989.
4. Bueso, E., **Ibañez, C.**, Sayas, E., Muñoz-Bertomeu, J., Gonzalez-Guzmán, M., Rodriguez, P.L., and Serrano, R. (2014a). *A forward genetic approach in Arabidopsis thaliana identifies a RING-type ubiquitin ligase as a novel determinant of seed longevity*. Plant Sci. 215–216, 110–116.
5. Bueso, E., Rodriguez, L., Lorenzo-Orts, L., Gonzalez-Guzman, M., Sayas, E., Muñoz-Bertomeu, J., **Ibañez, C.**, Serrano, R., and Rodriguez, P.L. (2014b). *The single-subunit RING-type E3 ubiquitin ligase RSL1 targets PYL4 and PYR1 ABA receptors in plasma membrane to modulate abscisic acid signaling*. Plant J. 80, 1057–1071.

Eidesstattliche Erklärung

Ich erkläre an Eides statt, dass ich die Arbeit selbstständig und ohne fremde Hilfe verfasst, keine anderen als die von mir angegebenen Quellen und Hilfsmittel benutzt und die den benutzten Werken wörtlich oder inhaltlich entnommenen Stellen als solche kenntlich gemacht habe.

Ort/Datum

Halle, 29.05.2017

A handwritten signature in blue ink, appearing to read 'C. Reed', with a horizontal line extending to the right.